


12-2013

Radiogenic Second Cancer Risk Differences in Female Hodgkin Lymphoma Patients Treated with Proton versus Photon Radiotherapies

Kenneth L. Homann

Follow this and additional works at: http://digitalcommons.library.tmc.edu/utgsbs_dissertations

 Part of the [Biological and Chemical Physics Commons](#), [Nuclear Commons](#), and the [Oncology Commons](#)

Recommended Citation

Homann, Kenneth L., "Radiogenic Second Cancer Risk Differences in Female Hodgkin Lymphoma Patients Treated with Proton versus Photon Radiotherapies" (2013). *UT GSBS Dissertations and Theses (Open Access)*. Paper 408.

This Dissertation (PhD) is brought to you for free and open access by the Graduate School of Biomedical Sciences at DigitalCommons@The Texas Medical Center. It has been accepted for inclusion in UT GSBS Dissertations and Theses (Open Access) by an authorized administrator of DigitalCommons@The Texas Medical Center. For more information, please contact laurel.sanders@library.tmc.edu.

**Radiogenic Second Cancer Risk Differences in Female
Hodgkin Lymphoma Patients Treated with Proton *versus*
Photon Radiotherapies**

by

Kenneth Lois Homann, M.S.

Approved

Wayne D. Newhauser, Ph.D. - Advisor

Rebecca M. Howell, Ph.D. - Co-Advisor

Dragan Mirkovic, Ph.D.

Carol J. Etzel, Ph.D.

Anita Mahajan, M.D.

Dean, The University of Texas Graduate School of Biomedical Sciences

**Radiogenic Second Cancer Risk Differences in Female
Hodgkin Lymphoma Patients Treated with Proton *versus*
Photon Radiotherapies**

A
DISSERTATION

Presented to the Faculty of
The University of Texas
Health Science Center at Houston
and
The University of Texas
M. D. Anderson Cancer Center
Graduate School of Biomedical Sciences

In Partial Fulfillment
of the Requirements
for the Degree of

DOCTOR OF PHILOSOPHY

by
Kenneth Lois Homann
M.S., The University of Texas Health Science Center at Houston, 2005
B.S., Northwestern State University, 2001

December 2013

© Copyright by Kenneth Lois Homann, 2013.

All rights reserved.

For Sarah and the soon to be Baby Girl Homann...

Acknowledgements

I would like to thank my two co-advisors, Drs. Wayne Newhauser and Rebecca Howell, for both the time and energy they have invested in guiding me through this project. Their doors have always been open when I've needed their help and guidance, and for that I am truly appreciative.

I would also like to thank the members of my advisory, candidacy examination, and supervisory committee: Dr. Carol Etzel, Dr. Dragan Mirkovic, Dr. Anita Mahajan, Dr. Philip Taddei, Dr. Uwe Titt, Dr. David Followill, Dr. Thomas Buchholz, and Dr. George Coutrakon. Without their support and expertise, the road to finishing up this undertaking would have been far more difficult.

I would also like to acknowledge my peers and colleagues who have helped me both personally and professionally as I've navigated through my studies over the last few years, including Dr. John Eley, Dr. Annelise Giebeler, Dr. Rui Zhang, Ms. Laura Rechner, and Ms. Scharlene Wilson. Their insight and humor along the way made this undertaking more enjoyable than I could have imagined.

No acknowledgement would be complete without including my family. My parents, Ronnie and Debbie Homann, and my brother, Scott Homann, have always been there for me. Their encouragement and belief in me since I was young have helped me to attain any accomplishments I have been fortunate enough to obtain.

Finally, I'd like to thank my wife, Sarah, for her unwavering love and support. I am so grateful that we get to share our lives together, and I cannot wait to see what the future holds for us as we travel this road together.

Table of Contents

Dedication	iv
Acknowledgements.....	v
List of Figures	ix
List of Tables.....	xii
Abstract	xiv
1. Introduction and Background	1
1.1. Hodgkin Lymphoma	1
1.2. Photon Therapy for Hodgkin Lymphoma.....	2
1.2.1. – History	2
1.2.2. - Delivery Techniques	3
1.2.3. – Stray Radiation	3
1.3. Proton Therapy for Hodgkin Lymphoma.....	4
1.3.1. – History	4
1.3.2. - Delivery Techniques	5
1.3.3. – Stray Radiation	6
1.4. Risks from Radiation Exposure.....	6
1.4.1. – Japanese Atomic Bomb Survivor Data and Risk Models	6
1.4.2. - Linear Non Threshold Radiogenic Second Cancer Models	8
1.5. Uncertainties Associated with Risk Calculations.....	9
1.5.1. – Atomic Bomb Survivor Risk versus Medically Radiated Patient Risk	9
1.5.2. - Rationale for Relative Risk Comparisons	9
1.6. Statement of the Problem	10
1.7. Hypothesis and Specific Aims.....	10
2. Specific Aim 1: Ratio of Relative Risk (RRR) for proton versus photon therapies of nine female HL patients	13
2.1. Introduction	13
2.2. Methods and Materials.....	13
2.2.1. – Patient Cohort	13
2.2.2. - Hodgkin Lymphoma Treatment Plans.....	14
2.2.3. – Dose from Stray Radiation	18

2.2.4. - Risk Models	23
2.2.5. – Statistical Tests for Significance	28
2.2.6. – Propagation of Uncertainties	32
2.2.7. – Patient Treatment Variation Effects on Risk Analysis	34
2.3. Results	37
2.3.1. – Characteristics of Patient Cohort	37
2.3.2. – Characteristics and Images of Patient Plans	41
2.3.3. – Characteristics and Images of Stray Dose Distributions.....	42
2.3.4. – Total Dose and Relative Risk Calculations.....	46
2.3.5. – Propagation of Uncertainties	49
2.3.6. – Ratio of Relative Risk.....	50
2.3.7. – Statistical Tests for Significance	54
2.3.8. – Patient Treatment Variation Effects on mean RRR.....	56
3. Specific Aim 2: Confidence intervals of predicted mean RR values.....	60
3.1. Introduction	60
3.2. Methods and Materials.....	60
3.2.1. – Adjusted Variables Used for the Sensitivity Tests.....	60
3.2.2. – Rationale for Sensitivity Tests	61
3.2.3. - Non-linear Dose Response Models.....	62
3.2.4. – RBE of Neutrons for Carcinogenesis.....	64
3.2.5. – Propagation of Uncertainties for Non-Linear Dose Response Models	64
3.2.6. – Sensitivity Analysis	68
3.2.7. – Mean RRR Extrema Comparisons.....	70
3.2. Results	70
3.3.1. – Sensitivity Test for Mean Neutron Dose	70
3.3.2. – Sensitivity Test for Total Mean Equivalent Dose.....	74
3.3.3. – Sensitivity Test for Mean Relative Risk (RR).....	74
3.3.4. – Sensitivity Test for the Propagation of Uncertainties	78
3.3.5. – Sensitivity Test for Mean RRR	78
3.3.6. – Mean RRR Extrema Comparisons.....	88
4. Discussion.....	96
4.1. Outcome of Specific Aim 1	96

4.2. Outcome of Specific Aim 2	97
4.3. Coherence with Existing Literature	99
4.4. Implications and Significance of Findings	103
4.5. Strengths of the Study.....	104
4.6. Limitations of the Study	106
4.7. Future Work	108
4.8. Conclusion	108
References.....	109
Vita	129

List of Figures

Figure 2-1 – Differences in patient CT setups	14
Figure 2-2 – Tumor volume and anatomy of interest	15
Figure 2-3 – Photon treatment field design	16
Figure 2-4 – Proton treatment field design.....	18
Figure 2-5 – Anthropomorphic phantom	20
Figure 2-6 – Photon low dose correction algorithm	22
Figure 2-7 – Sign test parameters	30
Figure 2-8 – Student’s t-test parameters	31
Figure 2-9 – Anatomical location of OAR relative to CTV	36
Figure 2-10 – Photon IMRT dose distribution example	41
Figure 2-11 – Proton primary dose distribution example.....	42
Figure 2-12 – Photon out-of-field analytical model -	43
Figure 2-13 – Proton treatment external neutron dose distribution example.....	44
Figure 2-14 – Proton treatment internal neutron dose distribution example	45
Figure 2-15 – Mean equivalent neutron dose for protons per patient per prescribed Gy – neutron $\overline{w}_R = 20$	46
Figure 2-16 – Mean equivalent dose to OAR – neutron $\overline{w}_R = 20$	47
Figure 2-17 – Mean relative risk to OAR (Sv) - neutron $\overline{w}_R = 20$ - LNT dose response model.....	48
Figure 2-18 – $\overline{RRR}_{j,k}$, PSPT vs IMRT, LNT dose response model, exposed age (e) = 26, attained age (a) = 46, neutron $\overline{w}_R = 20$	51
Figure 2-19 – $\overline{RRR}_{j,k}$, IMPT vs IMRT, LNT dose response model, exposed age (e) = 26, attained age (a) = 46, neutron $\overline{w}_R = 20$	53
Figure 2-20 – \overline{RRR}_j , proton plans vs IMRT, LNT dose response model, exposed age (e) = 26, attained age (a) = 46, neutron $\overline{w}_R = 20$	54
Figure 2-21 – Correlation between $\overline{RRR}_{j,k}$ and age at exposure (years)	57
Figure 2-22 – Correlation between $\overline{RRR}_{j,k}$ and volume of total lung (cc).....	58
Figure 3-1 – Risk calculation differences between dose response models used.....	64
Figure 3-2 – Mean equivalent neutron dose per prescribed Gy by varying neutron \overline{w}_R – breast (cSv/Gy).....	71

Figure 3-3 – Mean equivalent neutron dose per prescribed Gy by varying neutron $\overline{w_R}$ – lung (cSv/Gy)..... 72

Figure 3-4 – Mean equivalent neutron dose per prescribed Gy by varying neutron $\overline{w_R}$ – thyroid (cSv/Gy)..... 73

Figure 3-5 – Mean total equivalent dose to OAR by varying neutron $\overline{w_R}$ value (Sv)..... 74

Figure 3-6 – Mean relative risk to OAR For each dose response model and neutron $\overline{w_R}$ value - exposed age 26, attained age = 46, response inflection point (α) = 0.025..... 75

Figure 3-7 – Mean relative risk to OAR For each dose response model and neutron $\overline{w_R}$ value - exposed age 26, attained age = 46, response inflection point (α) = 0.090..... 76

Figure 3-8 – % decrease in RR compared to LNT model RR – all patients averaged together 77

Figure 3-9 – $\overline{RRR_{j,k}}$ for all patients and OARs, PSPT vs IMRT, exposed age = 26, attained age (a) = 46, neutron $\overline{w_R} = 20$, response inflection pt (α) = 0.025 79

Figure 3-10 – $\overline{RRR_{j,k}}$ for all patients and OARs, PSPT vs IMRT, exposed age = 26, attained age (a) = 46, neutron $\overline{w_R} = 20$, response inflection pt (α) = 0.025 80

Figure 3-11 – $\overline{RRR_{j,k}}$ – BREAST ONLY – proton plans vs IMRT, exposed age (e) = 26, attained age (a) = 46, neutron $w_R = 20$, All α 81

Figure 3-12 – $\overline{RRR_{j,k}}$ – LUNG ONLY – proton plans vs IMRT, exposed age (e) = 26, attained age (a) = 46, neutron $\overline{w_R} = 20$, All α 82

Figure 3-13 – $\overline{RRR_{j,k}}$ – THYROID ONLY – proton plans vs IMRT, exposed age (e) = 26, attained age (a) = 46, neutron $\overline{w_R} = 20$, All α 83

Figure 3-14 – Sign test of $\overline{RRR_{j,k}}$ for proton treatments vs IMRT, exposed age (e) = 26, attained age (a) = 46, neutron $\overline{w_R} = 20$, all dose response models, all α 85

Figure 3-15 – $\overline{RRR_j}$ for a given OAR for all patients, proton plans vs IMRT, exposed age (e) = 26, attained age (a) = 46, neutron $\overline{w_R} = 20$, all dose response models, all α 87

Figure 3-16 – $\overline{RRR_j}$ for a given OAR for all patients, PSPT vs IMRT, exposed age (e) = 26, attained age (a) = 46, neutron $\overline{w_R}$, all α 88

Figure 3-17 – Extrema $\overline{RRR_j}$ for PSPT vs IMRT, exposed age (e), attained age (a), α , and neutron $\overline{w_R} = 20$ 89

Figure 3-18 – Sign test $\overline{RRR_{j,k}}$ extrema for PSPT vs IMRT, exposed age (e), attained age (a), neutron $\overline{w_R} = 20$, all dose response models, and α 90

Figure 4-1 – Axial slices of Patient #7 highlighting increased dose from the IMRT plan vs the PSPT plan..... 99

Figure 4-2 – Comparison of Cella *et al*, 2013 mean RRR values to this work 100

Figure 4-3 – Example of risk visualization tools 106

List of Tables

Table 2-1 – Photon therapy patient data.....	17
Table 2-2 – Proton therapy patient data - Selected host and treatment factors	18
Table 2-3 – Flow diagram of different mean RRR calculations	27
Table 2-4 – LNT uncertainty terms and stated uncertainty for assigned variables	34
Table 2-5 – Host characteristics per patient – demographics	37
Table 2-6 – Host characteristics per patient – breast	38
Table 2-7 – Host characteristics per patient – lung	38
Table 2-8 – Host characteristics per patient – thyroid.....	39
Table 2-9 – Treatment characteristics per patient – CTV	40
Table 2-10 – Treatment characteristics per patient – beam setup.....	40
Table 2-11 – Percent increase in mean dose to OARs after photon scatter dose model correction .	43
Table 2-12 – % contribution breakdown of propagation of uncertainty error for LNT dose response model	49
Table 2-13 – \overline{RRR} for LNT dose response model, PSPT plan comparison	50
Table 2-14 – \overline{RRR} for LNT dose response model, IMPT plan comparison.....	52
Table 2-15 – Sign test results, LNT dose response model, exposed age (e) = 26, attained age (a) = 46, neutron $\overline{w}_R = 20$	55
Table 2-16 – Student’s t-test results, LNT dose response model, exposed age (e) = 26, attained age (a) = 46, neutron $\overline{w}_R = 20$	56
Table 2-17 – Summary of all major finding from Aim 1	59
Table 3-1 – Linear Plateau uncertainty terms and stated uncertainty for assigned variables	66
Table 3-2 – Linear Exponential uncertainty terms and stated uncertainty for assigned variables	68
Table 3-3 – Breakdown of figures and tables described in section 3.2.6	69
Table 3-4 – Mean RRR extrema values for sensitivity parameters	70
Table 3-5 – Mean neutron dose contributions averaged over all patients (cSv/Prescribed Gy).....	71
Table 3-6 – % contribution breakdown of propagation of uncertainty error for dose response models.....	78
Table 3-7 – Student’s t-test of $\overline{RRR}_{j,k}$ for proton treatments vs IMRT, exposed age (e) = 26, attained age (a) = 46, neutron $\overline{w}_R = 20$, all dose response models, all α	86

Table 3-8 – Student’s t-test of $\overline{RRR}_{j,k}$ extrema for PSPT vs IMRT, exposed age (e), attained age (a), neutron $\overline{w}_R = 20$, all dose response models, and α	91
Table 3-9 – Summary of all major finding from Aim 2 - comparisons to Aim 1.....	93
Table 3-10 – Summary of all major finding from Aim 2 - neutron \overline{w}_R variation.....	94
Table 3-11 – Summary of all major finding from Aim 2 - extrema comparison.....	95

Radiogenic Second Cancer Risk Differences in Female Hodgkin Lymphoma Patients Treated with Proton *versus* Photon Radiotherapies

Publication No. _____

Kenneth Lois Homann, M.S.

Hodgkin Lymphoma (HL) is the most common cancer diagnosis of young adults in the United States. Advances in curative treatments for HL, including the use of photon radiation therapy (RT) techniques, have increased 10 year survival rates to approximately 90% among young patients. These RT treatments, however, contribute to an increased incidence of radiogenic second cancer (RSC) formation to the healthy tissue surrounding the tumor volume relative to the general population. These RSCs are the leading cause of death among long-term HL survivors. Proton therapy has been shown to reduce the therapeutic dose, and therefore, the risk of developing a RSC, to healthy tissue relative to HL photon therapy. Current commercial treatment planning systems (TPS) do not account for stray radiation doses for these treatments, however. The impact of these contributions on RSC incidence was previously unknown.

The relative risk (RR) of developing a RSC following treatment with proton therapy compared to the current standard of care, photon intensity modulate radiation therapy (IMRT), was determined for the breast, lung, and thyroid (OARs) of nine HL patients. Treatment plans were developed and therapeutic doses were calculated with commercial TPSs. Stray dose contributions were measured with thermoluminescent dosimeters (TLD) in anthropomorphic phantom for the IMRT treatments and simulated using Monte Carlo techniques that model a passive scattering treatment nozzle and each individual patient's anatomy and treatment setup. RSC risks were calculated using the Biological Effects of Ionizing Radiation VII (BEIR VII) and Radiation Risk Assessment Tool (RadRAT) risk models. Sensitivity tests varied the dose response model, relative biological effectiveness (RBE) of neutrons for carcinogenesis, age of exposure, and attained age for each patient to characterize the uncertainty of the RSC RR results.

The risk analysis showed that the majority of comparisons indicated a lower RSC risk after proton therapy than photon IMRT, but were not statistically significant unless the values of all patients for a given OAR were averaged together. Our findings, for the first time, revealed that it is important to include stray dose contributions and their uncertainties when comparing the RSC risks after different treatment techniques for HL. Furthermore, our findings clearly demonstrated the importance of personalized dose and risk calculations for modern radiotherapy for HL.

1. Introduction and Background

1.1. Hodgkin Lymphoma

Hodgkin lymphoma (HL) is a form of cancer originating from the white blood cells, or lymphocytes. Over 9,000 people in the United States are diagnosed with HL each year (Howlader et al., 2013). HL was first described by English physician Thomas Hodgkin in 1832 (Hodgkin, 1832) who suggested the first reference to the condition was made by Italian physician Marcello Malpighi in 1666. It affects all ages of the population, but nearly 60% of new cases occur before the age of 44 (Macmahon, 1957, Ries and SEER Program (National Cancer Institute (U.S.)), 2007, Howlader et al., 2013). HL is the most common cancer diagnosis of young adult patients in the United States (Bleyer et al., 2006).

Until the 1940's, a diagnosis of HL was generally considered fatal. Due to advances in both radiological and systematic treatment technologies, however, it is now one of the most curable cancers (Cox and Ha, 1999, Armitage, 2010) and has a 10 year survival rate of ~90% for diagnosis during childhood and adolescents (Constine et al., 2008). With these increased survival rates, however, come complications due to the treatments successfully used to treat HL, including radiogenic second cancers (RSC).

RSCs are defined as cancers that are at least partially brought about by the radiation dose administered during the treatment of the primary cancer (e.g. HL). Recent epidemiological studies have shown nearly 1 in 6 new cancers in the United States are a second primary cancer (Wood et al., 2012). In the Childhood Cancer Survivorship Study (CCSS) the overall cumulative incidence of a second primary cancer (excluding nonmelanoma skin cancer) was 7.9% at 30 years follow up, and was twice as likely to occur in patients exposed to radiation as those who did not receive radiation (Friedman et al., 2010).

HL survivors have the highest risk of developing a RSC amongst young patients. In the CCSS, HL survivors represented 13.4% of the cohort but 33.8% of all RSCs (Meadows et al., 2009). After HL therapy, RSCs generally develop after a median latency period of 5-10 years with the increased risk prevalent for at least 30 years (Hodgson et al., 2007a). The 30 year cumulative RSC incidence for HL survivors (excluding nonmelanoma skin cancer) was 10.9% for males and 26.1% for females with no indication that these rates will plateau beyond that time frame (Bhatia et al., 2003, Constine et al., 2008, Castellino et al., 2011). In addition, RSCs are the leading cause of death for HL survivors (Ng et al., 2002, Aleman et al., 2003).

The CCSS and young adult studies that many of these papers examined followed patients irradiated between the years 1970-1986. They have advocated that the reduction in exposure from current treatment techniques, such as those examined in this work, will likely result in a decrease in RSC incidence (Friedman et al., 2010, Travis et al., 2012, Berrington de Gonzalez et al., 2013). In light of this evidence, comparing new radiation treatments that can minimize dose to the normal tissue surrounding HL tumor volumes could prove beneficial in the long term health of HL survivors.

1.2. Photon Therapy for Hodgkin Lymphoma

1.2.1. - History

In the first half of the 20th century, radiation alone was used to treat HL. During the 1920's Gilbert (1939) determined that radiation administered to non-clinically involved lymph nodes was important for improving outcomes. The doses given during that era however, were low compared to the amounts delivered today, so HL was considered incurable. Peters (1950) reported a curable effect due to radiation alone, but it wasn't until with the introduction of the mantle field, also known as extended field radiation therapy (EFRT) in the early 1960's that definitive studies helped bring about widespread use of radiation for curative purposes of HL EFRT includes not only the gross tumor volume (GTV) but also the surrounding lymphatic pathways that are judged to be at risk of harboring subclinical disease (Kaplan, 1962, Easson and Russell, 1963). Further refinements of the radiation technique (Rosenberg and Kaplan, 1982) brought about the first ever decline in mortality rates of HL in the early 1970's (Devesa et al., 1987).

Despite the improved survival rates, secondary morbidities, including RSCs, were high for HL patients. The introduction of chemotherapy reagents, specifically for this work, the regimen consisting of adriamycin, bleomycin, vinblastine, and dacarbazine (known as ABVD) (Bonadonna et al., 1975), led to improved outcomes and a reduction in both radiation field size and dose delivered to achieve equal or better outcomes compared to radiation alone for early stage HL patients (Engert et al., 2007, Ferme et al., 2007).

These reduced-field-size treatments, called involved field radiation therapy (IFRT), were introduced by Cham et al. (1976). They reduced the field size to only the known areas of involvement, relying on the chemotherapy regimens to assist in the control and eradication of the cancer cells in the surrounding lymphatics. Comparison studies of EFRT to IFRT with ABVD regimens revealed similar outcomes with significantly less morbidities for IFRT compared to EFRT (Engert et al., 2003). Clinical trials investigating the possibility of eliminating radiation therapy in

favor of chemotherapy treatments have proven less effective (Macdonald et al., 2007, Meyer et al., 2012) further reinforcing the need for radiation treatments for HL patients.

1.2.2. - Delivery Techniques

There are two main ways of delivering IFRT treatments. The first and older technique is three dimensional conformal radiation therapy (3DCRT). For HL treatments, this technique is usually delivered in a two-field configuration with parallel opposed antero-posterior (AP) fields. The field shape, which conforms to the extended margins (i.e. of the Planning Tumor Volume (PTV)) of the intended tumor shape, is formed with an external cerrobend beam block (Powers et al., 1973), or more commonly today, with the use of a tungsten multi-leaf collimator (MLC) (Brahme, 1988).

The emergence of intensity modulated radiation therapy (IMRT) (Kallman et al., 1988, Webb, 1992, Bortfeld et al., 1994) , which is the second technique used to deliver the IFRT treatment, has replaced 3DCRT for many tumor sites. IMRT is most frequently administered in a co-planar 5-9 beam arrangement around the patient.

IMRT modifies the beam intensities of the photon beam to better conform to the tumor volume by moving the leaves of the MLC in and out of the field. Currently, this is the standard of care at our institution for photon HL treatments. All of our patients, save one, had five beams delivered. The other one was a six-field configuration. Several studies compared the dose distributions of 3DCRT vs IMRT and showed IMRT to be comparable or better at delivering less dose to the normal tissue (Diez et al., 2007, Paumier et al., 2011, Koeck et al., 2012).

IMRT has been shown to reduce the cumulative dose to OARs relative to 3DCRT. However, due to the increased number of beams and monitor units (MU) needed to deliver the prescribed dose relative to 3DCRT and the increased volume of the OARs that the additional beams must traverse, IMRT treatment bathe a larger volume of healthy tissue with low dosages of radiation (Hall and Wu, 2003, Bortfeld, 2006, Weber et al., 2011, Cella et al., 2013). The effects of this difference in the dose distribution in the long term is currently unknown, but will be tracked closely as more patients reach later stages of their follow-ups, and is a main impetus for this work.

1.2.3. - Stray Radiation

Radiation outside of the intended treatment volume is defined as stray radiation. Its presence delivers unwanted dose to healthy tissue in the body and is a source of concern with respect to RSC risks. IMRT treatments typically deliver an increased amount of stray radiation relative to 3DCRT. There are three main components of stray radiation for photon IMRT treatments, two of which are relevant for this work.

The first are leakage photons, which emanate from the shielding of the linear accelerator head. Leakage radiation dominates in distances far from the field edge (i.e. the 50% isodose line for IMRT plans). Measurements have shown that these doses are usually less than or equal to 0.1% of the prescribed dose (Nath et al., 1994).

The second source of stray radiation is scatter dose. This form dominates near the treatment field and originates both from within the patient and again from the treatment head. Kase et al. (1983) found that a larger percentage of scatter dose came from the treatment head than within the patient.

The third source of radiation are photoneutrons which originate in the linear accelerator head, specifically from the flattening filter, primary collimator, electron target, and accelerator jaws. Photoneutron production is limited to photon energies that exceed 8 MeV. Studies of high energy IMRT treatments have shown doses to healthy tissue of over 1% of the prescribed dose for OARs close to the treatment field (Followill et al., 1997, Kry et al., 2005, Howell et al., 2006a). As this adds a significant amount of dose to the patient, IMRT treatments are usually treated with low energy photons below the photoneutron production threshold. This was the case for this work.

Additionally, accounting for this stray radiation has been shown to be deficient in commercial treatment planning systems (TPS). Howell et al. (2010a) and Joosten et al. (2011) showed that while TPSs generally do a good job of accounting for dose within the treatment field and in anatomical regions with dose down to 5% of the prescribed dose, beyond this point they can under-report doses by up to 60%. This low dose region has minimal acute effect on the patient but can be of concern with respect to RSC, and was accounted for in this work.

1.3. Proton Therapy for Hodgkin Lymphoma

1.3.1. - History

Due to the known potential to reduce radiation exposure to surrounding normal tissue of mediastinal HL patients (De Laney and Kooy, 2008), proton treatments were examined. Proton therapy was first explored for HL treatments in the 1970's when Archambeau et al. (1974) found that proton therapy reduced the dose to the irradiated healthy tissue by half when compared to photon therapy. Widespread clinical use of proton therapy was not economically feasible until the 1990's, however, and has only gained a larger foothold in the radiotherapy community since the turn of the 21st century (Levin et al., 2005).

Proton therapy was originally used for intracranial (Kjellberg et al., 1962, Kjellberg et al., 1983) and ocular (Munzenrider et al., 1980, Gragoudas, 1986, Munzenrider, 1999) lesions. The implementation of 3D Computed Tomography (CT) and as a consequence, 3D visualization of patient anatomy and dose distributions opened the door for treatments outside of the cranium. For

Hodgkin's treatments, an HL specific prospective phase II study showed that a comparison between 3DCRT, IMRT, and proton therapy showed that proton treatments best spared dose to healthy OARs while maintaining tumor coverage (Hoppe et al., 2012).

1.3.2. - Delivery Techniques

There are two different methods for delivering proton beams to the patient, one which employs a passive delivery system (henceforth called PSPT) and one that delivers dose with a dynamic or spot scanning approach (which we will call IMPT). At our institution, PSPT is currently the technique used to treat HL patients.

PSPT was first developed for larger-field proton treatments by Koehler et al. (1977). It uses a series of scatterers to systematically shape a uniform proton distribution to up to 30 cm in diameter. The details of the PSPT system are as follows: A proton pencil beam a few mm in diameter is extracted from a cyclotron or synchrotron system which produced the original proton beam. The pencil beam then encounters a rotating range-modulation wheel (RMW) made of varying thicknesses of acrylic. These various thicknesses degrade the initial energy of the proton beam, which varies the distance in the patient the proton beam will travel (called the range).

By modulating the proton beam range, a spread out Bragg peak (SOBP), which is the combination of all unique Bragg peaks from the protons of various energy is formed. This ensures coverage of the tumor in the beam direction. The lateral borders of the proton beam are formed from a scattering foil placed downstream of the RMW which spreads out the original proton beam. These lateral borders are further shaped to match the lateral extent of the intended treatment by collimators even further downstream. At the end of the chain, one final beam modifier called the range compensator is used. This device, of various thicknesses which is shaped as a function of the distal target border, takes the available protons of various energy produced by the RMW and degrades them further to match the off-axis depth of the target.

IMPT is an actively scanning beam delivery system that removes the physical components of the modulation chain seen in PSPT. To shape the beam to the target, the proton pencil beam is magnetically scanned across the region of interest. To account for depth changes to the target, the beam is delivered in discrete iso-energy layers. After completely covering the given target depth, the accelerating structure resets and produces a proton pencil beam of a different energy that corresponds to the new depth needed.

Usually, the PSPT is considered more robust and less prone to changes in patient anatomy or positioning during treatment than IMPT. IMPT deliveries are theoretically able to conform their dose distribution to both the deep and shallow extents of the target selecting the necessary proton

energies for each spot scanned. PSPT is able to conform to the deep portion of the target, but not the shallow.

Some early follow up data has been reported to indicate a reduction in RSC for proton treatment vs photon therapy, but the median follow up time at the time of publication was less than 8 years (Chung et al., 2008) while multiple studies have indicated mean latency periods of 10 years or greater for the lung and breast (Travis et al., 2002, Travis et al., 2003)

1.3.3. – Stray Radiation

As in photon therapy, proton treatments also deliver a non-intended dose to healthy tissue inside and outside of the specified treatment area. For protons, this stray component consists mainly of high energy neutrons. In this work, the neutron dose is split into two components, named external and internal neutrons. Polf and Newhauser (2005) showed that the main source of external neutrons for PSPT treatments was the RMW. In addition, external neutron contributions increase with increased SOBP width, proton beam energy, un-collimated proton field size, and decreasing aperture size (Yan et al., 2002, Zheng et al., 2008, Taddei et al., 2008).

Since there is no RMW in IMPT, or any other component of the proton nozzle for that matter, the external neutron component is negligible in IMPT plans (Schneider et al., 2002) and was therefore not calculated for these plans. Internal neutrons, which originate in the patient, are present in both the PSPT and IMPT plans.

Neutrons have large uncertainties associated with their relative biological effectiveness (RBE) relative to photons. Whereas photon treatment assumes an RBE value of 1.0, Kellerer et al. (2006) have indicated that a recent analyses of atomic bomb survivors gives a 95% confidence interval for neutrons of 4-400. While this encompasses the furthest extent of the possible neutron RBE values, other works have stated more likely values between 10 (Newhauser et al., 2009) and 30 (Brenner and Hall, 2008). It is because of the large uncertainty, that this value will be varied for sensitivity tests in this work.

1.4. Risks from Radiation Exposure

1.4.1. – Japanese Atomic Bomb Survivor Data and Risk Models

Ionizing radiation has long been known to assist in the killing of cancer cells. A by-product of this therapeutic use, of course, is the exposure of healthy tissue to the damaging effects of radiation as well. Despite the use of radiation to treat human maladies for over a century, data that provides accurate dosimetry and a statistically significant sample size that can predict long term effects from exposure are difficult to accrue.

The largest cohort with the longest follow-up time after initial exposure is the Life Span Study (LSS) cohort of survivors of the atomic bombings of Hiroshima and Nagasaki at the end of World War II in 1945 (Beebe et al., 1962, Preston et al., 2007, Ozasa et al., 2012). Begun in 1950, the LSS follows the 120,000 survivors of the atomic bombings of Hiroshima and Nagasaki. The LSS is generally considered the most complete, and more importantly, statistically significant, radiation exposed cohort on record due to its extended follow up period as well as the size of the cohort studied.

While not exclusively used, the LSS data forms the backbone of all calculations used in the National Cancer Institute (NCI) Radiation Risk Assessment Tool (RadRAT) (Berrington de Gonzalez et al., 2012) and the National Academy of Sciences Biological Effects of Ionizing Radiation (BEIR) VII – Phase 2 Report (National Research Council (U.S.). Committee to Assess Health Risks from Exposure to Low Level of Ionizing Radiation., 2006) RSC risk models, which were used in this work.

The LSS cohort offers many advantages for being used to calculate RSC risk (National Research Council (U.S.). Committee to Assess Health Risks from Exposure to Low Level of Ionizing Radiation., 2006). Due to the nature of the exposure, there is no bias in the selection of those exposed as both sexes and all ages at exposure are included. The long follow-up times also provide significant amount of data to determine the change in RSC risks as a function of time since exposure. Additionally, dose measurements are well categorized and tracking of patients since exposure has been thorough, allowing for extensive analysis of potential confounders or effect modifications.

While there are many advantages, there are some shortcomings with respect to transporting this exposure to a medically exposed population. Exposures were less than 3 Sv for nearly the entire cohort, which is much less than would be expected in a therapeutic exposure. The models were only designed to account for exposures up to these values, which introduced uncertainty at exposures above its threshold. Finally, no dose fractionation occurred during exposure so any potential reduction of risk due to cellular repair or repopulation is not accounted for either.

The subjects were also Japanese making transportation of the risk coefficients to other populations not straightforward. The exposures from detonation were also whole body instead of localized to a specific OAR as with radiotherapy. While this has benefits (all OARS receive the same dose so differences in radiosensitivity can be differentiated), it is not the manner which patients are treated in most instances. Even with these shortcomings, however, the LSS is the most complete and thorough radiation exposed cohort available and is the basis for the risk models used in this work.

1.4.2. - Linear Non Threshold Radiogenic Second Cancer Models

The two risk models used in this work, BEIR VII and RadRAT, were derived from the LSS study group to quantitatively determine an individual's risk of developing a RSC. These models were derived from the same radiation epidemiology studies. Relative to BEIR VII, the RadRAT study was released more recently and offered a significant amount of additional data that allowed us to benchmark our work to ensure our calculations were correct. In addition, the RadRAT publication added several individual risk models for additional OARs that were not examined in BEIR VII which could be of use for future works. Three OARs were examined using these two models: breast, lung, and thyroid. Each have unique RSC risk values that can be calculated from the mean dose calculated to the OAR of interest, the exposed age of the patient (e), and the age the person lives to (attained age) (a).

The BEIR VII/RadRAT lung model was developed for both the right and left components of the organ together and was derived from the LSS cohort. The BEIR VII/RadRAT breast model was also calculated for the total breast and uses the LSS data but incorporated medically exposed populations from Preston et al. (2002) as well. These two models were found to be largely interchangeable with the only difference being the modification of the risk coefficient (β) from the Japanese population to an American population. The BEIR VII/RadRAT thyroid model used the LSS and other cohorts to determine the dose response shape. The additional cohorts were taken largely from the work of Ron et al. (1995) which included medically exposed populations.

These models all follow the dose response model called Linear Non Threshold (LNT) which states that as the dose increases, the risk of developing a RSC increases linearly. The BEIR VII and RadRAT models both simulate these response shapes. Multiple HL studies have further strengthened this approach to RSC risk for both the breast and lung. Breast studies have found an approximately linear dose response relation for breast RSC risk with no evidence of a downturn at dose of greater than 30 Gy (Travis et al., 2003, Guibout et al., 2005, Inskip et al., 2009) for both children and young adults. The lung also has shown an LNT response albeit in patients older than our patient cohort for this study. Primary lung cancer studies of patients irradiated at 50 years of age showed a linear dose/risk response even at doses above 40 Gy (Travis et al., 2002, Gilbert et al., 2003)

The thyroid dose response, however, has been shown to vary from the LNT in medically exposed populations. In two recent studies, a linear exponential model, which shows an increase in the risk similar to the LNT until doses exceed a certain threshold (20-30 Gy in this instance) where it then begins to decrease, fit the data best (de Vathaire et al., 1999, Bhatti et al., 2010). The BEIR VII/RadRAT models indicate an LNT model for thyroid because their models are intended for doses

below the 30 Gy threshold (Giebeler et al., 2011). It is this limitation which necessitated adjusting the LNT model to account for non-linear dose responses in this work.

1.5. Uncertainties Associated with Risk Calculations

1.5.1. – Atomic Bomb Survivor Risk versus Medically Radiated Patient Risk

As has been pointed out, there is substantial uncertainty associated with transporting the risk models from their intended population and intended dose range to that of a medically exposed cohort. In general, medically exposed population's RSC risk was less than the LSS cohort (Berrington de Gonzalez et al., 2013) for breast (Preston et al., 2002) and lung (Gilbert et al., 2003), sometimes by over an order of magnitude. The thyroid BEIR VII/RadRAT models were closer to medically exposed patient cohort studies, but this was because the data used for that publication included fractionated dose exposure (Ron et al., 1995).

Even the medical epidemiology studies covered in above sections which state that the LNT model fits RSC risks the best are subject to uncertainty. Follow up times are still short for newer radiation techniques (< 20 years), and the range of possible values are statistically variable enough to introduce the possibility of another type of dose response. Other risk studies incorporated models fitted to medically exposed populations with downturns at higher doses for the lung and breast as well (Schneider et al., 2011).

Finally, the LSS risk models are designed for photon exposures. Multiple researchers have preached a cautious approach to assuming certain RSC responses outside of the limitations places on the risk models examined (Hall, 2006, Newhauser and Durante, 2011, Berrington de Gonzalez et al., 2012). To account for these many different sources of uncertainty, sensitivity tests, which vary many of these factors, were used to determine a range of possible results.

1.5.2. - Rationale for Relative Risk Comparisons

In light of this uncertainty, we took a cautious approach to assessing RSC risk to different treatments. The endpoint of our work is a metric we have termed the ratio of relative risks (RRR). The RRR compares two separate treatments by dividing their calculated risks by each other. Doing this allows us to largely remove mutual confounders that are either currently disputed or unknown which could introduce additional uncertainty to the final risk analysis such as patient demographics or specific risk/Gy coefficients.

Doing this also prohibits us from making definitive absolute risk statements, but we can use current epidemiology studies to inform our relative findings. For example, secondary thyroid cancer is 6-7 times less common among HL survivors than the breast and lung and only represented 2.7% of solid tumors from the cohort (Hodgson et al., 2007a). Calculating the RRR allows us to still draw

meaningful conclusions about two comparable treatment solutions while minimizing our uncertainties as much as possible.

1.6. Statement of the Problem

Proton therapy has been shown to reduce dose to healthy tissue in HL studies while maintaining equal dosimetric coverage of the tumor compared to photon treatments (Schneider et al., 2000, Chera et al., 2009, Andolino et al., 2011, Cella et al., 2013). However, there are no studies which include both therapeutic and out-of-field dosimetry for contemporary proton and photon treatment plans. Without taking into account all sources of dose, risk comparisons are less reliable.

In addition, further uncertainties associated with dosimetric radiobiological uncertainties, such as the dose response model for each exposed organ of interest and the RBE of neutrons for carcinogenesis (neutron $\overline{w_R}$), can lead to even more significant decreases in confidence for comparisons of proton versus photon radiation treatments of HL, even when the dose is fully taken into account.

Our goal was to calculate the risk of developing a RSC after eliminating two major sources of uncertainty by: 1) including an accurate incorporation of all additional dose sources not predicted by commercial TPSs and 2) introducing a set of sensitivity tests that take into account the known radiobiological uncertainties associated with RSC risk calculations by varying their contribution across a known range of possible values. By doing these tasks, further clarity and confidence regarding the various possible treatment configurations used to treat HL with respect to predicted RSC risk were achieved.

1.7. Hypothesis and Specific Aims

The hypothesis of this work is **patients treated for supra-diaphragmatic HL will have a significantly lower predicted risk of developing a RSC ($\overline{RRR} < 1$, $p \leq 0.05$) while maintaining the same dosimetric coverage of the tumor when treated with proton *versus* photon IMRT**, which was tested by the following two specific aims:

Specific Aim 1: Compare the predicted mean Ratio of Relative Risk (\overline{RRR}) for proton versus photon IMRT of nine female HL patients.

The objective of this aim was to determine if proton therapy would reduce dose to healthy tissue in HL patients with supra-diaphragmatic tumors compared to the current standard of care at our

institution (photon IMRT), thus lowering the predicted RSC risk using reasonable assumptions for the dose response model and neutron \overline{w}_R .

We tested this specific aim by using the approach of conducting a paired data, *in-silico* study that calculates dose for both proton and photon plans on nine female HL patients. For this we used the combination of a commercial treatment planning system (TPS) to calculate the in-field or therapeutic dose, and an analytical model for the photon plan and Monte Carlo techniques for the proton plans to calculate the stray and neutron dose contribution, respectively.

The RSC risk was then calculated for the total breast, total lung, and thyroid using risk models from the literature (National Research Council (U.S.). Committee to Assess Health Risks from Exposure to Low Level of Ionizing Radiation., 2006, Berrington de Gonzalez et al., 2012) for both proton and photon plans. The sign and student t-test was used to determine if one treatment technique provided a statistically significant reduction in predicted RSC risk.

The rationale for this aim is currently that clinicians have incomplete knowledge to make an informed, evidenced based decision that quantitatively takes into consideration RSC risk for the determination of the most appropriate standard of care for female HL patients. It was our expectation that proton treatments would provide a significant reduction in dose, and therefore, predicted RSC risk, to the female total breast, total lung, and thyroid for supra-diaphragmatic HL tumors.

Such a finding would be of importance because comparisons of predicted RSC risk will provide a rationale for selecting a treatment technique, not just for their curative properties, but for their potential to prevent RSCs, as well.

Specific Aim 2: Determine confidence intervals of predicted \overline{RRR} values

The objective of this aim is to determine if uncertainties, including varying neutron \overline{w}_R and the dose response function of the BEIR VII and RadRAT LNT models, were large enough to affect the final conclusion of the predicted RSC risk outcomes found from the first aim. We tested this specific aim by using the approach of sensitivity tests which vary both the shape of the dose response curve for each exposed organ at risk (OAR) as well as the value of the neutron \overline{w}_R when calculating the mean equivalent dose (\overline{H}) to a given OAR.

These sensitivity tests incorporated a reasonable range of uncertainties for each of these parameters. Analysis of this interval of potential \overline{RRR} values, in concert with a rigorous propagation of errors following the methods of Fontenot et al. (2010), showed whether or not these uncertainties changed the qualitative findings of the overall study from specific aim 1. The sign and Student's t-test were again used to determine if one treatment technique provided a statistically significant

reduction in predicted RSC risk.

The rationale for this aim is that limited understanding of uncertainties in radiobiological parameters is an obstacle to confidently using predicted risk results in a clinical setting. By varying the values associated with these radiobiological parameters, we determined within plausible confidence intervals if our \overline{RRR} values were still statistically significant.

It was our expectation that these sensitivity tests, combined with rigorous uncertainty analysis, would show that while radiobiological uncertainties were large, they were sufficiently small to draw statistically significant conclusions. Such a finding would be of importance because it would allow increased confidence in the conclusions determined from specific aim 1.

2. Specific Aim 1: Ratio of Relative Risk (RRR) for proton versus photon therapies of nine female HL patients

2.1. Introduction

An analysis on the differences in the risk of developing a radiogenic second cancer (RSC) between various treatment plan types and techniques was conducted for a paired data, *in-silico* clinical trial for a population of Hodgkin lymphoma (HL) patients. In particular, we (1) calculated dose for both proton and photon radiation therapy (RT) treatment plans for nine female patients, (2) calculated the RSC risk for several organs, and (3) used the sign test and Student's t-test to determine if one treatment technique provided a statistically significant reduction in predicted RSC risk relative to the other treatment. Section 2.2.1 describes the selection of the patients studied in this work. Section 2.2.2 describes the parameters used for the creation of the HL treatment parameters. Section 2.2.3 details the calculation techniques and models used to account for the stray dose. Section 2.2.4 explains the rationale behind the selection of the various risk equations and endpoints selected for this work. Section 2.2.5 describes the statistical tests used on our results. Section 2.2.6 walks through the error analysis for our risk calculations, and 2.2.7 describes the different parameters studied to determine if there were any trends or correlations between these factors and their subsequent mean RRR values.

2.2. Methods and Materials

2.2.1. – Patient Cohort

Patients were selected using the following inclusion criteria. All patients received proton therapy at our institution between July 2007 and December 2011. The consecutive sampling method was employed. All patients were diagnosed with Stage II (eight of nine patients) or Stage IIIA (one patient – Patient #8) Classical Nodular Sclerosis Hodgkin Lymphoma. The disease was also confined to the supra-diaphragmatic region of the torso, which accounts for roughly 90% of all Stage II disease (Krikorian et al., 1986). Exclusion criteria included males since the male breast is at lower risk for RSC than female breast. Patients treated with photon therapy were also excluded because their patient setup and apparatus used for immobilization differ from proton therapy patients. Treatment plans and other pertinent data from nine female patients with an average age of 25.3 years old at the time of treatment (standard deviation of 9.89 years) were retrospectively collected under a protocol approved by the MD Anderson Cancer Center Institutional Review Board (IRB). A preliminary sample size analysis was performed using data from two previous studies that conducted similar studies on HL patients (Chera et al., 2009, Andolino et al., 2011). This analysis showed that

nine patients would provide sufficient statistical power (>80% with an alpha level of 5%) to detect whether photon or proton treatments yielded a lower mean RSC risk. Assuming a Ratio of Relative Risk (RRR) of approximately 0.5, which was the average RRR for the Chera *et al* and Andolino *et al* works (*i.e.*, one treatment, either photon or proton, would decrease the risk of a RSC to a particular organ by a factor of ~2).

2.2.2. - Hodgkin Lymphoma Treatment Plans

Treatment records were extracted from the institution's archives. These records included computed tomography (CT) simulation with the patient in the supine position. The CT image covered superiorly from the top of the head or chin to the base of the diaphragm (see Figure 2.1). The patients' arms were placed either at their sides or over their heads. Thermoplastic immobilization mask and head rests were used for all patients.

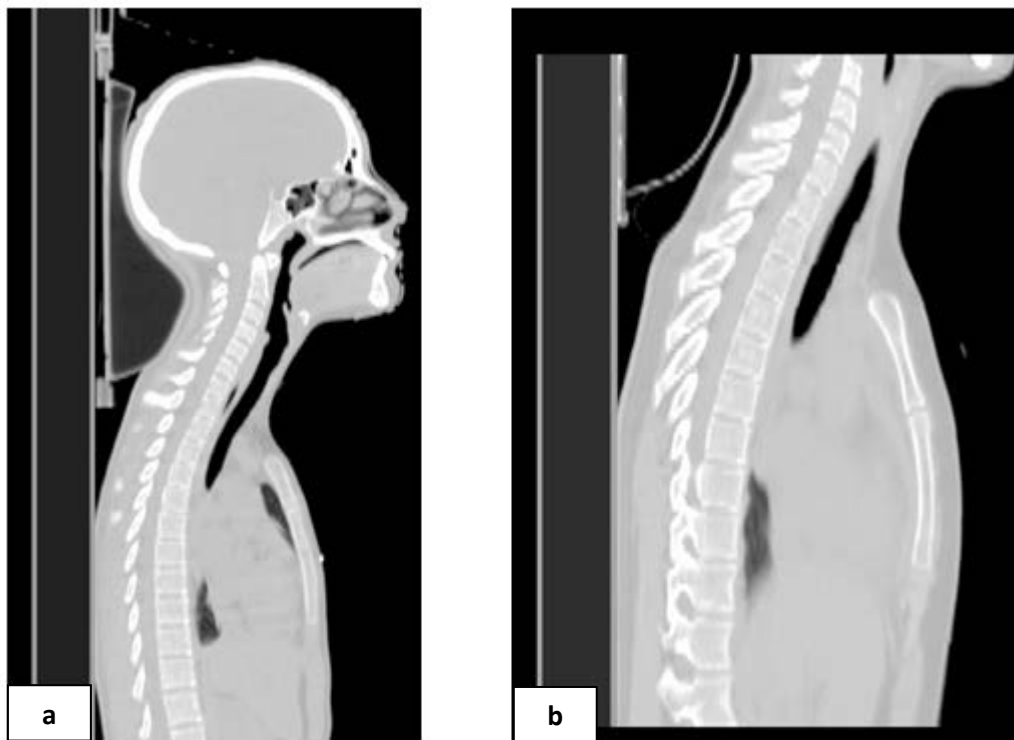


Figure 2-1 – Differences in patient CT setups - Sagittal view of Patient a) #3 and b) #4. These two images display the differences in the superior border in the CT images for the various patients. Each has an immobilization mask and head rest while being in the supine treatment position. Since the patients selected for this study have already been treated, clinical CT data sets were extracted from the data archive at our institution leading to minor differences in their respective images. For example, some CT data sets include the entire head while others only extend superiorly to the chin. For all patients, regardless of which data set was used, all organs of interest (OAR) for this study were fully included in the scans.

For each CT scan, tumor volumes and organs at risk (OAR) were delineated by either a board certified medical physicist or medical dosimetrist and then reviewed and approved by a board

certified radiation oncologist. Of particular interest for our study were the Gross Tumor Volume (GTV), Clinical Tumor Volume (CTV), and Planning Tumor Volume (PTV) as defined by the International Commission on Radiation Units and Measurements Report (ICRU) 62 (Wambersie et al., 1999) (Figure 2.2a) and OARs including breast (both right and left), lung (both right and left), and thyroid (Figure 2.2b). Both the right and left were contoured individually for the breast and lung and then combined using Boolean logic for the purposes of calculating the risk.

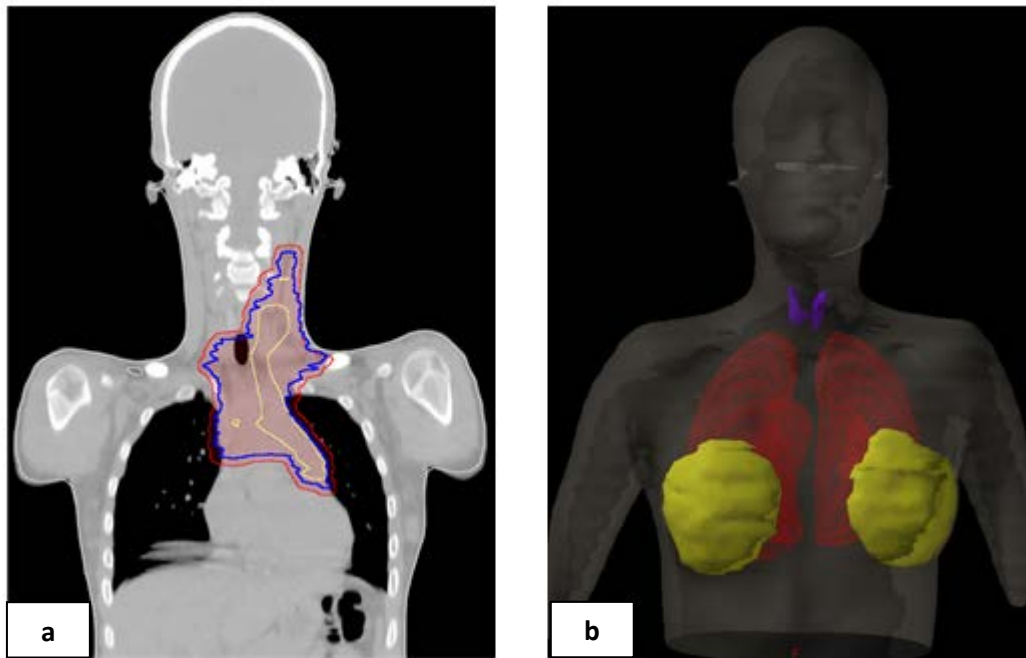


Figure 2-2– Tumor volume and anatomy of interest - Images of Patient #9 **a)** Coronal view. The GTV (yellow), CTV (blue), and PTV (red shaded area) are delineated. Each patient's tumor location was unique, but all patients in this study had supra-diaphragmatic HL tumor locations. **b)** 3D skin rendering (coronal view) showing OARs for patient shown in Figure 2.3. Total breast (yellow), total lung (red), and thyroid (purple).

Since the patient cohort was retrospectively selected and the treatment plans were designed by multiple dosimetrists, new photon and proton treatment plans were created for all nine patients to ensure consistent treatment field construction throughout and current standards of care at our institution. There are a wide range of dose prescriptions that can be given for HL patients depending on their specific prognosis and use in concert with chemotherapy agents. These values can range from 20-40 Gy (Hansen and Roach, 2010). The total prescribed dose was 36.0 Gy relative biological effectiveness (RBE) (*i.e.*, $32.7 \text{ Gy} \times 1.1$ to reflect the biological effectiveness of protons relative to photons) and 36.0 Gy for the proton and photon treatment plans, respectively. The use of the generic RBE factor of 1.1 for proton plans follows the recommendations on dose prescription and reporting

in International Commission on Radiation units and Measurements (ICRU) Report 78 (Wambersie et al., 2007) and is consistent with the clinical practice at our institution.

2.2.2.i. Photon treatment plans

There are two main treatment techniques used for HL: the historical extended field radiation therapy treatment (EFRT) and the more current involved field radiation therapy treatment (IFRT). An IFRT technique was used for the photon treatment plans. IFRT has largely replaced EFRT treatments (Kaplan, 1962), *i.e.*, mantle field irradiation, and only includes the involved lymphatic regions (Cham et al., 1976, Connors et al., 1987) (Figure 2.3). IFRT can be treated using either conventional 3D conformal radiationtherapy (3DCRT) or intensity modulated radiation therapy (IMRT). For our study, a 6 MV step and shoot IMRT treatment technique, consisting of either a five or six beam co-planar geometry was chosen. This technique is currently the standard of care for HL patients treated with photon therapy at our institution. Treatment plans were developed using a commercial treatment planning system (TPS) (Eclipse, Version 8.9.08, Varian Medical Systems, Palo Alto, CA). Dose distributions were calculated using the Anisotropic Analytical Algorithm (AAA) (Eclipse, Version 8.9.08, Varian Medical Systems, Palo Alto, CA). The optimization objective was to deliver the prescribed dose to 100% of the PTV.

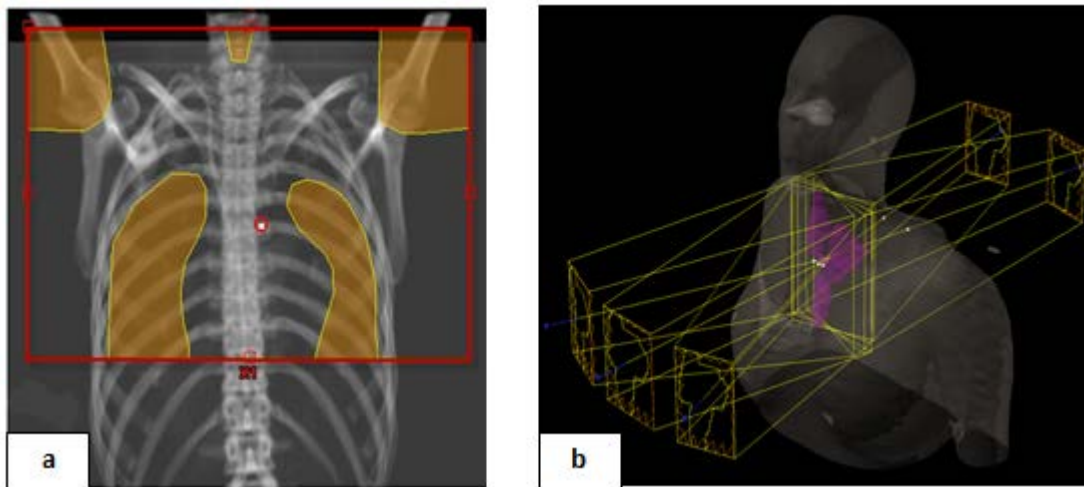


Figure 2-3 – Photon treatment field design - Images of Patient #3 a) Field size of a Hodgkin Lymphoma mantle field or extended field photon irradiation. Mantle fields cover all lymphatic sites above the diaphragm, including the cervical, supraclavicular, infraclavicular, axillary, mediastinal, and hilar nodes while blocking the lungs, humoral heads, and thyroid. b) 5 field IMRT setup and field size for a Hodgkin Lymphoma IFRT irradiation. Note the difference in the area of exposed tissue for the EFRT treatment in Figure 2.4a *versus* the IFRT Figure in 2.4b. The CTV is rendered in purple.

Additionally, selected photon beam characteristics as well as the age of each individual patient are listed in Table 2.1.

Table 2-1 – Photon therapy patient data - Selected host and treatment factors for HL photon treatments

Patient #	Age at Exposure (e) (Years)	Photon Energy (MV)	Treatment Gantry Angles (degrees)						Collimator X and Y Jaws (cm)					
			Field 1	Field 2	Field 3	Field 4	Field 5	Field 6	Field 1	Field 2	Field 3	Field 4	Field 5	Field 6
1	26	6	0	49	165	200	325	-	13.3 x 11.3	12.3 x 11.3	13.6 x 11.3	13.3 x 11.0	12.0 x 11.3	-
2	28	6	0	20	70	170	190	340	20.5 x 17.8	20.7 x 17.8	15.0 x 18.3	21.5 x 17.5	20.5 x 17.3	21.0 x 17.5
3	42	6	0	20	170	190	340	-	14.4 x 17.0	12.5 x 16.8	14.0 x 16.8	13.3 x 16.8	13.0 x 17.0	-
4	31	6	0	20	170	190	340	-	14.0 x 23.8	14.4 x 23.5	14.3 x 23.8	14.3 x 24.3	14.8 x 23.8	-
5	36	6	0	51	151	211	309	-	16.1 x 15.1	12.5 x 15.5	15.5 x 15.3	13.8 x 14.3	12.9 x 14.3	-
6	25	6	0	51	151	211	309	-	21.4 x 16.8	17.5 x 17.0	19.5 x 16.8	20.2 x 17.0	15.5 x 17.1	-
7	15	6	0	20	170	190	340	-	16.3 x 15.8	15.8 x 15.6	14.8 x 15.3	16.3 x 15.3	13.3 x 15.8	-
8	10	6	0	20	170	190	340	-	11.0 x 14.1	10.3 x 13.8	12.1 x 13.6	11.1 x 13.6	12.3 x 14.1	-
9	15	6	0	20	170	190	340	-	13.8 x 20.8	13.8 x 21.3	14.3 x 21.3	14.3 x 21.1	13.6 x 20.5	-

2.2.2.ii. Proton treatment plans

For each patient, two separate proton treatment plans were examined, a passively-scattered proton therapy plan (PSPT) and an intensity modulated proton therapy plan (IMPT). The differences between the two plans were in the inclusion or exclusion of various components of the stray neutron dose (which will be discussed in more detail in Section 2.2.3 below).

The PSPT plan was constructed following the prevailing standard of care in 2012 at our institution. In accordance with ICRU recommendations (Wambersie et al., 2007), lateral, proximal, and distal margins were added on a field by field basis to account for the dose distribution uncertainties of the CTV. For a given patient, the number of fields and their orientations for both the PSPT and IMPT treatment plans were the same (either a one or two field configuration) (Figure 2.4). All proton plans were developed using a commercial TPS (Eclipse, Version 8.9.08, Varian Medical Systems, Palo Alto, CA), and dose was calculated using the Proton Convolution Superposition Algorithm (Eclipse, Version 8.9.08, Varian Medical Systems, Palo Alto, CA) (Schaffner, 2008), which was previously validated (Newhauser et al., 2007a)

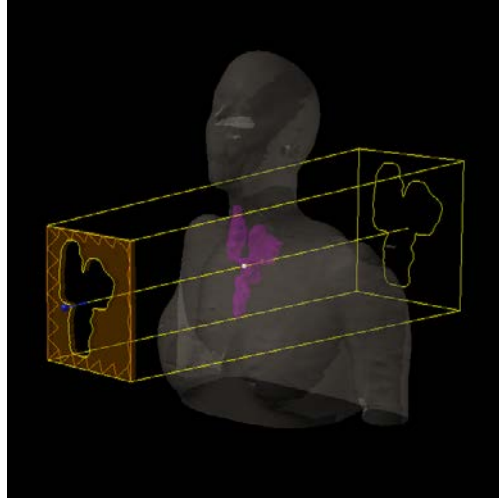


Figure 2-4 – Proton treatment field design - 3D skin rendering highlights aperture design for a one-field proton treatment. The CTV (which the aperture is designed to cover) is rendered in purple.

Selected proton beam characteristics as well as the age of each individual patient are shown in Table 2.2.

Table 2-2 – Proton therapy patient data - Selected host and treatment factors

Patient #	Age at Exposure (e) (Years)	Proton Energy at Nozzle Entrance (MeV)		Gantry Angle (degrees)		Snout Size - Small (10X10 cm ²), Medium (18X18 cm ²), Large (25X25 cm ²)		Nominal Spread Out Bragg Peak (SOBP) Width (cm)		Nominal Range in Patient Water Equivalent Thickness (cm)	
		Field 1	Field 2	Field 1	Field 2	Field 1	Field 2	Field 1	Field 2	Field 1	Field 2
1	26	140	180	0	90	Medium	Medium	8	12	8.9	15.9
2	28	225	250	0	180	Large	Large	13	14	17	21.9
3	42	140	-	0	-	Medium	-	8	-	8.8	-
4	31	160	250	0	180	Large	Large	8	12	9.6	22.5
5	36	160	225	100	340	Medium	Medium	11	14	20.7	12.3
6	25	160	-	0	-	Large	-	10	-	10.9	-
7	15	160	200	0	95	Medium	Medium	10	12	13	17.9
8	10	140	180	0	180	Medium	Medium	9	11	9.7	16.1
9	15	160	225	0	180	Large	Large	9	11	10	17.4

2.2.3. – Dose from Stray Radiation

There are two components of dose, the therapeutic dose, i.e., dose from the treatment field, and the stray dose, i.e., the dose outside the treatment field. Contemporary TPS have been shown to accurately calculate this therapeutic absorbed dose for photon and proton beams to within 2% of the measured value (Ramsey et al., 1999, Van Esch et al., 2006), which is acceptable for the endpoints of this study.

Despite this accuracy within the therapeutic 5% isodose line, the TPS did not accurately calculate or did not attempt to calculate stray absorbed dose below that value (Howell et al., 2010a, Joosten et al., 2011). Thus, the therapeutic component of dose to individual OARs was directly taken from the TPS, but the stray dose component was determined using supplemental approaches.

In particular, stray radiation doses from photon therapy were determined using an analytical model, and stray radiation doses from proton therapy were calculated using Monte Carlo simulations.

For each OAR (denoted by the subscript, j), the therapeutic and stray doses were calculated for each photon and proton treatment plan. Therapeutic and stray dose were added together to give the total absorbed dose for each treatment plan. The equivalent dose (Sv) was then found by multiplying the therapeutic and stray components of the total absorbed dose by their respective mean radiation weighting factors, $\overline{w_R}$

$$\overline{H}_j = \left(\overline{D_{Ther_j}} * \overline{w_{R_{Ther}}} \right) + \left(\overline{D_{Stray_j}} * \overline{w_{R_{Stray}}} \right) \quad (\text{Eq. 2.1})$$

where \overline{H}_j is the mean equivalent dose (Sv) to the OAR, j ; $\overline{D_{Ther_j}}$ is the mean absorbed dose (Gy) to the OAR, j , from the therapeutic component of the beam; $\overline{D_{Stray_j}}$ is the mean absorbed dose (Gy) to the OAR, j , from the stray component of the beam; $\overline{w_{R_{Ther}}}$ is the mean radiation weighting factor from the therapeutic component of the beam; and $\overline{w_{R_{Stray}}}$ is the mean radiation weighting factor from the stray component of the beam. For this work the $\overline{w_{R_{Ther}}}$ and $\overline{w_{R_{Stray}}}$ are the same for a given particle. They are listed for all particles of interest are listed below:

- Photons
 - $\overline{w_R} = 1.0$ which is the clinically used value at MD Anderson
- Protons
 - $\overline{w_R} = 1.1$ which is the clinically used value at MD Anderson
- Neutrons
 - $\overline{w_R} = 20.0$ was selected as a reasonable, median value as studies have suggested values between roughly 10 (Newhauser et al., 2009) and 30 (Brenner and Hall, 2008) can be used with a fair amount of confidence. The selection of this parameter is highly controversial (Kellerer et al., 2006, Brenner and Hall, 2008); therefore, the $\overline{w_R}$ for neutrons value was varied in Aim 2 as part of our sensitivity tests.

2.2.3.i. Stray dose for the photon treatment

For photon treatments, out-of-field stray photon dose calculations below 5% of the prescribed dose have been shown to under report dose by up to 60-70% (Howell et al., 2010a, Joosten et al., 2011). Commercial photon treatment planning systems also do not calculate neutron dose produced by the linear accelerator for high energy photon treatments using beam energies above ~10 MV. None of our studies included photons at or above 10 MV, so photoneutrons were not considered in this work.

The stray dose was calculated using an analytical absorbed dose calculation model designed

following the methodology from Howell *et al* (2010b). This methodology is reviewed below for the convenience of the reader. A 6 MV HL treatment plan was designed for a commercial male dosimetry phantom (ATOM, CIRS, Inc., Norfolk, VA) on the commercial TPS (Figure 2.5). 4-5 lithium fluoride thermoluminescent dosimeters (TLD-100) were placed inside the phantom at pre-determined locations relative to the 50% isodose line from the treatment plan. These locations were identified and transferred to the correct location inside the phantom as a result of it being cut into identifiable axial slices, both on the phantom itself as well as on its CT images on the TPS.

The closest distance a given slice was from the 50% isodose line (in cm) was measured using the TPS. The TLD-100 dosimeters were placed in the particular slice which was a known distance from the 50% isodose line. The treatment plan was delivered on a commercial medical linear accelerator (Varian 2100C, Varian Medical Systems, Palo Alto, CA) which is calibrated monthly for in-field dose using the American Association of Physicists in Medicine Task Group 51 protocol (Almond *et al.*, 1999) at our institution and commissioned for clinical use.



Figure 2-5 – Anthropomorphic phantom - Photograph of the anthropomorphic phantom used for the TLD measurements the prescribed dose.

Following irradiation, the TLDs were individually read at an established laboratory traceable to standards from a National protocol consistent with Accredited Dosimetry Calibration Laboratory (ADCL) procedures. The reading procedure accounted for energy response, linearity, and dosimeter fading. The uncertainty for each TLD was $< 3.0\%$ (Kirby *et al.*, 1986, Kirby *et al.*, 1992). Each TLD dose reading was determined from a calibration coefficient derived from a set of reference TLDs taken from the same batch as the measurement TLDs. The reference TLDs were irradiated by a

Cobalt-60 unit traceable to the ADCL and the National Institute of Standards and Technology (NIST). The measured absorbed doses were normalized per absorbed dose delivered to the isocenter and were reported in centi-Sievert per delivered Gray to isocenter (cSv/Gy_{iso}) (Eq. 2.2).

$$\frac{H_{TLD}}{D_{Iso}} = \frac{D_{TLD} * \overline{w_R}}{D_{Iso}} \quad (Eq. 2.2)$$

where H_{TLD} is the equivalent dose delivered to the TLD (cSv), D_{Iso} is dose delivered to isocenter (Gy_{iso}), D_{TLD} is the absorbed dose delivered to the TLD, and $\overline{w_R}$ is the mean radiation weighting factor for photons, which equals 1.0.

TLD doses were plotted vs distance from the 50% isodose line. An analytical model was fit to the plot to describe this relationship between dose and distance from field edge (defined as the 50% prescribed isodose line) for the photon IMRT HL treatment. The equation which best fit the data was a power function of the form:

$$\frac{H_{TLD}}{D_{Iso}} = 69.311 * x_{50}^{-1.503} \quad (Eq. 2.3)$$

where H_{TLD} is the equivalent dose delivered to the TLD (cSv), D_{Iso} is dose delivered to isocenter (Gy_{iso}), and x_{50} is the distance in cm the TLD is from the 50% isodose line.

Using the computer programming language Matlab[®] (Version R2012a (7.14.0.739), Mathworks[®], Natick, MA), an algorithm was devised to incorporate the analytical model (Eq. 2.2) on a voxel by voxel basis to the portion of the OAR that fell below the coverage of the 5% isodose line. x_{50} was found and then input into Eq. 2.3 and multiplied by the prescription dose of 36 Gy. H_{TLD} replaced the original TPS value. This process was repeated for voxels in the breast, lungs, and thyroid of each patient. Figure 2.6 describes the process.

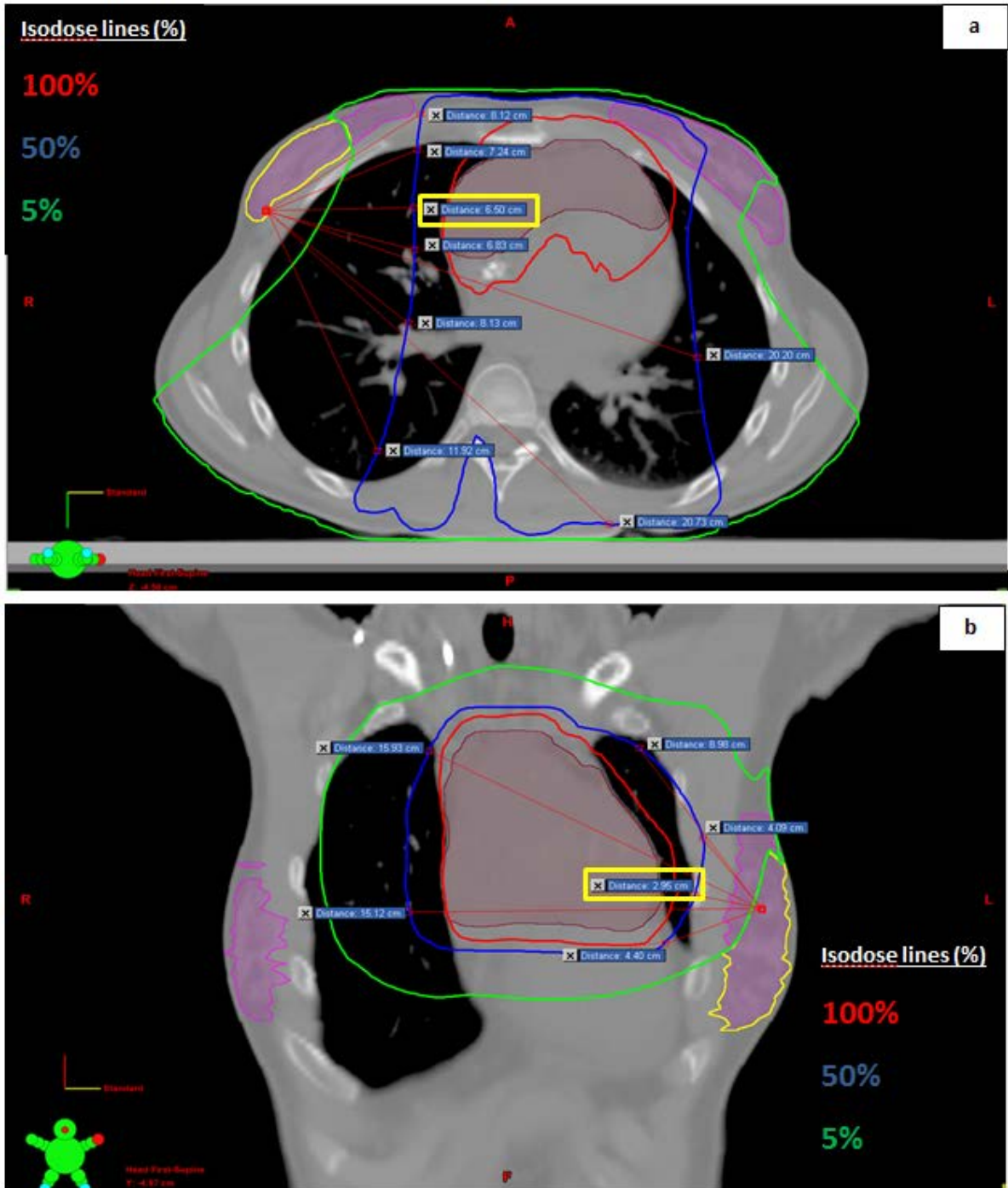


Figure 2-6 – Photon low dose correction algorithm - For both images, the pink shaded area represents the breasts, the maroon shaded area represents the CTV, and the yellow outlined area represents the portion of the breast that is below the 5% isodose line. a) Axial slice of Patient #1. The screenshot depicts a small sample of how the algorithm steps through each voxel located on the 50% isodose line to determine the shortest distance to a given voxel in the right breast outside of the 5% isodose line. After checking each distance in all three dimensions, the minimum is determined (yellow box) and designated as x_{50} . b) Sagittal slice of Patient #1 displaying the same algorithm steps to find the closest distance to the 50% isodose line as a) but in a different dimension for a different voxel in the left breast.

2.2.3.ii. Stray dose for the proton treatment

Stray radiation in proton therapy is due to secondary neutron formation from proton-induced nuclear reactions in the treatment apparatus as well as within the patient (Agosteo et al., 1998, Yan et al., 2002, Jiang et al., 2005, Taddei et al., 2008, Zheng et al., 2008, Agosteo et al., 2008, Perez-Andujar et al., 2009, Newhauser et al., 2009, Zhang et al., 2010). These neutrons are designated as external and internal neutrons, respectively. As noted above, for the proton treatment plans, the commercial TPS did not calculate neutron doses to the patient, which can exceed 1% of the prescribed dose to the patient in proton treatments (Taddei et al., 2009, Taddei et al., 2010a).

The neutron dose for the proton treatment plans was calculated using Monte Carlo methods. Monte Carlo uses statistical methods to estimate solutions for stochastic problems. The Monte Carlo N-Particle eXtended (MCNPX) version 2.7c transport code, developed at Los Alamos National Laboratory was used. The accuracy of MCNPX for simulation of a proton therapy nozzle treatment was validated both within our group and by others (Fontenot et al., 2005, Newhauser et al., 2005, Polf and Newhauser, 2005, Titt et al., 2006, Tayama et al., 2006, Moyers et al., 2008). In order to use the patient-specific treatment information from the commercial TPS for each individual patient, parameters were imported into the MCNPX-based Monte Carlo Proton Treatment Planning System (MCP RTP) described by Zheng *et al* (2006) and Newhauser *et al* (2007b).

We followed the methods of Newhauser *et al* (2009) to estimate the H/D values for both PSPT and IMPT, which have also been used in several other studies (Taddei et al., 2009, Taddei et al., 2010a, Rechner et al., 2012a). Using these established methods allowed us to make clinically realistic simulations of both PSPT and IMPT with a single simulation model. This was an important feature in avoiding the introduction of systematic bias when comparing internal *versus* external neutron exposures.

2.2.4. - Risk Models

2.2.4.i. RadRAT and BEIR VII

The National Cancer Institute (NCI) Radiation Risk Assessment Tool (RadRAT) (Berrington de Gonzalez et al., 2012) and the National Academy of Sciences Biological Effects of Ionizing Radiation (BEIR) VII – Phase 2 Report (National Research Council (U.S.). Committee to Assess Health Risks from Exposure to Low Level of Ionizing Radiation., 2006) were used to quantify the RSC risk for our patient studies. RadRAT is based largely on BEIR VII, which used the data from the Life Span Study (LSS) (Beebe et al., 1962, Preston et al., 2007, Ozasa et al., 2012) to derive RSC risk models.

BEIR VII calculates the Excess Relative Risk (ERR) of RSCs on a per organ basis as a function of sex, organ irradiated, dose to organ, age at exposure, and attained age (age lived to). The ERR is

defined as the ratio of RSC incidence of a radiation exposed population versus an unexposed population minus 1, or

$$ERR = \frac{RSC\ incidence_{Exposed\ Population}}{RSC\ incidence_{Unexposed\ Population}} - 1 \quad (Eq. 2.4)$$

The BEIR VII risk model is based upon the linear non-threshold (LNT) model which states that as dose increases, the risk of developing a second cancer linearly increases as well. While the thyroid has been shown to not follow the LNT model at higher doses (Sigurdson et al., 2005, Ronckers et al., 2006, Bhatti et al., 2010), the majority of studies of medically irradiated populations have reported that risk of developing RSCs in most organs increases linearly with dose (NCRP, 2011, Berrington de Gonzalez et al., 2013).

With the exception of breast (for which RadRAT did not provide an equation for ERR calculations), RadRAT uses the same ERR equations and coefficients as BEIR VII, but also has risk models for several additional OARs compared to BEIR VII, such as esophagus, which can be used for future studies. Since there was no ERR calculations for breast in RadRAT, the ERR was calculated using the BEIR VII equation for breast.

2.2.4.ii. Relative Risk (RR) calculations

The doses discussed in Section 2.2.3 above were calculated on a voxelized grid of 4 mm spatial resolution in the x-, y-, and z- dimensions of a Cartesian coordinate system. Each voxel was assigned an equivalent dose value (H_i). These equivalent dose values were then input into an in-house Matlab[®] program we developed to calculate ERR. Risk calculations were performed on a voxelized grid of 5 mm spatial resolution (mean ERR differences between 4 and 5 mm resolutions were on average less than 0.5%).

The program calculated and displayed the ERR on a voxel by voxel basis in the same manner as the TPS calculated dose. Previous works either calculated risk values based off of mean organ dose (Schneider et al., 2000, Newhauser et al., 2009, Fontenot et al., 2009, Taddei et al., 2010a, Taddei et al., 2010b) or the Dose Volume Histogram (DVH) data (Hodgson et al., 2007b, Andolino et al., 2011, Rechner et al., 2012a, Cella et al., 2013). Calculating voxel by voxel removed the loss of spatial risk information for visualization while maintaining the ability to tabulate the mean dose and risk information as needed.

Since BEIR VII and RadRAT had unique risk equations for each OAR (total breast using BEIR VII, total lung and thyroid using RadRAT) in the study, it was necessary to be able to determine which voxel were contained within the specified OARs. To accomplish this task, the program was designed to automatically identify and catalog the affiliated OAR of each voxel based upon the OAR

contours drawn in the TPS. Eq. 2.4-2.7 were used to calculate the ERR *for each voxel* for each OAR.

For breast

$$ERR_{LNT,i} = \beta_j * H_{j,i} * \left(\frac{a}{60}\right)^{-2} \quad (Eq. 2.5)$$

where $ERR_{LNT,i}$ is the ERR using the organ specific LNT risk model calculated to voxel i ; β_j is the ERR/Sv for exposure at exposed age (e) of 30+ at attained age (a) of 60; $H_{j,i}$ is the Equivalent Dose (Sv) found using Eq. 2.1 to the voxel i of a given OAR, j ; and a is the attained age in years.

For lung,

at age of exposure less than 30 years old,

$$ERR_{LNT,i} = \beta_j * H_{j,i} * e^{[\gamma_j * (e-30)]} * \left(\frac{a}{60}\right)^{\eta_j} \quad (Eq. 2.6)$$

where γ_j is the per decade increase in age at exposure over the range 0-30 years (always negative) for a given OAR, j ; e is the age at exposure in years and η_j is the exponent of attained age (always negative) for a given OAR, j .

at age of exposure equal to or greater than 30 years old

$$ERR_{LNT,i} = \beta_j * H_{j,i} * \left(\frac{a}{60}\right)^{\eta_j} \quad (Eq. 2.7)$$

For thyroid,

$$ERR_{LNT,i} = \beta_j * H_{j,i} * e^{[\gamma_j * (e-30)]} \quad (Eq. 2.8)$$

The $ERR_{LNT,i}$ was then converted to Relative Risk (RR) (Kaplan and Garrick, 1981) *for each voxel*. The definition of RR is

$$RR = \frac{RSC \text{ incidence}_{Exposed \text{ Populaion}}}{RSC \text{ incidence}_{Unexposed \text{ Populaion}}} = ERR + 1 \quad (Eq. 2.9)$$

The RR *for a voxel* ($RR_{LNT,i}$) was calculated using

$$RR_{LNT,i} = ERR_{LNT,i} + 1 \quad (Eq. 2.10)$$

where $ERR_{LNT,i}$ was taken from Eq. 2.5, 2.6, 2.7, or 2.8.

After $RR_{LNT,i}$ in *each voxel* in the OAR was calculated for RR, the mean RR for that OAR was found using

$$\overline{RR}_{JLNT} = \frac{\sum_i RR_{LNT,i}}{i} \quad (Eq. 2.11)$$

In this equation, $\overline{RR}_{j,LNT}$ is the mean RR for the j^{th} OAR for a given treatment plan, $RR_{LNT,i}$ is the RR for an individual voxel contained within the j^{th} OAR, and i is the number of voxels contained within the j^{th} OAR.

2.2.4.iii. Ratio of Relative Risk (RRR)

The endpoint of this work, and the metric we used to determine which treatment plan provided the lowest risk of developing a RSC, was the Ratio of Relative Risk (*RRR*). *RRR* is calculated by dividing the RR for a given treatment plan by the RR of the IMRT photon treatment plan as shown in Eq. 2.12.

$$RRR = \frac{RR_{Treatment\ Plan}}{RR_{IMRT\ Photon\ Plan}} \quad (Eq. 2.12)$$

In Eq. 2.12, *RRR* is the Ratio of Relative Risk, $RR_{Treatment\ Plan}$ is the Relative Risk of a specified treatment plan (in this work it will be one of the proton treatment plans), and $RR_{IMRT\ Photon\ Plan}$ is the Relative Risk of the IMRT photon treatment plan.

There were two endpoints examined using the *RRR* formula. To assist in clarifying the differences between the various *RRR* calculations, the reader is directed to Table 2.3. They are now examined in detail individually.

1. Mean *RRR* for a given organ and a given patient (white squares in Table 2.3)

$$\overline{RRR}_{j,k} = \frac{1}{L_{j,k}} \sum_{i=1}^{L_{j,k}} RRR_{i,j,k} \quad (Eq. 2.13)$$

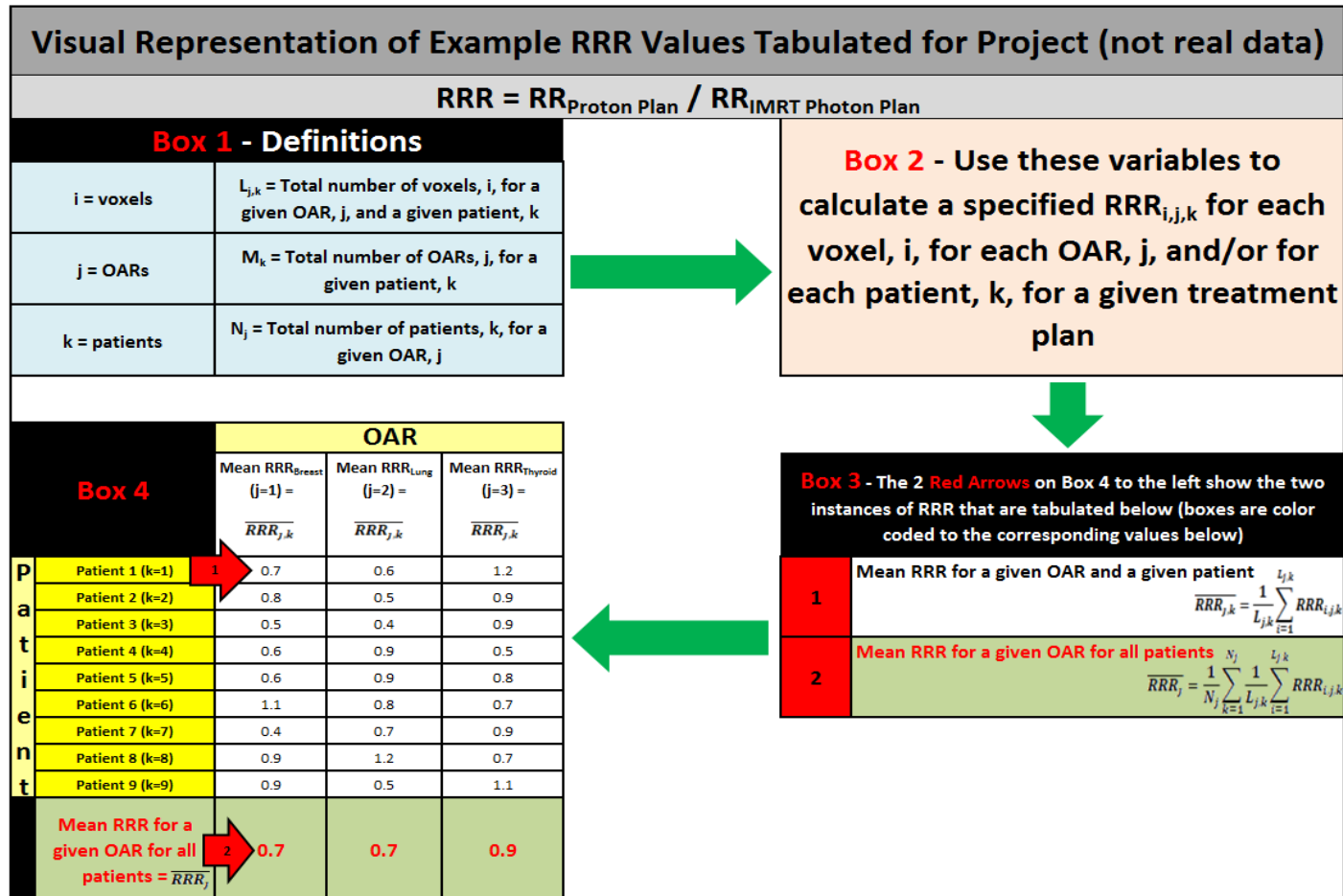
where $\overline{RRR}_{j,k}$ is the mean *RRR* for all voxels, i , contained in a given OAR, j , and a given patient, k ; $L_{j,k}$ is the total number of voxels, i , of the j^{th} OAR of the k^{th} patient; and $RRR_{i,j,k}$ is the calculated *RRR* for the i^{th} voxel of the j^{th} OAR of the k^{th} patient.

2. Mean *RRR* for a given OAR for all patients (green squares in Table 2.3)

$$\overline{RRR}_j = \frac{1}{N_j} \sum_{k=1}^{N_j} \frac{1}{L_{j,k}} \sum_{i=1}^{L_{j,k}} RRR_{i,j,k} \quad (Eq. 2.14)$$

where \overline{RRR}_j is the mean *RRR* for all voxels, i , and all patients, k , for a given OAR, j ; N_j is the total number of patients for a given OAR, j ; $L_{j,k}$ is the total number of voxels, i , of the j^{th} OAR of the k^{th} patient; and $RRR_{i,j,k}$ is the calculated *RRR* for the i^{th} voxel of the j^{th} OAR of the k^{th} patient.

Table 2-3 – Flow diagram of different mean RRR calculations - Depicts the different mean RRR endpoints examined for this work. Start at Box 1 and follow the green arrows to follow the logical progression of the graph. Box1 defines the variables used in the mean RRR equations. Box 2 states what the variables will be used to calculate. Box 3 defines the 5 different RRR endpoints that were calculated. Box 4 provides the visual representation of how those 2 RRR endpoints were calculated and how they relate to each other (via the red arrows).



When calculating the RSC risk to each organ, organs that have two distinct left and right portions (*i.e.*, breast, lung) were calculated together rather than individually as this was the technique used in the risk models. To explore the influence of exposed (e) and attained (a) ages, each patient had a full risk calculation done for exposed ages (e) of 10, 26, and 42. These ages corresponded to the minimum, mean, and maximum age of our patient cohort, respectively. Each of these exposed ages were calculated in combination with an attained age (a) of the given exposed age + 20 years and the given exposed age + 50 years.

To avoid inundating the text with data, a representative patient was used to display the data for Aim 1. Three variables were held constant which included

- Exposed Age of Patient - 26 (the mean age of our patient cohort)
- Attained Age of Patient - 46 (= 26+20, which is roughly equivalent to the median time for a RSC to develop in an HL patient treated with radiation (Friedman et al., 2010))
- Neutron radiation weighting factor (neutron $\overline{w_R}$) = 20

These variables will be varied in Aim 2 to determine any change in outcomes.

2.2.5. – Statistical Tests for Significance

Two standard statistical tests were conducted to determine the statistical significance for $\overline{RRR_{j,k}}$ for each OAR of interest (*i.e.* breast, lung, thyroid): the sign test and the Student’s t-test (Rosner, 2011). Since we are comparing $\overline{RRR_{j,k}}$ to 1 rather than another distribution, these tests were classified as a one sample inference. In addition, both were two-sided tests of significance because, a priori, it was unclear if the $\overline{RRR_{j,k}}$ would always be > or < than 1.

2.2.5.i. Sign test

The sign test is a non-parametric test (does not assume a Gaussian distribution of the data) that determines whether two samples are from the same distribution. It is relatively insensitive to outliers as it disregards the magnitude of the difference between the comparisons. $\overline{RRR_{j,k}}$ had three possible outcomes:

1. $\overline{RRR_{j,k}} = 1$ – The photon and proton plan had equal RSC risks
2. $\overline{RRR_{j,k}} > 1$ – The photon plan had lower RSC risk
3. $\overline{RRR_{j,k}} < 1$ – The proton plan had lower RSC risk

$\overline{RRR_{j,k}}$ was designated as (+) if it was greater than 1 and (-) if it was less than 1. The null hypothesis was $H_0: P(+) = P(-)$ and the alternate hypothesis was $H_1: P(+) \neq P(-)$, where $P(\pm)$ is the probability of a + or –, respectively. To determine significance one can test how many patients showed a $\overline{RRR_{j,k}} > 1$ or < 1 for each OAR. Since this is a two tailed sign test, you can determine if

either the proton or photon plans show a significant difference in RSC risk as we will show below. For this work we chose to count the number of patients with a $\overline{RRR}_{j,k} < 1$ for each OAR.

Equation 2.15 is the test parameter used to determine the number of patients per OAR (out of a total number of patients, n=9) that would need to have a $\overline{RRR}_{j,k}$ value of > 1 to conclude with an $\alpha = 0.05$ (where α is the significance level that denotes the probability of a type I statistical error which would reject H_0 when H_0 is actually true) that proton plans have a lower risk of RSC compared to their corresponding photon plans. Note from Figure 2.7 and Eq. 2.15 that the number of patients with a $\overline{RRR}_{j,k} < 1$, C , must be a number greater than C_2 .

$$C > C_2 = \frac{n}{2} + \frac{1}{2} + \left(z_{(1-\alpha/2)} * \sqrt{\frac{n}{4}} \right) \quad (\text{Eq. 2.15})$$

where C is the number of patients with a $\overline{RRR}_{j,k} < 1$, C_2 is the upper critical value which equals the number of patients out of the total number of patients examined (n , which for our purposes is 9) that must have a $\overline{RRR}_{j,k} < 1$ to have statistical significance at the $\alpha = 0.05$ level, and Z is the test statistic derived from the normal distribution (which for $\alpha = 0.05$ is $z_{(1-.025)} = 1.96$) (Rosner, 2011). For our studies (where $n = 9$), C must be ≥ 8 patients in order to state that the proton plans administered to our patient population have a statistically significant lower $\overline{RRR}_{j,k}$ than our patient population's corresponding photon plan.

Conversely, Equation 2.16 is the test parameter used to determine the number of patients (out of our total number of patients, $n = 9$) that would need to have a $\overline{RRR}_{j,k}$ value of less than 1 to conclude with an $\alpha = 0.05$ (where α is the significance level that denotes the probability of a type I statistical error which would reject H_0 when H_0 is actually true) that photon plans have a lower risk of RSC compared to their corresponding proton plans. Note from Figure 2.7 and Eq. 2.16 that the number of patients with a $\overline{RRR}_{j,k} < 1$, C , must be a number less than C_1 .

$$C < C_1 = \frac{n}{2} - \frac{1}{2} - \left(z_{(1-\alpha/2)} * \sqrt{\frac{n}{4}} \right) \quad (\text{Eq. 2.16})$$

where C is the number of patients with a $\overline{RRR}_{j,k} < 1$, C_1 is the lower critical value which is the number of patients out of the total number of patients examined (n , which for our purposes is 9) that must have a $\overline{RRR}_{j,k} < 1$ to have statistical significance at the $\alpha = 0.05$ level, and Z is the test statistic derived from the normal distribution (which for $\alpha = 0.05$ is $z_{(1-.025)} = 1.96$) (Rosner, 2011). For our studies (where $n = 9$), C must be < 1 patient in order to state that the photon plans administered

to our patient population have a statistically significant lower $\overline{RRR}_{j,k}$ than our patient population's corresponding proton plan.

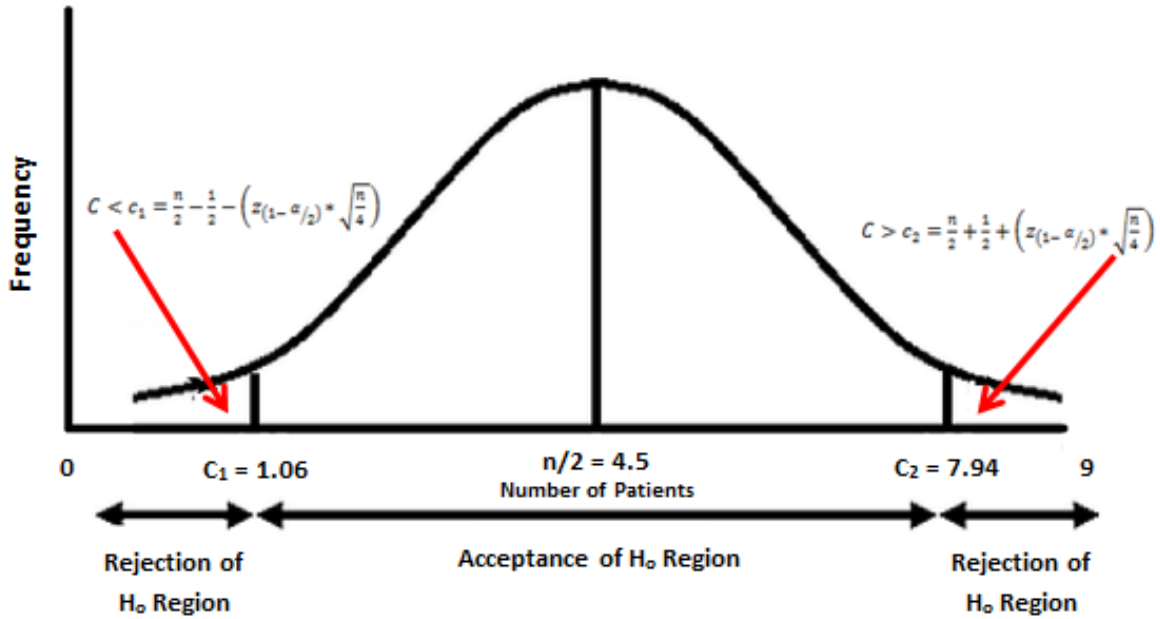


Figure 2-7 – Sign test parameters - Cartoon depicting the values of C needed to determine statistical significance of whether or not either proton or photon plans have a lower $\overline{RRR}_{j,k}$ compared to the other. If $C < C_1$ then the photon plans have a statistically significant lower $\overline{RRR}_{j,k}$. If $C > C_2$ then the proton plans have a statistically significant lower $\overline{RRR}_{j,k}$. C_1 , C_2 , and $n/2$ are given numerical values that correlate to the number of patients required to obtain significance.

2.2.5.ii. Student's t-test

Student's t-test is a parametric test that determines if the mean of a sample distribution is from the same distribution as the population mean. The parametric assumptions of the test may not be reasonable to assume given our small sample size. For pedagogical reasons, however, it was thought appropriate to examine in this work. As with the sign test, we can test if either the proton or photon plan have statistically significant $\overline{RRR}_{j,k}$ values relative to the other for each OAR. The null hypothesis $H_0: \overline{RRR}_{j,k} = 1$ was compared to the alternate hypothesis: $H_1: \overline{RRR}_{j,k} \neq 1$, with a two-sided significance level (α) of 0.05, the test statistic t was computed (Rosner, 2011) according to

$$t = \frac{\bar{x} - \mu_0}{s / \sqrt{n}} \quad (\text{Eq. 2.17})$$

where \bar{x} is the sample mean, μ_0 is the expected or population mean (equal to 1 here), s is the sample standard deviation, and n is the sample size (equal to 9 here).

This value was then compared to Eq. 2.17 and 2.19. If t is less than or equal to the value calculated for Eq. 2.19 (C_1), then the proton plans have a lower mean RSC risk. If the test statistic, t , is more than or equal to the value calculated in Eq. 2.19 (C_2), then the photon plans have a lower mean RSC risk.

$$t \leq C_1 = t_{[n-1, (\frac{\alpha}{2})]} \quad (\text{Eq. 2.18})$$

where C_1 is the lower critical value that indicates that a proton plan has a statistically significant lower mean RSC risk compared to its corresponding photon plan, n is the sample size (equal to 9 here), and α is the significance level (equal to 0.05 here), H_0 is rejected. For our study ($n=9$), $t = -2.306$.

$$t > C_2 = t_{[n-1, (1-\frac{\alpha}{2})]} \quad (\text{Eq. 2.19})$$

where C_2 is the upper critical value that indicates that a photon plan has a statistically significant lower mean RSC risk compared to its corresponding proton plan, n is the sample size (equal to 9 here), and α is the significance level (equal to 0.05 here), H_0 is rejected. For our study ($n=9$), $t = 2.306$. The acceptance and rejection regions are shown in Figure 2.8 below.

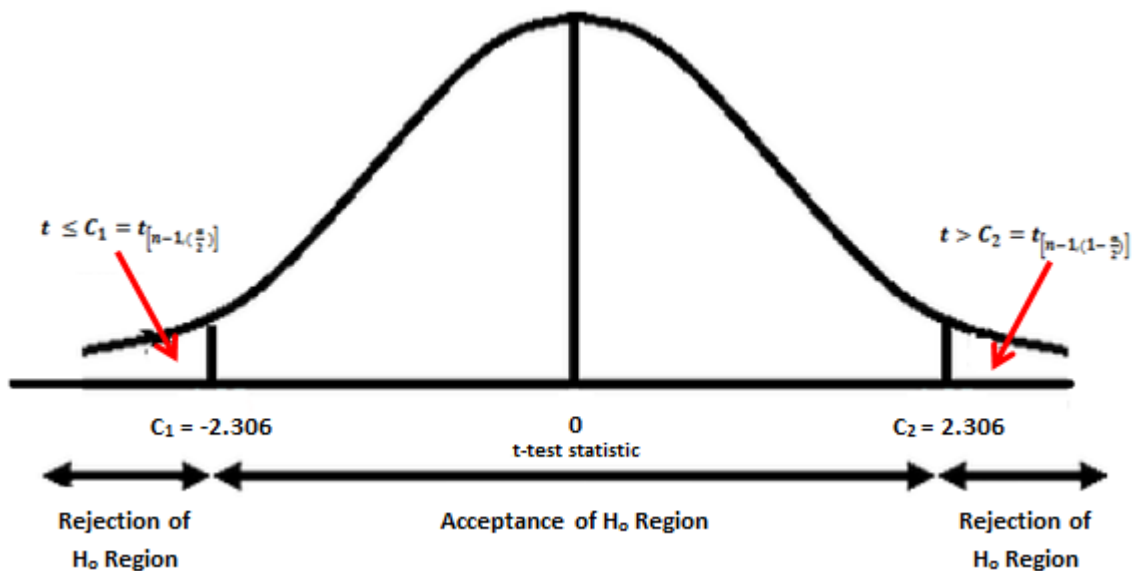


Figure 2-8 – Student’s t-test parameters - Cartoon depicting the values of t needed to determine statistical significance of whether or not either proton or photon plans have a lower $\overline{RRR}_{j,k}$ compared to the other. If $t \leq C_1$ then the proton plans have a statistically significant lower $\overline{RRR}_{j,k}$. If $t > C_2$ then the photon plans have a statistically significant lower $\overline{RRR}_{j,k}$. C_1 and C_2 , are given numerical values that correlate to the number of patients required to obtain significance.

2.2.6. – Propagation of Uncertainties

To account for uncertainty in the \overline{RRR} calculations, error propagation was used. We adapted the formula for the \overline{RRR} uncertainty from Fontenot *et al* (2010) and Rechner *et al* (2012a). Error

propagation was calculated for each instance of Eq. 2.13: $\overline{RRR}_{j,k} = \frac{1}{L_{j,k}} \sum_{i=1}^{L_{j,k}} RRR_{i,j,k}$.

Recall from Eq. 2.12 that $\overline{RRR} = \frac{\overline{RR_{Proton}}}{\overline{RR_{Photon IMRT}}}$, and can be reduced further from Eq. 2.9 to $RR = ERR + 1$. To simplify the calculation, the ERR calculations (Eqs. 2.5-2.8) were simplified to the following general form (Eq. 2.20):

$$\overline{ERR_{T,LNT_{j,k}}} = \beta_j * C_{j,k} * \overline{H_{T_{j,k}}} \quad (\text{Eq. 2.20})$$

Where $\overline{ERR_{T,LNT_{j,k}}}$ is the mean ERR calculated for a given OAR, j , and for a given patient, k , of treatment plan, T ; β_j is the ERR/Sv for exposure at exposed age (e) of 30+ at attained age (a) of 60 for a given OAR, j ; $C_{j,k}$ is a constant calculated for a given exposed age (e), attained age (a), per decade increase in age at exposure over the range 0-30 years (γ_j) for a given OAR, j , for a given exponent of attained age (η_j) for a given patient, k ; and $\overline{H_{T_{j,k}}}$ is the mean equivalent dose (Sv) found using Eq. 2.1 for a given OAR, j , for a given patient, k , of treatment plan, T .

Combining the above equations gives the general form of the equation with which we propagated the uncertainties (Eq. 2.21):

$$\overline{RRR_{LNT_{j,k}}} = \frac{\overline{RR_{Proton,LNT_{j,k}}}}{\overline{RR_{Photon IMRT,LNT_{j,k}}}} = \frac{\overline{ERR_{Proton,LNT_{j,k}}}+1}{\overline{ERR_{Photon IMRT,LNT_{j,k}}}+1} = \frac{(\beta_j * C_{j,k} * \overline{H_{Proton_{j,k}}})+1}{(\beta_j * C_{j,k} * \overline{H_{Photon IMRT_{j,k}}})+1} \quad (\text{Eq. 2.21})$$

Where $\overline{RRR_{LNT_{j,k}}}$ is the \overline{RRR} using the LNT dose response model, $\overline{RR_{Proton,LNT_{j,k}}}$ is the mean RR for a given proton treatment plan using the LNT dose response model, $\overline{RR_{Photon IMRT,LNT_{j,k}}}$ is the mean RR for a given photon IMRT treatment plan using the LNT dose response model, $\overline{ERR_{Proton,LNT_{j,k}}}$ is the mean ERR for a given proton treatment plan using the LNT dose response model, $\overline{ERR_{Photon IMRT,LNT_{j,k}}}$ is the mean ERR for a given photon IMRT treatment plan using the LNT dose response model, $\overline{H_{Proton_{j,k}}}$ is the total mean equivalent dose (Sv) for a given proton treatment plan, $\overline{H_{Photon IMRT_{j,k}}}$ is the total mean equivalent dose (Sv) for a given photon IMRT treatment plan, and β_j and $C_{j,k}$ are the same quantities described in Eq. 2.20. To avoid

receptiveness, it should be understood that all quantities of the form $\overline{X_{Y,j,k}}$ indicate for a given OAR, j , and for a given patient, k .

To propagate errors, the derivative of each variable with respect to the quantity we wished to propagate was taken. Taking Eq. 2.21, the equation for the propagation of errors for the mean RRR, $\overline{RRR_{LNT,j,k}}$, was as follows:

$$\begin{aligned} \sigma_{\overline{RRR_{LNT,j,k}}}^2 &= \left(\frac{\partial \overline{RRR_{LNT,j,k}}}{\partial \beta_j} \right)^2 \sigma_{\beta_j}^2 + \left(\frac{\partial \overline{RRR_{LNT,j,k}}}{\partial C_{j,k}} \right)^2 \sigma_{C_{j,k}}^2 + \left(\frac{\partial \overline{RRR_{LNT,j,k}}}{\partial \overline{H_{Proton,j,k}}} \right)^2 \sigma_{\overline{H_{Proton,j,k}}}^2 + \\ &\left(\frac{\partial \overline{RRR_{LNT,j,k}}}{\partial \overline{H_{Photon IMRT,j,k}}} \right)^2 \sigma_{\overline{H_{Photon IMRT,j,k}}}^2 \end{aligned} \quad (\text{Eq. 2.22})$$

Where $\overline{RRR_{LNT,j,k}}$, $\overline{H_{Proton,j,k}}$, $\overline{H_{Photon IMRT,j,k}}$, β_j , $C_{j,k}$ are the same quantities defined in Eq. 2.21, $\sigma_{\overline{RRR_{LNT,j,k}}}$ is the uncertainty in $\overline{RRR_{LNT,j,k}}$, σ_{β_j} is the known uncertainty in β_j , $\sigma_{C_{j,k}}$ is the known uncertainty in $C_{j,k}$, $\sigma_{\overline{H_{Proton,j,k}}}$ is the known uncertainty in $\overline{H_{Proton,j,k}}$, and $\sigma_{\overline{H_{Photon IMRT,j,k}}}$ is the known uncertainty in $\overline{H_{Photon IMRT,j,k}}$.

Table 2.4 defines the calculated derivatives and the known uncertainties of each variable for the LNT dose response model. In Aim 2 there were unique equations calculated for the other dose response models examined.

Table 2-4 – LNT uncertainty terms and stated uncertainty for assigned variables

Quantities	Uncertainty Terms/Stated Uncertainty		
$\left(\frac{\partial \overline{RRR}_{LNT_{j,k}}}{\partial \beta_j}\right)$	$\frac{\left\{\left(\beta_j * C_{j,k} * \overline{H}_{Photon\ IMRT_{j,k}} + 1\right) * \left(C_{j,k} * \overline{H}_{Proton_{j,k}}\right)\right\} - \left\{\left(\beta_j * C_{j,k} * \overline{H}_{Proton_{j,k}} + 1\right) * \left(C_{j,k} * \overline{H}_{Photon\ IMRT_{j,k}}\right)\right\}}{\left(\beta_j * C_{j,k} * \overline{H}_{Photon\ IMRT_{j,k}} + 1\right)^2}$		
σ_{β_j}	Breast – 0.14 ERR/Sv	Lung – 0.29 ERR/Sv	Thyroid – 0.91 ERR/Sv
$\left(\frac{\partial \overline{RRR}_{LNT_{j,k}}}{\partial C_{j,k}}\right)$	$\frac{\left\{\left(\beta_j * C_{j,k} * \overline{H}_{Photon\ IMRT_{j,k}}\right) * \left(\beta_j * \overline{H}_{Proton_{j,k}}\right)\right\} - \left\{\left(\beta_j * C_{j,k} * \overline{H}_{Proton_{j,k}}\right) * \left(\beta_j * \overline{H}_{Photon\ IMRT_{j,k}}\right)\right\}}{\left(\beta_j * C_{j,k} * \overline{H}_{Photon\ IMRT_{j,k}} + 1\right)^2}$		
$\sigma_{C_{j,k}}$	0		
$\left(\frac{\partial \overline{RRR}_{LNT_{j,k}}}{\partial \overline{H}_{Proton_{j,k}}}\right)$	$\frac{1}{\left(\overline{H}_{Photon\ IMRT_{j,k}} + 1\right)}$		
$\sigma_{\overline{H}_{Proton_{j,k}}}$	5% of $\overline{H}_{Proton_{j,k}}$		
$\left(\frac{\partial \overline{RRR}_{LNT_{j,k}}}{\partial \overline{H}_{Photon\ IMRT_{j,k}}}\right)$	$\frac{\left(1 - \overline{H}_{Proton_{j,k}}\right)}{\left(\overline{H}_{Photon\ IMRT_{j,k}} + 1\right)^2}$		
$\sigma_{\overline{H}_{Photon\ IMRT_{j,k}}}$	3% of $\overline{H}_{Photon\ IMRT_{j,k}}$		

For this work, the uncertainty of β_j was found by consulting both BEIR VII (for breast) and RadRAT (for lung and thyroid). $\pm 2\sigma$ is given for β_j . The values are not symmetric so $\pm\sigma$ was averaged and multiplied by 2 to give the value used for σ_{β_j} for each OAR. $C_{j,k}$ was assumed to have no uncertainty associated with it. The uncertainty in β_j is considered large enough to encompass any necessary variation in $C_{j,k}$ (Berrington de Gonzalez et al., 2012). Using values from Fontenot *et al* (2010) and Rechner *et al* (2012a), $\sigma_{\overline{H}_{Proton_{j,k}}}$ and $\sigma_{\overline{H}_{Photon\ IMRT_{j,k}}}$ were conservatively selected to be 5% and 3% of their given mean total equivalent doses, respectively.

2.2.7. – Patient Treatment Variation Effects on Risk Analysis

In addition to checking statistical differences, we also looked at possible correlations between the patient and/or tumor characteristics and the subsequent \overline{RRR} . Treatment and host specific factors were accounted for each patient by comparing the specified factor to $\overline{RRR}_{j,k}$ and looking for any correlation with the Coefficient of Determination (R^2), which is a linear regression model that accounts for the percentage of variance to the data accounted for by the model used to describe it. The coefficient of determination runs from 0 to 1. The closer the value to 0, the less the regression model improves the prediction over the mean model (i.e. the data mean). A value equal to 1 indicates perfect prediction. The CTV was used as the reference contour since it is the same for both photon and proton plans.

2.2.7.i. Host factors

- a. Age (Years) at exposure (e)
- b. Body Mass Index (BMI) (kg/m^2)
- c. OAR volume (cc)
- d. Patient width at the CTV centroid location
 - i. Lateral width (cm)
 - ii. Anterio-Posterior (AP) width (cm)
- e. Percent of OAR volume contained within the Photon IMRT 50% isodose line (%)
- f. Anatomical location of OAR relative to CTV (See Figure 2.9)

2.2.7.ii. Treatment factors

a. CTV volume (cc)

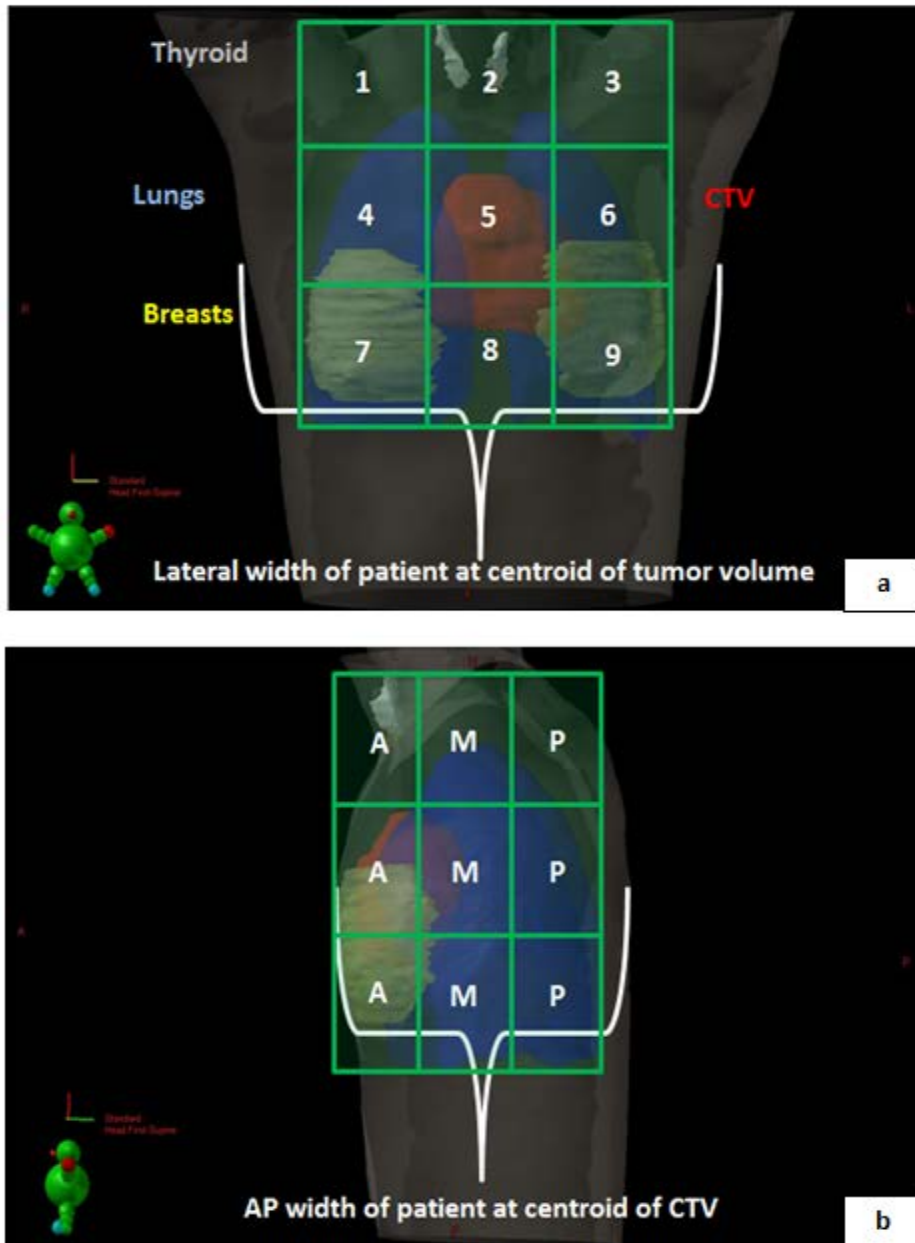


Figure 2-9 – Anatomical location of OAR relative to CTV – a) Antero-Posterior (AP) rendering of Patient #1 showing the CTV (red), breast (yellow), lungs (blue), and thyroid (gray). The green box encapsulates the furthest extent of these OARs in the lateral and superior/inferior (SI) directions. It is then divided into 9 boxes as shown by dividing the full width and height of the box by 3. The location of the OARs and CTV is determined by the location of the center of mass of that particular contour. b) Sagittal rendering of Patient #1. The figure continues to show the green box but this time in the AP direction. As in Figure 2.9a, the green box covers the extent of the OARs, but this time in the AP and SI directions and is equally divided into 9 different boxes. A stands for “Anterior”, M stands for “Medial”, and P stands for “Posterior”. They are combined with the numbering lines to form a total of 27 boxes (9 boxes each in the “A”, “M”, and “P” designations). As an example, the CTV centroid would be designated as “A5” while the thyroid centroid is located in “A2”.

2.3. Results

2.3.1. – Characteristics of Patient Cohort

The patient cohort consisted of 9 patients who each had unique characteristics for both their host and treatment factors.

2.3.1.i. Host factors

Host factors, including each individual patient’s demographics (age, height, weight, BMI) and OAR (breasts, lungs, thyroid) characteristics are included in Tables 2.5-2.8.

Table 2-5 – Host characteristics per patient – demographics - Compilation of various host factors for the HL cohort. With the exception of the youngest patient (Patient #8) there was fairly similar height, weight, and BMI values across the cohort

Patient #	Age at Exposure (e) (Years)	Height (cm)	Weight (kg)	Body Mass Index (BMI) (kg/m ²)
1	26	168.0	57.6	20.4
2	28	162.6	63.5	24.0
3	42	158.0	64.6	25.9
4	31	161.0	58.1	22.4
5	36	161.0	62.7	24.2
6	25	163.0	53.6	20.2
7	15	157.2	58.8	23.8
8	10	146.5	36.9	17.2
9	15	160.0	50.0	19.5
Average	25.3	159.7	56.2	22.0
Standard Deviation	9.9	5.5	8.1	2.6

Table 2-6 – Host characteristics per patient – breast - Breast characteristics of all 9 patients. The total volume in cubic centimeters (cc) was found for each breast as well as the two combined (Total Breast). As a point of reference, the percentage of the total breast contained within the open field of the photon IMRT treatment (designated as the 50% isodose line) was found to determine any possible correlations between proximity of the specified OAR to the tumor volume and the mean RRR value. The breast had the second largest average percentage of tissue contained within the 50% isodose line of the three examined OARs. The location designated as the Left and Right Breast Centroid Region corresponds to the description in Figure 2.9.

Patient #	Volume - Left Breast (cc)	Volume - Right Breast (cc)	Volume - Total Breast (cc)	Total Breast % within 50% line of photon IMRT plan (%)	Left Breast Centroid Region	Right Breast Centroid Region
1	138.8	124.2	262.9	11.6	A9	A7
2	744.0	588.9	1332.9	52.1	A6	A4
3	531.9	610.8	1142.7	0.0	A9	A7
4	477.6	481.5	959.1	13.8	A6	A7
5	570.3	559.1	1129.4	15.2	A6	A4
6	313.1	270.8	583.9	28.9	A6	A4
7	533.7	571.6	1105.3	10.3	A6	A4
8	88.6	97.4	186.0	10.0	A6	A4
9	233.2	256.0	489.1	3.1	A9	A7
Average	403.5	395.6	799.1	16.1	-	-
Standard Deviation	207.9	196.2	399.6	14.8	-	-

Table 2-7 – Host characteristics per patient – lung - Lung characteristics of all 9 patients. The total volume in cubic centimeters (cc) was found for each lung as well as the two combined (Total Lung). As a point of reference, the percentage of the total lung contained within the open field of the photon IMRT treatment (designated as the 50% isodose line) was found to determine any possible correlations between proximity of the specified OAR to the tumor volume and the mean RRR value. The lung had the largest average percentage of tissue contained within the 50% isodose line of the three examined OARs. The location designated as the Left and Right Lung Centroid Region corresponds to the description in Figure 2.9.

Patient #	Volume - Left Lung (cc)	Volume - Right Lung (cc)	Volume - Total Lung (cc)	Total Lung % within 50% line of photon IMRT plan (%)	Left Lung Centroid Region	Righth Lung Centroid Region
1	1009.7	1496.6	2506.3	22.5	M6	M4
2	577.2	802.4	1379.6	37.5	P6	P4
3	764.2	966.5	1730.7	13.4	P6	M4
4	1090.4	1337.9	2428.2	36.7	M6	M4
5	654.2	1034.2	1688.5	26.2	P6	M4
6	911.8	998.8	1910.5	58.1	P6	P4
7	894.1	1014.1	1908.2	16.6	P6	M4
8	476.9	645.7	1122.6	26.2	M6	M4
9	1052.2	1313.4	2365.6	21.1	P6	M4
Average	825.6	1067.7	1893.3	28.7	-	-
Standard Deviation	206.5	254.9	448.7	12.9	-	-

Table 2-8 – Host characteristics per patient – thyroid -Thyroid characteristics for all 9 patients. Due to its small size, the thyroid was considered as a whole rather than with a right and left side. The total volume in cubic centimeters (cc) was found. As a point of reference, the percentage of the thyroid contained within the open field of the photon IMRT treatment (designated as the 50% isodose line) was found to determine any possible correlations between proximity of the specified OAR to the tumor volume and the mean RRR value. The location designated as Thyroid Centroid Region corresponds to the description in Figure 2.9.

Patient #	Volume - Thyroid (cc)	Thyroid % within 50% line of photon IMRT plan (%)	Thyroid Centroid Region
1	6.6	0.0	A2
2	13.0	0.0	M2
3	5.9	38.6	M2
4	6.6	22.4	A2
5	5.5	27.4	M2
6	4.6	0.0	M2
7	7.2	27.8	M2
8	4.4	15.8	A2
9	6.3	69.9	M2
Average	6.7	22.4	-
Standard Deviation	2.4	21.4	-

The patient cohort gave a large variation in volume for the breasts and lungs while the thyroid, due to its small size and standard position in the body, was fairly uniform. For all three OARs, the percentage of the volume within the 50% isodose line for the photon IMRT plan varied considerably.

2.3.1.ii. Treatment factors

Treatment factors, which were dictated by the CTV volume and location for each patient, are listed in Table 2.9. The CTV Centroid Region corresponds to the description in Figure 2.9. The patient width at the centroid of the CTV was found both in the lateral and AP direction of the patient to establish how much tissue would be traversed when treating the tumor volume.

Table 2-9 – Treatment characteristics per patient – CTV - Characteristics of the CTV volume and location for all 9 patients. CTV volumes varied substantially from patient to patient, but on average, the width of the patient at the centroid of the CTV in both the lateral and AP directions did not. As was to be expected, the CTV was found in the middle third laterally and in the anterior two thirds for all patients. However, 4 of the 9 patients were in either the superior or inferior third of the patient box described in Figure 2.9 which could impact the RRR values later in the results for the various OARs.

Patient #	Volume - CTV (cc)	Patient Width at Centroid of CTV Slice - Lateral (cm)	Patient Width at Centroid of CTV Slice - Anterior-Posterior (AP) (cm)	CTV Centroid Region
1	267.6	23.1	19.5	A5
2	787.3	36.1	21.2	M5
3	151.2	23.6	15.5	M2
4	383.1	29.6	20.2	A5
5	337.8	30.4	15.9	M5
6	530.9	27.1	19.3	M8
7	211.7	31.9	15.6	M2
8	204.4	23.8	13.1	M5
9	329.5	37.8	13.1	M2
Average	355.9	29.3	17.0	-
Standard Deviation	186.2	5.1	2.9	-

Table 2-10 – Treatment characteristics per patient – beam setup - Characteristics of treatment beam orientation and approach for all 9 patients. The majority of the patients used the same number of beams for the photon IMRT (5) and the proton (2) treatments. When possible, equivalent angles were used to reduce variation from patient to patient. However, in order to obtain appropriate tumor volume coverage, adjustments were made when necessary. It is important to note that the plans were designed to sufficiently cover the tumor volume with the prescribed dose and not to optimize risk reduction.

Patient #	Arms Up or Down	# of Beams - Photon IMRT	Beam Angles - Photon IMRT (°)	# of Beams - Proton	Beam Angles - Proton (°)
1	Up	5	0, 49, 165, 200, 325	2	0, 90
2	Up	6	0, 20, 70, 170, 190, 340	2	0, 180
3	Down	5	0, 20, 170, 190, 340	1	0
4	Up	5	0, 20, 170, 190, 340	2	0, 180
5	Up	5	0, 51, 151, 211, 309	2	0, 285
6	Up	5	0, 51, 151, 211, 309	1	0
7	Up	6	0, 20, 70, 170, 190, 340	2	0, 95
8	Up	5	0, 20, 170, 190, 340	2	0, 180
9	Down	5	0, 20, 170, 190, 340	2	0, 180

2.3.2. – Characteristics and Images of Patient Plans

Example dose distributions and values are shown for a representative patient (Patient #2) to highlight the differences between the various treatment techniques and dose sources.

2.3.2.i. Photon treatment plan

As was expected, the photon dose distributions from the largely 5 field IMRT (Table 2.1) dose distributions deposited low doses to larger volumes of the normal tissue and OAR in order to adequately cover the CTV. Efforts were made to remove extraneous dose from the OARs as long as it did not compromise the tumor volume dose prescription.

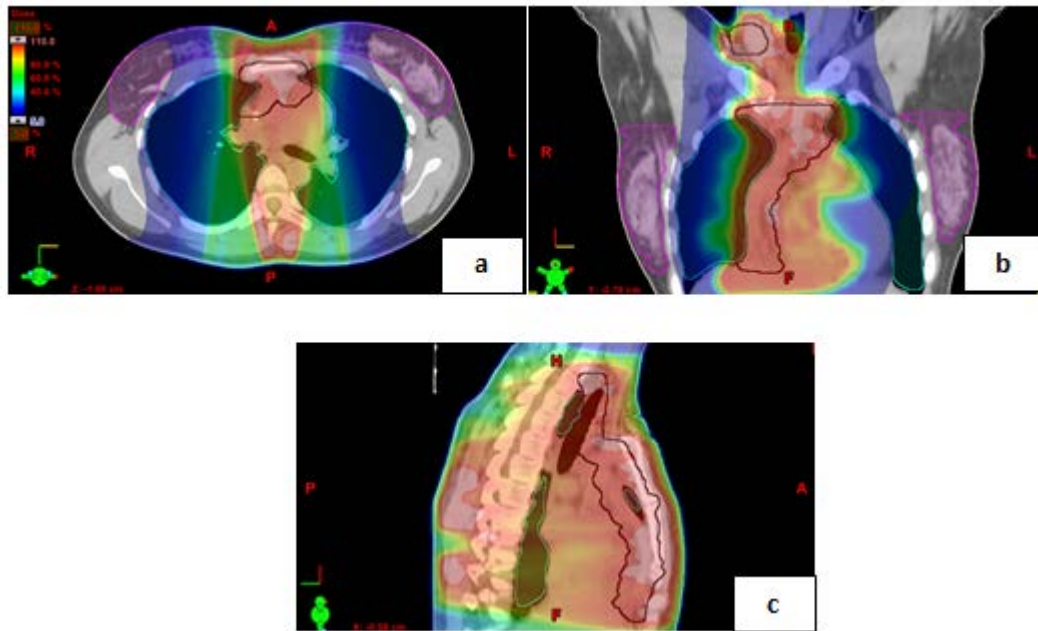


Figure 2-10 – Photon IMRT dose distribution example - Colorwash of the dose distribution (100% = 36 Sv) for Patient #4. The CTV (rendered in black), breast (rendered in magenta), lung (rendered in sky blue) and thyroid (rendered in yellow) are visible in the various orientations. a) Axial, b) Coronal, and c) Sagittal renderings showing a 5 field setup for the photon IMRT treatment plan.

2.3.2.ii. Proton treatment plans

The proton treatment plans included the dose found only from the commercial TPS. One can clearly see the reduction in the low level dose to tissue outside of the intended treatment volume. This portion does not cover the neutron dose contributions, however, which will be shown in the next section.

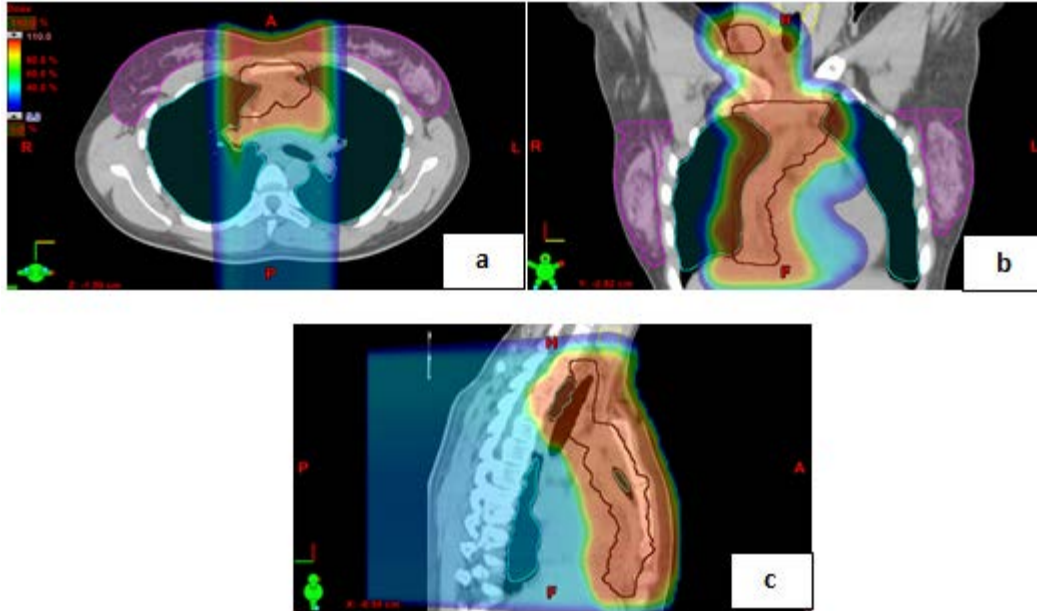


Figure 2-11 – Proton primary dose distribution example - Colorwash of the dose distribution (100% = 36 Sv) for Patient #4. The CTV (rendered in black), breast (rendered in magenta), lung (rendered in sky blue) and thyroid (rendered in yellow) are visible in the various orientations. a) Axial, b) Coronal, and c) Sagittal renderings showing a 2 field AP/PA setup for the proton PSPT treatment plan. Note the reduced doses outside the treatment volume relative to the photon IMRT plan.

2.3.3. – Characteristics and Images of Stray Dose Distributions

The addition of the stray dose not included in the commercial TPS is shown here. Visualization of the photon stray dose calculation below the 5% isodose line of the commercial TPS is not included in this study, but the dose distributions of the neutron contributions, both external and internal, from the proton treatment plans are shown.

2.3.3.i. Stray dose for the photon treatment plan

The equation which best fit the data was a power function (Eq. 2.3) that correlated to the TLD measured data with an R^2 value of 0.9879. The following graph shows the fit of the TLD dose measurements to the equation used to replace the voxels below the 5% isodose threshold.

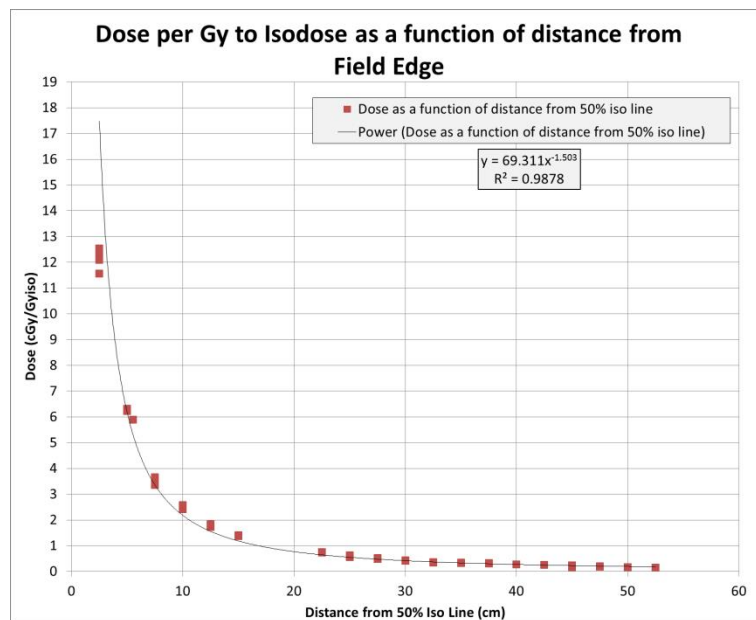


Figure 2-12 – Photon out-of-field analytical model - Comparison of TLD dose measurements in the anthropomorphic phantom as a distance from the 50% isodose line. The power function shows a strong correlation of determination to the data.

Table 2.11 shows the increase in the mean dose after the application of the analytical model to regions of the various OARS that fell below the 5% isodose line in the commercial TPS.

Table 2-11 – Percent increase in mean dose to OARs after photon scatter dose model correction - Percent Increase (%) in the mean dose to each OAR averaged over all patients after the photon scatter dose model was implemented. Since this model was only used on voxels which were below the 5% isodose value, only a small portion of the voxels received a modification. A significant enough adjustment in the mean dose to an OAR that results in a change in the mean RRR from > 1 (indicating the mean dose to the photon plan was less than the proton plan) to < 1 (indicating the opposite) is worth noting. This occurred for the total breast and total lung. For total breast one PSPT plan (Patient #5) decreased the mean RRR from > 1 to < 1 as a result of the increased dose. For the IMPT plan, 3 patients (#1,4, and 5) decreased the mean RRR from >1 to < 1. The average increase in mean dose for these three patients after the scatter correction was added was 15.3%. For total lung, no changes were observed for the PSPT comparison and only Patient #8 changed when comparing IMPT.

	Breast	Lung	Thyroid
Mean Dose for IMXT Plan of All Patients <u>Before</u> Correction (Sv)	6.64	11.92	11.09
Mean Dose for IMXT Plan of All Patients <u>After</u> Correction (Sv)	7.60	12.23	11.60
Percent Increase in Mean Dose to OAR (%)	14.48	2.60	4.56

2.3.3.ii. Stray dose for the proton treatment plans

The addition of the Monte Carlo calculated neutron dose is displayed below. The mean radiation weighting factors, $\overline{w_R}$, applied to the neutron calculations was 20 (Eq. 2.1). External neutron images are shown in Figure 2.13 and internal neutrons are shown in Figure 2.14.

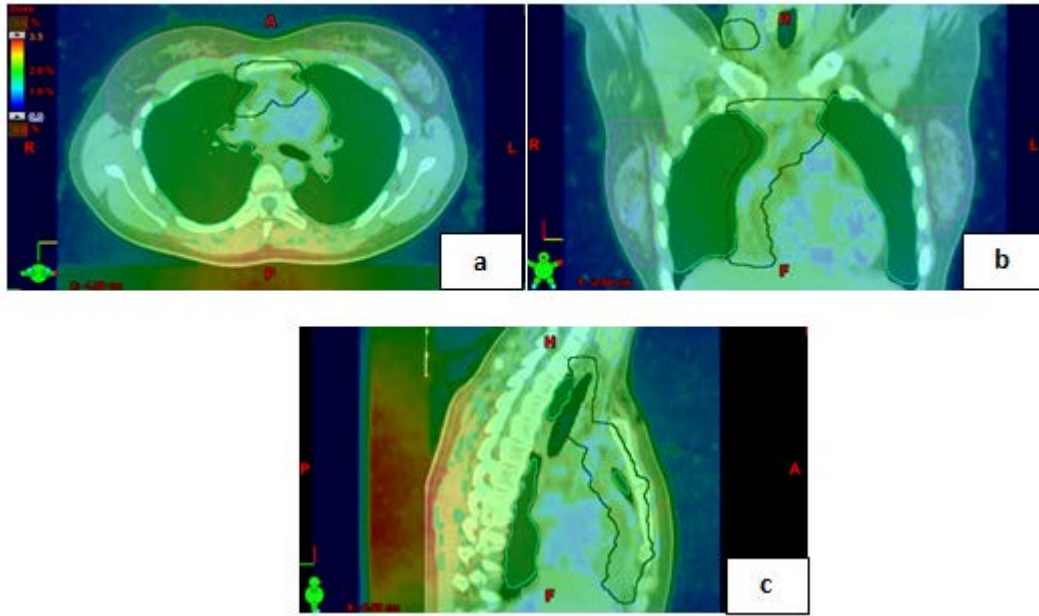


Figure 2-13 – Proton treatment external neutron dose distribution example - Colorwash of the external neutron dose (neutron $\overline{w_R} = 20$) distribution (100% = 36 Sv) for Patient #4. The CTV (rendered in black), breast (rendered in magenta), lung (rendered in sky blue) and thyroid (rendered in yellow) are visible in the various orientations. a) Axial, b) Coronal, and c) Sagittal renderings showing a 2 field AP/PA setup for the proton PSPT treatment plan. Note that the dose distribution range shown is only up to 3.5% of the prescribed dose. The external neutron dose is fairly evenly distributed throughout the patient as was expected due to the formation occurring upstream in the treatment nozzle.

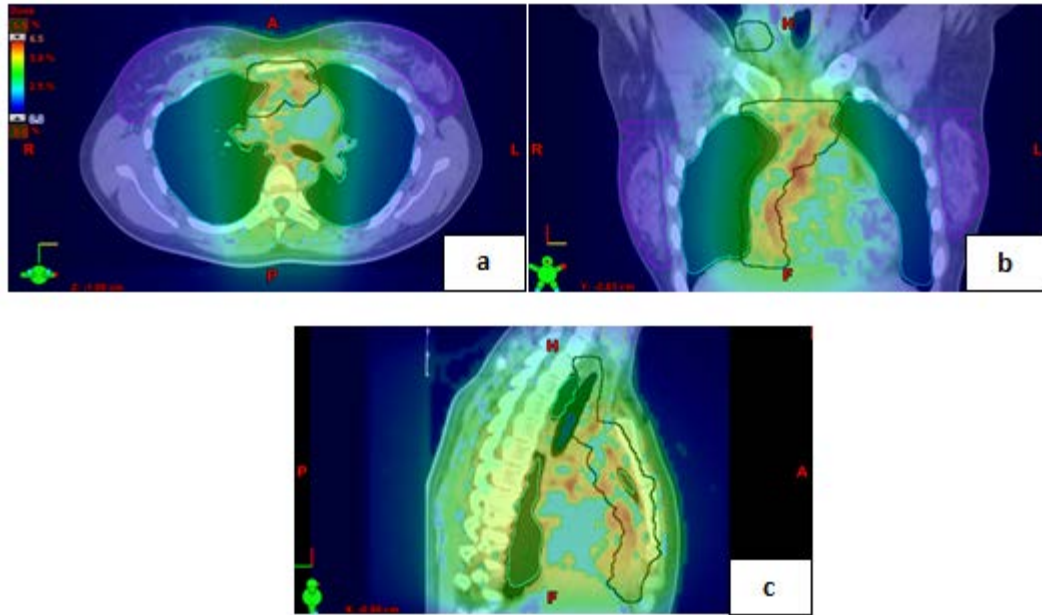


Figure 2-14 – Proton treatment internal neutron dose distribution example - Colorwash of the internal neutron dose (neutron $\overline{w}_R = 20$) distribution (100% = 36 Sv) for Patient #4. The CTV (rendered in black), breast (rendered in magenta), lung (rendered in sky blue) and thyroid (rendered in yellow) are visible in the various orientations. a) Axial, b) Coronal, and c) Sagittal renderings showing a 2 field AP/PA setup for the proton PSPT treatment plan. Note that the dose distribution range shown is only up to 6.5% of the prescribed dose. The internal neutron dose is concentrated in the vicinity of the treatment volume since production mainly occurs inside the treatment field.

The mean equivalent dose for neutrons per prescribed Gray to the tumor volume (cSv/Gy) in the OARs are shown in Figure 2.15 assuming neutron $\overline{w}_R = 20$. To determine the total mean equivalent dose (cSv), multiple the value by the prescribed dose of 36 Gy.

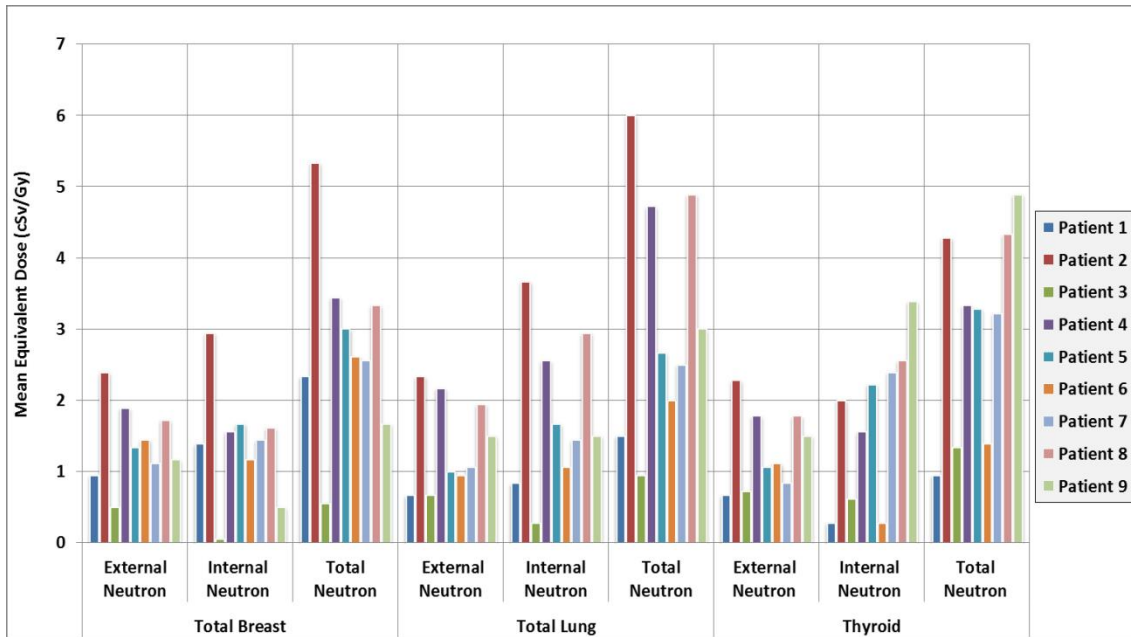


Figure 2-15 – Mean equivalent neutron dose for protons per patient per prescribed Gy – neutron $\overline{w_R} = 20$
 - Graph depicting the breakdown of neutron equivalent dose contributions per patient per Gy prescribed dose with neutron $w_r = 20$. Averaged over all patients, the mean total neutron equivalent dose contribution was 2.8 cSv/Gy for total breast, 3.1 cSv/Gy for total lung, and 3.0 cSv/Gy for thyroid.

2.3.4. – Total Dose and Relative Risk Calculations

In order to ultimately determine the RRR, the equivalent dose (Sv) and relative risk (RR) for each treatment must be calculated. Figure 2.16 shows the mean equivalent dose for each OAR for each treatment plan. Recall that these values include the adjusted scatter dose beyond the 5% isodose line for the photon IMRT plan and the neutron dose for both proton plans. Figure 2.17 shows the RR for the same endpoints.

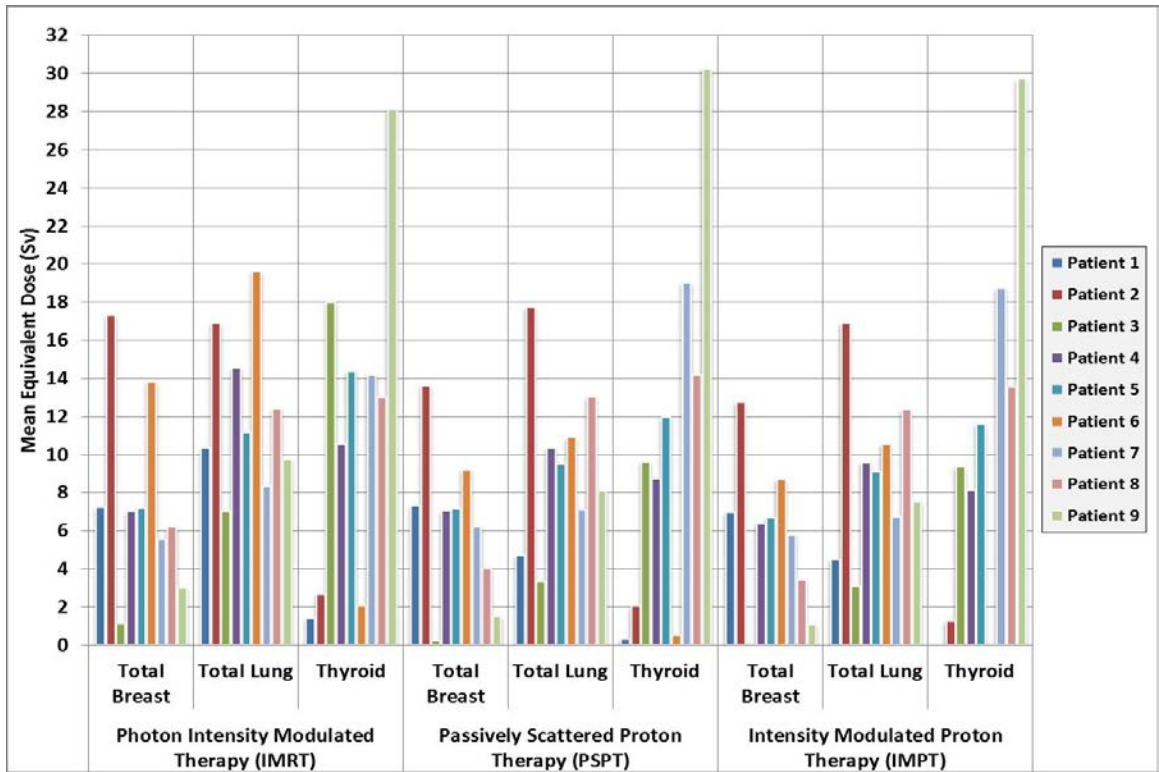


Figure 2-16 – Mean equivalent dose to OAR – neutron $\overline{w}_R = 20$ - Graph showing the mean equivalent dose to each OAR for the various treatment plans for the prescribed 36 Gy treatment. While there are several examples contrary to this trend, in general, IMPT < PSPT < IMRT with respect to the mean equivalent dose per organ. PSPT > IMPT slightly since the IMPT plans do not include external neutron dose.

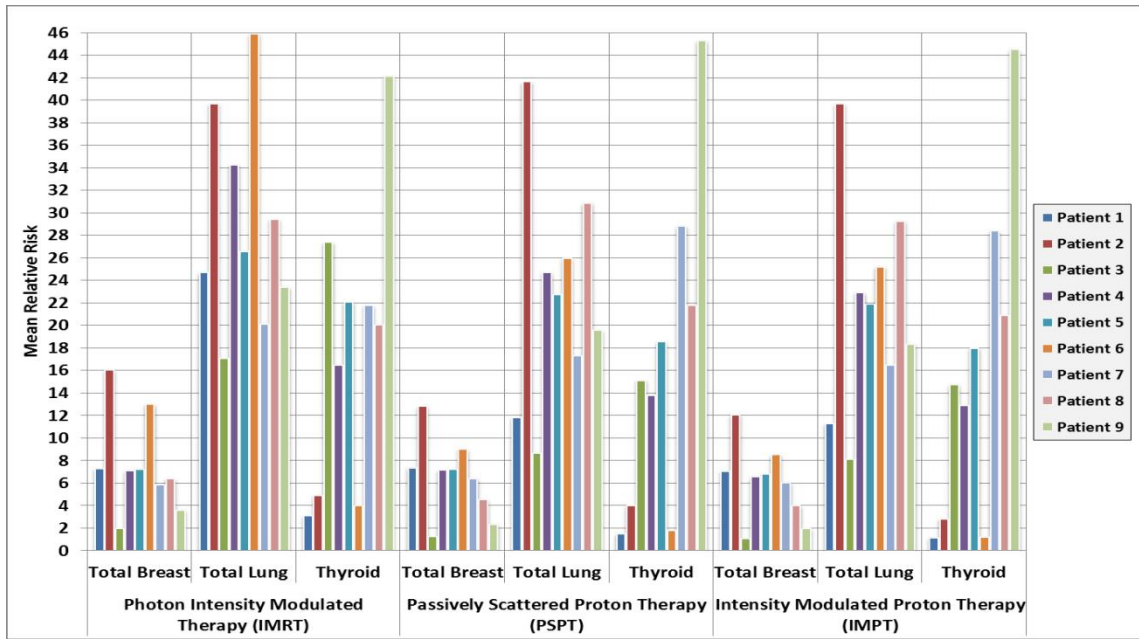


Figure 2-17 – Mean relative risk to OAR (Sv) - neutron $\bar{w}_R = 20$ - LNT dose response model - Graph showing the mean RR for each OAR for the various treatment plans for the prescribed 36 Gy treatment. Since this is based off of the LNT dose response model, the same trends seen in Figure 2.14 are mirrored here. Unlike the dose, however, we see the differences in the risk models of different OARs for relatively similar dose values. Note the dose for the breast and lung for the IMRT plan and then compare the ~ 3x increase in lung risk relative to the corresponding breast risk.

2.3.5. – Propagation of Uncertainties

Since the values found using the derived propagation of uncertainty from Table 2.4 are used in all of the \overline{RRR} data forthcoming, a small interlude is inserted here to elaborate on which factors contributed the most to the uncertainty. The individual components of Eq. 2.22 were averaged per organ for the nine patients and calculated to determine which component contributed the greatest portion to the uncertainty values. The Table 2.12 shows the breakdown.

Table 2-12 – % contribution breakdown of propagation of uncertainty error for LNT dose response model - Shows the breakdown of which component is most responsible for the error in the Mean RRR calculations. Overwhelmingly the proton dose is the largest source of error for all three OARs. This was largely due to the lack of dependence the proton and photon components have on β (see Table 2.4). There was a wide variation within the OARs as to the source of the uncertainty as well. This was a result of the uncertainty (σ) in β relative to the nominal β value of the particular OAR. For example, lung has a much larger nominal β (1.40) relative to its σ (0.29) compared to thyroid, which has almost equivalent β and σ (1.05 and 0.91, respectively).

Organ	$\left(\frac{\partial \overline{RRR}_{LNT_j}}{\partial \beta_j}\right)^2 \sigma_{\beta_j}^2$	$\left(\frac{\partial \overline{RRR}_{LNT_j}}{\partial C_j}\right)^2 \sigma_{C_j}^2$	$\left(\frac{\partial \overline{RRR}_{LNT_j}}{\partial H_{Proton_j}}\right)^2 \sigma_{H_{Proton_j}}^2$	$\left(\frac{\partial \overline{RRR}_{LNT_j}}{\partial H_{Photon\ IMRT_j}}\right)^2 \sigma_{H_{Photon\ IMRT_j}}^2$
Breast	4%	-	93%	3%
Lung	0%	-	83%	17%
Thyroid	10%	-	89%	1%

2.3.6. – Ratio of Relative Risk

After calculation of the mean RR for each treatment plan, the various \overline{RRR} discussed in Table 2.3 were calculated. Table 2.13 shows the PSPT \overline{RRR} s and their specific uncertainties (from for Eq. 2.13).

Table 2-13 \overline{RRR} –for LNT dose response model, PSPT plan comparison - All mean \overline{RRR} s ($\overline{RRR}_{j,k}$, \overline{RRR}_j) with their respective uncertainties are shown for the Proton PSPT plan vs the Photon IMRT plan. The majority of $\overline{RRR}_{j,k}$ are < 1 , but several patients for specific OARs showed $\overline{RRR}_{j,k} > 1$ indicating the lack of a class solution for all patients or OARs. All \overline{RRR}_j were < 1 , however.

Mean RRR		OAR		
		Mean RRR Breast $\overline{RRR}_{j,k}$	Mean RRR Lung $\overline{RRR}_{j,k}$	Mean RRR Thyroid $\overline{RRR}_{j,k}$
Treatment Plan	Proton - PSPT			
Dose Response Model	LNT			
Response Inflection Pt (α)	-			
Exposed Age (e)	26			
Attained Age (a)	46			
Neutron W_r	20			
Patient	Patient 1	1.01 ± 0.10	0.48 ± 0.05	0.48 ± 0.25
	Patient 2	0.80 ± 0.08	1.05 ± 0.11	0.82 ± 0.08
	Patient 3	0.62 ± 0.11	0.51 ± 0.05	0.55 ± 0.06
	Patient 4	1.01 ± 0.10	0.72 ± 0.07	0.84 ± 0.08
	Patient 5	1.00 ± 0.10	0.86 ± 0.09	0.84 ± 0.09
	Patient 6	0.69 ± 0.07	0.57 ± 0.06	0.44 ± 0.20
	Patient 7	1.09 ± 0.10	0.86 ± 0.08	1.32 ± 0.14
	Patient 8	0.71 ± 0.07	1.05 ± 0.11	1.09 ± 0.11
	Patient 9	0.64 ± 0.07	0.84 ± 0.08	1.07 ± 0.12
	Mean RRR for a Given OAR for All Patients \overline{RRR}_j	0.84 ± 0.03	0.77 ± 0.03	0.83 ± 0.05

Figure 2.18 shows a graphical representation of each individual $\overline{RRR}_{j,k}$ in Table 2.13 and their associated uncertainties.

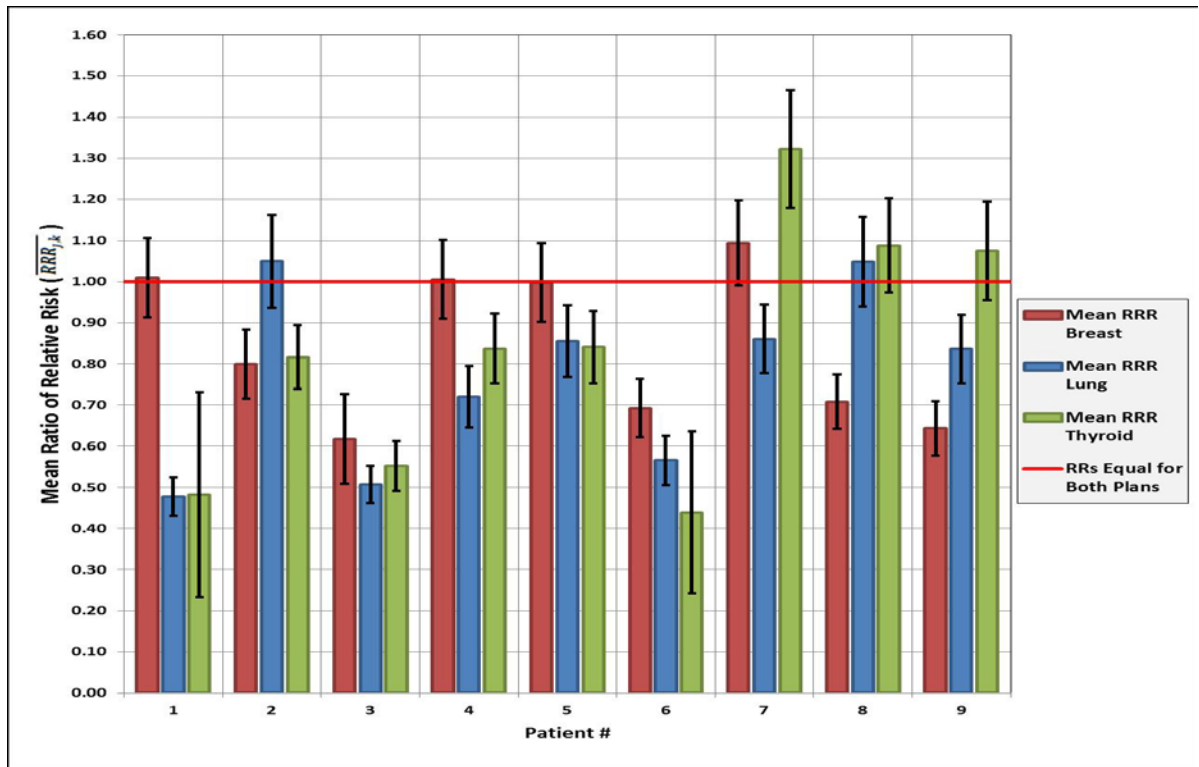


Figure 2-18 – $\overline{RRR}_{j,k}$, PSPT vs IMRT, LNT dose response model, exposed age (e) = 26, attained age (a) = 46, neutron $\overline{w}_R = 20$ - Each of the three OARs are shown for all 9 patients. The red line is set at 1 and is used to indicate whether the specific OAR for each patient shows a decreased risk of RSC for the proton treatment (< 1) or the photon treatment (> 1). 18 out of the 27 individual OARs in the graph have values below 1 (including error bars). Of note, the patients with the lowest $\overline{RRR}_{j,k}$ (Patient #3 and #6) had only 1 field proton plans and patients with the highest $\overline{RRR}_{j,k}$ (Patients #7, #8, and #9) were significantly younger than the average age of the cohort.

Table 2.14 and Figure 2.19 display the same information as Table 2.13 and Figure 2.18, respectively, but for the Proton IMPT plan vs the Photon IMRT plan rather than the Proton PSPT plan.

Table 2-14 – \overline{RRR} for LNT dose response model, IMPT plan comparison - All mean RRRs ($\overline{RRR}_{j,k}$, \overline{RRR}_j) with their respective uncertainties are shown for the Proton IMPT plan vs the Photon IMRT plan. All mean RRRs are lower with the IMPT plan compared to the PSPT, which was expected due to the absence of the external neutron dose. There are still several patients for specific OARs which showed $\overline{RRR}_{j,k} > 1$ but that number is reduced. As with PSPT all \overline{RRR}_j were < 1 .

Mean RRR		OAR		
		Mean RRR _{Breast}	Mean RRR _{Lung}	Mean RRR _{Thyroid}
Treatment Plan	Proton - IMPT	$\overline{RRR}_{j,k}$	$\overline{RRR}_{j,k}$	$\overline{RRR}_{j,k}$
Dose Response Model	LNT			
Response Inflection Pt (α)	-			
Exposed Age (e)	26			
Attained Age (a)	46			
Neutron W_r	20			
Patient	Patient 1			
	Patient 2	0.75 ± 0.08	1.00 ± 0.11	0.57 ± 0.12
	Patient 3	0.54 ± 0.13	0.47 ± 0.04	0.54 ± 0.06
	Patient 4	0.92 ± 0.09	0.67 ± 0.07	0.78 ± 0.08
	Patient 5	0.94 ± 0.09	0.82 ± 0.08	0.82 ± 0.09
	Patient 6	0.66 ± 0.07	0.55 ± 0.06	0.29 ± 0.25
	Patient 7	1.03 ± 0.10	0.82 ± 0.08	1.30 ± 0.14
	Patient 8	0.62 ± 0.06	0.99 ± 0.10	1.04 ± 0.11
	Patient 9	0.54 ± 0.08	0.78 ± 0.08	1.06 ± 0.12
	Mean RRR for a Given OAR for All Patients \overline{RRR}_j	0.77 ± 0.03	0.73 ± 0.03	0.75 ± 0.05

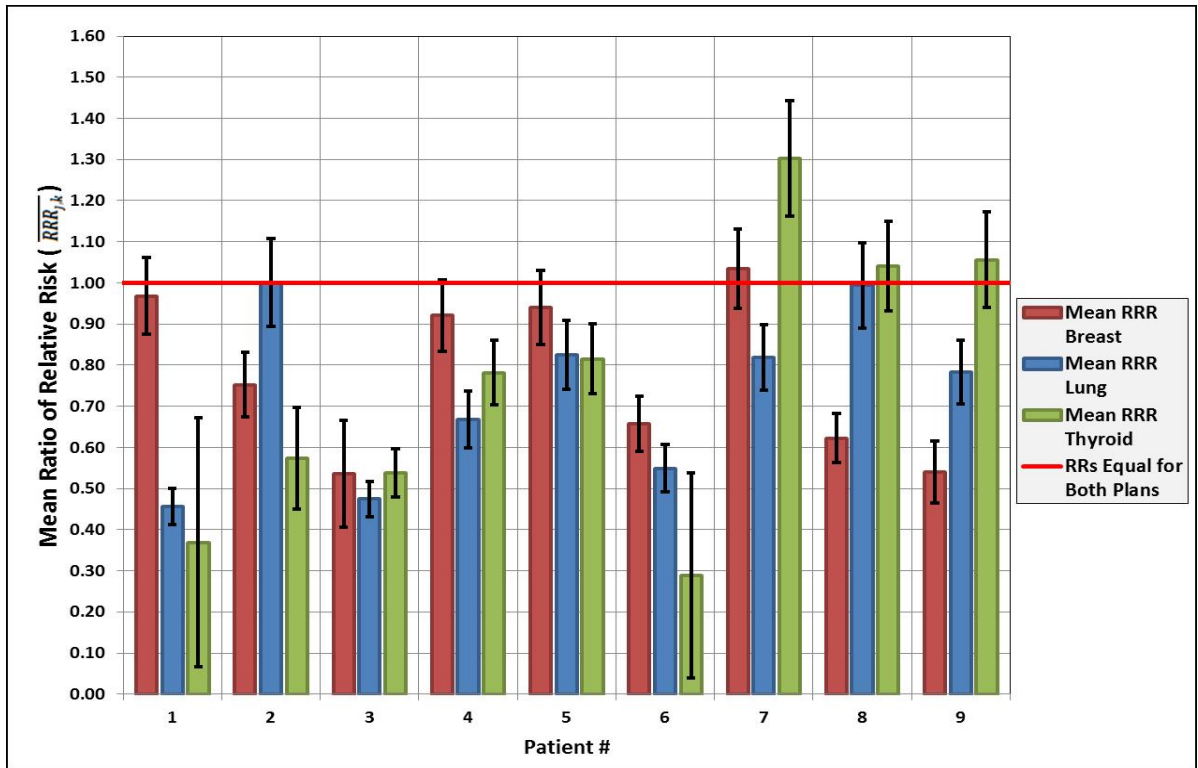


Figure 2-19 – $\overline{RRR}_{j,k}$, IMPT vs IMRT, LNT dose response model, exposed age (e) = 26, attained age (a) = 46, neutron $\overline{w}_R = 20$ - Each of the three OARs are shown for all 9 patients. The red line is set at 1 and is used to indicate whether the specific OAR shows a decreased risk of RSC for the proton treatment (< 1) or the photon treatment (> 1). 18 out of the 27 individual OARs in the graph have values below 1 (including error bars). Again, the patients with the lowest $\overline{RRR}_{j,k}$ (Patient #3 and #6) had only 1 field proton plans and patients with the highest $\overline{RRR}_{j,k}$ (Patients #7, #8, and #9) were significantly younger than the average age of the cohort.

Graph for \overline{RRR}_j which compare the values for the Proton PSPT plan vs the Proton IMPT plan is shown in Figure 2.20.

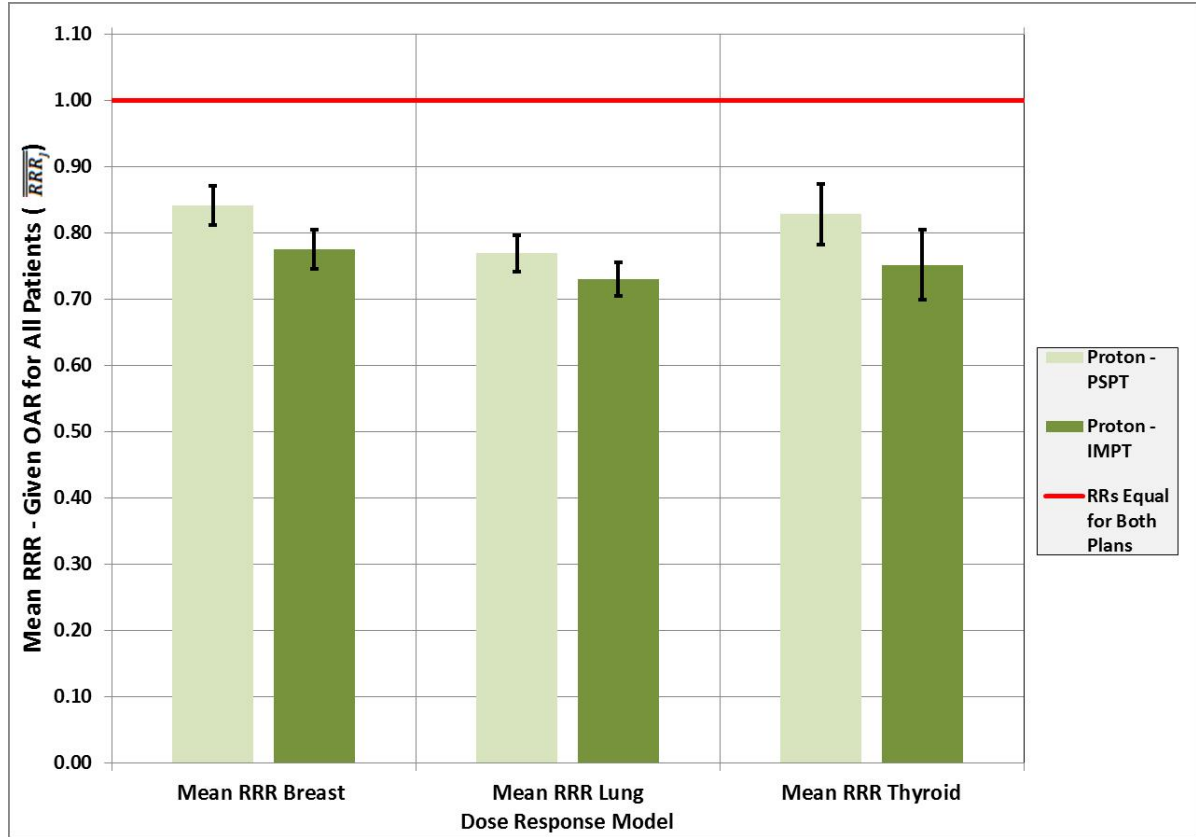


Figure 2-20 – \overline{RRR}_j , proton plans vs IMRT, LNT dose response model, exposed age (e) = 26, attained age (a) = 46, neutron $\overline{w}_R = 20$ - Again, the IMPT plan has a lower \overline{RRR}_j compared to the PSPT plan. The red line is set at 1 and is used to indicate whether the specific bar graph shows a decreased risk of RSC for the proton treatment (< 1) or the photon treatment (> 1). All iterations showed a lower risk of RSC for the proton plans compared to their respective photon plan.

2.3.7. – Statistical Tests for Significance

The Sign and Student’s T-test were calculated for each patient’s $\overline{RRR}_{j,k}$ and tabulated in the tables below. Statistical significance was stated (if any was found) for both the Proton PSPT and IMPT plans and for all of the OARs. In addition, the uncertainty of each $\overline{RRR}_{j,k}$ was taken into account by comparing the number of plans < 1 for the nominal $\overline{RRR}_{j,k}$ values, the nominal $\overline{RRR}_{j,k}$ plus the associated uncertainty, and the nominal $\overline{RRR}_{j,k}$ minus the associated uncertainty.

2.3.7.i. Sign Test

The sign test indicated that for the nine patients considered, the proton PSPT plan was not significantly different from the photon plans when comparing their values for each OAR ($\overline{RRR}_{j,k}$). For the proton IMPT plan vs IMRT comparisons, results showed a significant reduction in RR for the IMPT plan for the nominal total breast and total lung. Results are shown in Table 2.15.

Table 2-15 – Sign test results, LNT dose response model, exposed age (e) = 26, attained age (a) = 46, neutron $\overline{w}_R = 20$ - Graph showing the sign test results for each individual OAR tested ($\overline{RRR}_{j,k}$). In order to show significance for the proton plan, at least 8 of the 9 patients had to have a $\overline{RRR}_{j,k}$ value < 1. For the photon plan to show significance, 1 or less of the 9 patients had to have a $\overline{RRR}_{j,k}$ value > 1. Columns with just the OAR name (i.e. Breast, Lung, Thyroid) indicates the nominal $\overline{RRR}_{j,k}$ values. Columns with the OAR name plus the calculated uncertainty (i.e. Breast w/ + Error, etc.) indicates the nominal $\overline{RRR}_{j,k}$ plus its corresponding error, and columns with the OAR name minus the calculated uncertainty (i.e. Breast w/ - Error, etc.) indicates the nominal $\overline{RRR}_{j,k}$ minus the corresponding error. Proton PSPT results are shown on top followed by the Proton IMPT results. Yellow boxes indicate instances of no significance between the given proton plan vs the photon IMRT plan. The PSPT plan showed no significant decrease in RSC risk compared to the IMRT plan. The IMPT plan showed a significant decrease in RSC risk compared to the IMRT plan for breast and lung.

Treatment Type Compared to IMRT	Parameters	Breast w/ - Error	Breast	Breast w/ + Error	Lung w/ - Error	Lung	Lung w/ + Error	Thyroid w/ - Error	Thyroid	Thyroid w/ + Error
PSPT	# of Patients with Mean $\overline{RRR} < 1$	9	6	5	9	7	7	8	6	6
	Treatment Modality Significantly Better?	Protons	None	None	Protons	None	None	Protons	None	None
IMPT	# of Patients with Mean $\overline{RRR} < 1$	9	8	5	9	8	7	8	6	6
	Treatment Modality Significantly Better?	Protons	Protons	None	Protons	Protons	None	Protons	None	None

2.3.7.ii. Student’s T-Test

Student’s t-test, which unlike the sign test, takes accounts of the magnitude of the mean RRRs, showed a significant decrease in RSC cancer risk for the Proton PSPT plan compared to the Photon IMRT plan. The thyroid was the only OAR that did not indicate a significant decrease in RSC cancer risk for the PSPT plan. For the Proton IMPT plan, results showed also showed a significant decrease in RSC cancer risk for total breast and total lung compared to the photon plan. Results are shown in Table 2.16.

Table 2-16 – Student’s t-test results, LNT dose response model, exposed age (e) = 26, attained age (a) = 46, neutron $\overline{w_R} = 20$ - Graph showing Student’s t-test results for each individual OAR tested ($\overline{RRR}_{j,k}$). Proton PSPT results are shown first followed by the Proton IMPT results. Since the t-test does not count the number of patients above or below the $\overline{RRR}_{j,k}$ value of 1 to calculate significance (it does take into account the magnitude of the mean RRR, however) the table only displays whether one modality or the other showed significance. The PSPT and IMPT plan showed a significant decrease in RSC risk compared to the IMRT plan for both the total breast and total lung. No significance was found for either plan with respect to the thyroid, however, unless the uncertainty was subtracted. Also of note, the IMRT plan showed no statistical significance in any iteration.

Treatment Type Compared to IMRT	Parameter	Breast w/ - Error	Breast	Breast w/ + Error	Lung w/ - Error	Lung	Lung w/ + Error	Thyroid w/ - Error	Thyroid	Thyroid w/ + Error
PSPT	Treatment Modality Significantly Better?	Protons	Protons	None	Protons	Protons	None	Protons	None	None
IMPT	Treatment Modality Significantly Better?	Protons	Protons	None	Protons	Protons	Protons	Protons	None	None

Statistical tests for this section show mixed results, depending on the test used and the OAR examined highlighting the need to analyze each patient and their subsequent unique treatment parameters in order to determine the correct plan to proceed with. Generally, however, the proton plan more often than not showed a better mean RR outcome than IMRT, which never showed a significant improvement compared to either proton plans.

2.3.8. – Patient Treatment Variation Effects on mean RRR

Treatment and host specific factors were compared for each patient by comparing the specified factor to $\overline{RRR}_{j,k}$ looking for any correlation via the coefficient of determination (R^2). As there was no indication that another model was to be expected, a linear fit was used for all plots. Correlations were examined between the mean RRR per patient and the following corresponding treatment and host specific characteristics (CTV was used as the reference contour since it is the same for both photon and proton plans): The different factors examined were CTV volume (cc), age (Years) at exposure (e), body mass index (BMI) (kg/m^2), OAR volume (cc), patient width at the CTV centroid location both in the lateral and antero-posterior directions, percent of OAR volume contained within the photon IMRT 50% isodose line (%), and anatomical location of OAR relative to CTV (See Figure 2.9a and 2.9b).

For the majority of parameters, minimal correlation was found. In the interest of space, we show only the parameters that had a R^2 value greater than 0.35 (on a scale of 0 to 1). The minimal R^2 value required to confidently determine a robust coefficient of determination is not set in the field, but a value of 0.35 does not generally indicate a strong correlation. However, a lower R^2 also does not mean there are no possible trends either, so we display only the values that demonstrated our

highest correlation. For this study a minimum correlation of at least 0.4 was found between the mean RRRs and the age (Years) at exposure (e) (thyroid only) and OAR volume (cc) (lung only).

The differences in the R^2 values were minimal between the PSPT and IMPT plans, so the subsequent tests for correlation below will only track the PSPT plans. The IMPT plans will be assumed to follow a similar outcome.

Figure 2.21 shows the coefficient of determination (R^2) between the $\overline{RRR}_{j,k}$ and the age in years at exposure (e). This was one of the few factors that a non-negligible correlation was found.

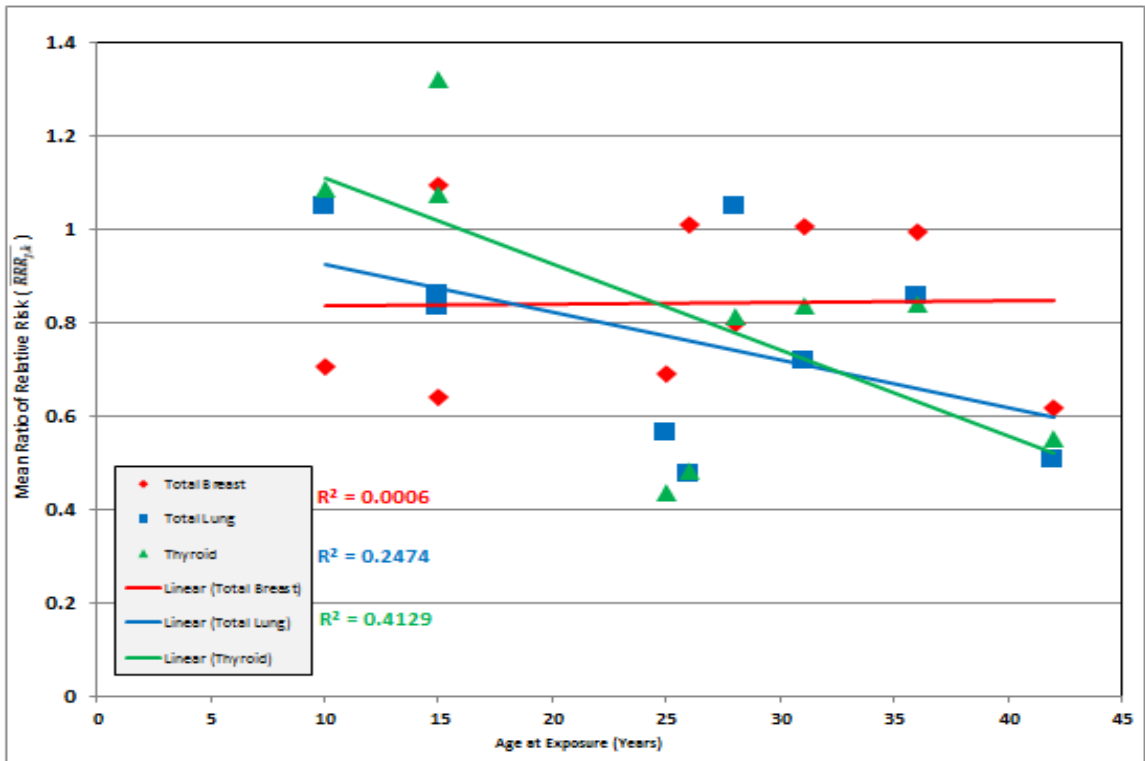


Figure 2-21 – Correlation between $\overline{RRR}_{j,k}$ and age at exposure (years) - The coefficient of determination (R^2) between the $\overline{RRR}_{j,k}$ (for Total Breast (red), Total Lung (blue), and Thyroid (green)) against the patient age at exposure (e). The points in the scatter plot represent the individual mean RRR values for each patient. The lines correspond to the points of the same color's trend line which was used to calculate R^2 . Total Lung and Thyroid (which had the highest correlation) showed weak correlation with the linear model.

Figure 2.22 shows the coefficient of determination (R^2) between the $\overline{RRR}_{j,k}$ and the volume of the total lung, which was the only OAR to show a correlation.

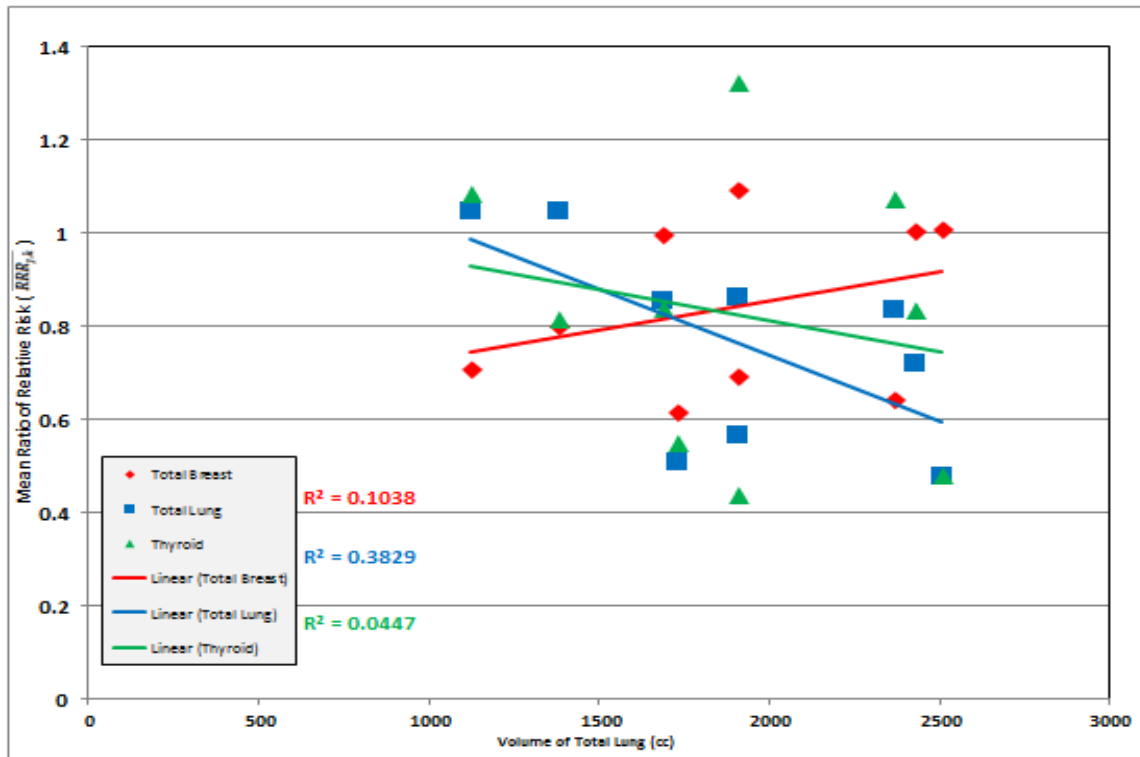


Figure 2-22 – Correlation between $\overline{RRR}_{j,k}$ and volume of total lung (cc) - The coefficient of determination (R^2) between the $\overline{RRR}_{j,k}$ (for Total Breast (red), Total Lung (blue), and Thyroid (green)) against the volume of the total lung (cc). The points in the scatter plot represent the individual mean RRR values for each patient. The lines correspond to the points of the same color's trend line which was used to calculate R^2 . Minimal correlation was found for the Lung $\overline{RRR}_{j,k}$.

A summary of the findings from Aim 1 are presented in Table 2.17 including statistical tests.

Table 2-17 – Summary of all major finding from Aim 1 – Breaks down the results by PSPT and IMPT tests compared to IMRT. Note that the column labeled “Mean for All 9 Patients” averages all 9 of the respective $\overline{RRR}_{j,k}$ values together. These values correspond to \overline{RRR}_j . A mark like this (*) indicates that the given proton plan significantly ($p \leq 0.05$) reduced the risk of RSC compared to IMRT.

Patient Parameters	Metric Examined	Corresponding Table	Mean for All 9 Patients	Sign Test	Student's T-Test	Comment	
e = 26, a = 46, LNT, neutron $\overline{W}_R = 20$	PSPT vs IMRT		Table 2.13				
		$\overline{RRR}_{j,k}$					
		Breast	0.84 ± .03	P = 0.503	P = 0.033*	Majority of tests showed decreased RSC risk for PSPT, but statistical significance was only seen if magnitude was taken into account	
		Lung	0.77 ± .03	P = 0.184	P = 0.013*		
		Thyroid	0.83 ± .05	P = 0.503	P = 0.124		
		IMPT vs IMRT		Table 2.14			
		$\overline{RRR}_{j,k}$					
		Breast	0.77 ± .03	P = 0.046*	P = 0.008*	Increased significance was seen for IMPT compared to PSPT. Thyroid still showed no significant difference in RSC risk between the two Plans	
		Lung	0.73 ± .03	P = 0.046*	P = 0.004*		
		Thyroid	0.75 ± .05	P = 0.503	P = 0.060		

3. Specific Aim 2: Confidence intervals of predicted mean RR values

3.1. Introduction

Specific Aim 1 was designed to limit patient variability when calculating the mean RRR. In that aim, the patients were assumed to have received their treatments at the same age ($e = 26$), attained the same age in life ($a = 46$), had the same mean RBE of neutrons for carcinogenesis radiation weighting factor ($\bar{w}_r = 20$), and had the same dose response model when calculating their risk (LNT).

Although those results led to a certain level of confidence, their outcomes fail to account for the wide range of variation (i.e. the age of exposure and the attained age) or the uncertainty in the values and/or models assigned (i.e the neutron \bar{w}_R and the dose response model). These limitations can lead to reduced confidence in the results. To address this issue, sensitivity tests, which varied these host and treatment factor parameters throughout their uncertainty intervals, were systematically conducted for each patient and compared.

Addressing and displaying every permutation for each variable would require an excessive amount of data. To alleviate this dilemma, select configurations which emphasize the changes (if any) in the outcome were selected. To further simplify the process and assist in easier comparisons to the previous results in this work, the patient parameters used in Aim 1 were also used in Aim 2 ($e = 26$, $a = 46$) for the majority of our analysis. Ages are varied only when the extrema of the mean RRR results are examined.

Section 3.2.1 lists the parameters included in the sensitivity tests. Section 3.2.2 details the rationale behind our sensitivity tests. Section 3.2.3 describes the impact of non-linear dose response models on the risk calculations from Aim 1. Section 3.2.4 describes varying \bar{w}_R for neutrons. Section 3.2.5 outlines the propagation of uncertainties for non-linear dose response models. Section 3.2.6 details our method of analyzing the results from the sensitivity tests. Finally, Section 3.2.7 describes a method to analyze extrema in our findings.

3.2. Methods and Materials

3.2.1. – Adjusted Variables Used for the Sensitivity Tests

The parameters varied for the sensitivity tests in Aim 2 were (Note: **Bold** if value was used previously for Aim 1)

- Exposed Age of Patient (e)
 - 10 – minimum age of patients in cohort study
 - **26 – mean age of patients in cohort study**
 - 42 – maximum age of patients in cohort study
- Attained Age of Patient (a)
 - e+20 (30, **46**, 62)
 - e+50 (60, 76, 92)
- Dose Response Model
 - **Linear Non Threshold (LNT)**
 - Linear Plateau (Lin Plat)
 - Linear Exponential (Lin Exp)
- Dose Response Model Inflection Point (α)
 - 0.090 – corresponds to an inflection point at 10 Sv
 - **0.025 – corresponds to an inflection point at 40 Sv. This parameter was not used for Aim 1 since α is not included in the LNT risk equation. However, when the sensitivity tests are conducted, this value rather than 0.090 was used since it more closely reflects the LNT model when used with the Lin Plat and Lin Exp models.**
- Mean RBE of neutrons for carcinogenesis radiation weighting factor (neutron $\overline{w_R}$)
 - 5
 - **20**
 - 35

All combinations of these parameters were examined for each patient (#1-9), treatment plan (Proton – PSPT, Proton – IMPT, Photon – IMRT), and OAR’s (Total Breast, Total Lung, Thyroid) various mean RRR values.

3.2.2. – Rationale for Sensitivity Tests

BEIR VII and RadRAT risk models were intended for whole body/organ, low dose photon exposures of ~2-3 Sv. BEIR VII and RadRAT also assume a linear non threshold (LNT) dose response model, which states that as dose increases; the risk of developing a second cancer linearly increases as well. In this work, our patient population deviated from these criteria as follows:

1. Low dose photon exposures
 - a. Portions of patients’ OARs were exposed to high dose values (potentially in excess of the prescribed dose of 36 Gy)

- b. Neutron doses and their possible radiobiological variations from photon exposures were not taken into account.
2. Dose response model
- a. While current epidemiological studies of medically irradiated RSC formation indicates most organs appear to follow the LNT response (Berrington de Gonzalez et al., 2013), follow-ups to this point still require larger patient cohorts and longer follow-up times before definitive conclusions can be drawn.
 - b. A small number of organs of interest, including the thyroid, have been shown to deviate from the linear RSC response of the LNT model at high dose exposures (Sigurdson et al., 2005, Ronckers et al., 2006, Bhatti et al., 2010).

While error and uncertainty are inherent in all experimentation, the values associated with these parameters can be quite large. While not always considered realistic or likely, they are still nonetheless worth examining. The rationale was to show the range of values for the RSC risk values if one takes into account these intervals. Doing so allowed us to quantify at what point, if any, a treatment technique (i.e. proton or photon) that was shown to be superior with respect to RSC risk for a given set of conditions no longer maintains that advantage.

Additionally, to account for the non-homogenous dose distributions in each patient, each voxel contained within the OAR was calculated for risk individually (or the specific sensitivity tests included in this section) and then summed and averaged to determine the average risk to the OAR.

3.2.3. - Non-linear Dose Response Models

RadRAT and BEIR VII use the LNT model to determine the risk values for a given dose to a patient's particular OAR. Two alternative dose response models that introduce a reduction in RSC incidence at higher dose levels due to cell response saturation or cell sterilization, named linear-plateau and linear-exponential, have been shown to be plausible solutions for RSC risk calculations (Lindsay et al., 2001, Hall, 2004, Dasu and Toma-Dasu, 2005, Schneider et al., 2005, Sigurdson et al., 2005, Ronckers et al., 2006, Bhatti et al., 2010). Using a format previously employed in our group (Fontenot et al., 2009, Rechner et al., 2012a), linear-plateau and linear-exponential models with inflection points at 10 Sv ($\alpha = 0.090$) and 40 Sv ($\alpha = 0.025$) were incorporated. These values were selected because they covered the range seen in previous follow-up studies involving medically exposed patient populations (Schneider and Kaser-Hotz, 2005, Travis, 2006, Fontenot et al., 2009).

For the non-linear dose response models above, in order to correctly calculate the RR and subsequently the RRR, the dose must be multiplied by the dose response model on a voxel by voxel basis due to the inhomogeneous dose distributions to the OAR following the same form as Eq. 2.9.

3.2.3.i. Linear-plateau equation

The equation for the linear-plateau dose response model was:

$$\overline{RR}_{Lin Plat} = \frac{\sum_i \frac{RR_{LNT_i}}{H_i^\alpha} (1 - e^{-(\alpha \cdot H_i)})}{i} \quad (\text{Eq. 3.1})$$

In this equations $\overline{RR}_{Lin Plat}$ is the modified mean RR using the linear-plateau dose response model, RR_{LNT_i} is the RR using the RadRAT or BEIR VII LNT risk model for an individual voxel, i , H_i is the Equivalent Dose (Sv) in voxel i , α is the tissue specific parameter that accounts for cell response saturation or cell sterilization (Fontenot et al., 2009, Rechner et al., 2012a), and i = individual voxel contained with the specified OAR.

3.2.3.ii. Linear-exponential equation

The equation for the linear-exponential dose response model is

$$\overline{RR}_{Lin Exp} = \frac{\sum_i RR_{LNT_i} \cdot e^{-(\alpha \cdot H_i)}}{i} \quad (\text{Eq. 3.2})$$

In this equations $\overline{RR}_{Lin Exp}$ is the modified mean RR using the linear-exponential dose response model, RR_{LNT_i} is the RR using the RadRAT LNT risk model for an individual voxel, i , H_i is the Equivalent Dose (Sv) in voxel i , α is the tissue specific parameter that accounts for cell response saturation or cell sterilization, and i is the individual voxel contained with the specified OAR. The various dose response models are shown in Figure 3.1.

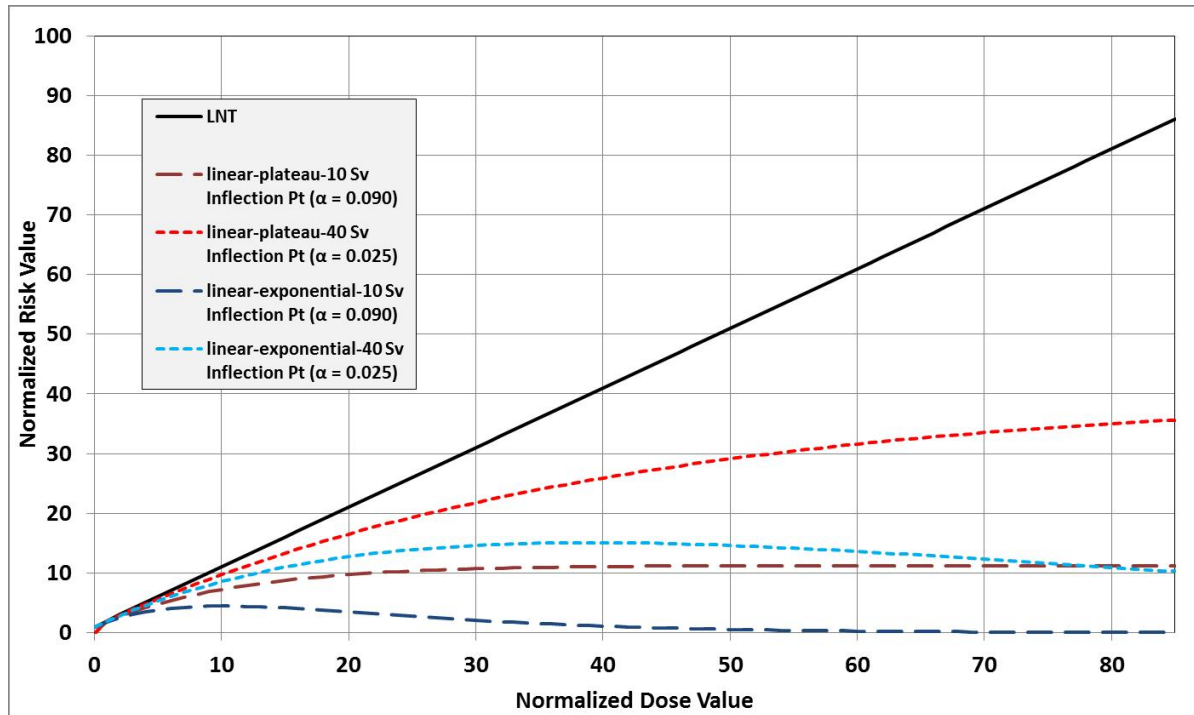


Figure 3-1 – Risk calculation differences between dose response models used - Graph highlighting the differences in risk values for a given dose input to the various dose response models. For the LNT model in this rendering (which the other models are based upon), the risk value increases by one unit for every one unit of increase in dose.

3.2.4. – RBE of Neutrons for Carcinogenesis

In addition to the dose response models, the mean RBE of neutrons for carcinogenesis radiation weighting factor (neutron $\overline{w_R}$) will be varied across the potential range of values. For this work, neutron $\overline{w_R}$ is defined as the radiological protection term. Since it is used for these purposes, the values could be considered conservative. The neutron $\overline{w_R}$ is defined as 1 for photon treatments. For neutrons the value has been stated to be as low as 4 and as high (although this is likely the very upper end of most conservative estimates) as 500 (Kellerer et al., 2006). While these numbers represent the extreme range of possibilities, various studies have estimated more plausible values between 4 and 35 (National Research Council (U.S.). Committee to Assess Health Risks from Exposure to Low Level of Ionizing Radiation., 2006, Brenner and Hall, 2008, Newhauser et al., 2009). Using Eq. 2.1 from earlier, the neutron $\overline{w_R}$ will be varied across the values of 5, 20, and 35 and analyzed for the various dose response models examined above.

3.2.5. – Propagation of Uncertainties for Non-Linear Dose Response Models

Similar to the LNT dose response model, error propagation was conducted on the equations of the Linear Plateau and Linear Exponential Dose Response Models. In addition to the components which comprise Eq. 2.24, an additional term is added to account for the tissue specific parameter that

accounts for cell response saturation or cell sterilization, α . For the Linear Plateau model, we used Eq. 3.3

$$\begin{aligned} \sigma_{\overline{RRR}_{Lin Plat_{j,k}}}^2 &= \left(\frac{\partial \overline{RRR}_{Lin Plat_{j,k}}}{\partial \beta_j} \right)^2 \sigma_{\beta_j}^2 + \left(\frac{\partial \overline{RRR}_{Lin Plat_{j,k}}}{\partial C_{j,k}} \right)^2 \sigma_{C_{j,k}}^2 + \left(\frac{\partial \overline{RRR}_{Lin Plat_{j,k}}}{\partial \overline{H}_{Proton_{j,k}}} \right)^2 \sigma_{\overline{H}_{Proton_{j,k}}}^2 + \\ &\left(\frac{\partial \overline{RRR}_{Lin Plat_{j,k}}}{\partial \overline{H}_{Photon IMRT_{j,k}}} \right)^2 \sigma_{\overline{H}_{Photon IMRT_{j,k}}}^2 + \left(\frac{\partial \overline{RRR}_{Lin Plat_{j,k}}}{\partial \alpha} \right)^2 \sigma_{\alpha}^2 \end{aligned} \quad (\text{Eq. 3.3})$$

Where $\overline{H}_{Proton_{j,k}}$, $\overline{H}_{Photon IMRT_{j,k}}$, β_j , $C_{j,k}$ are the same quantities defined in Eq. 2.22, $\overline{RRR}_{Lin Plat_{j,k}}$ is the mean RRR using the Linear Plateau dose response model, $\sigma_{\overline{RRR}_{Lin Plat_{j,k}}}$ is the uncertainty in $\overline{RRR}_{Lin Plat_{j,k}}$, α is the tissue specific parameter that accounts for cell response saturation or cell sterilization (Fontenot et al., 2009, Rechner et al., 2012a), σ_{β_j} is the known uncertainty in β_j , $\sigma_{C_{j,k}}$ is the known uncertainty in $C_{j,k}$, $\sigma_{\overline{H}_{Proton_{j,k}}}$ is the known uncertainty in $\overline{H}_{Proton_{j,k}}$, $\sigma_{\overline{H}_{Photon IMRT_{j,k}}}$ is the known uncertainty in $\overline{H}_{Photon IMRT_{j,k}}$, and σ_{α} is the known uncertainty in α .

Table 3-1 – Linear Plateau uncertainty terms and stated uncertainty for assigned variables

Quantities	Uncertainty Terms/Stated Uncertainty		
$\left(\frac{\partial RRR_{Lin Plat_{j,k}}}{\partial \beta_j}\right)$	$\left\{ \frac{C_{j,k}(1 - e^{-\alpha \overline{H}_{Proton_{j,k}}})}{\left[\beta_j * C_{j,k} + \left(\frac{1}{\overline{H}_{Photon IMRT_{j,k}}}\right)\right] (1 - e^{-\alpha \overline{H}_{Photon IMRT_{j,k}}})} \right\} \left\{ 1 - \frac{\left[\beta_j * C_{j,k} + \left(\frac{1}{\overline{H}_{Proton_{j,k}}}\right)\right]}{\beta_j * C_{j,k} + \left(\frac{1}{\overline{H}_{Photon IMRT_{j,k}}}\right)} \right\}$		
σ_{β_j}	Breast – 0.14 ERR/Sv	Lung – 0.29 ERR/Sv	Thyroid – 0.91 ERR/Sv
$\left(\frac{\partial RRR_{Lin Plat_{j,k}}}{\partial C_{j,k}}\right)$	$\left\{ \frac{\beta_j(1 - e^{-\alpha \overline{H}_{Proton_{j,k}}})}{\left[\beta_j * C_{j,k} + \left(\frac{1}{\overline{H}_{Photon IMRT_{j,k}}}\right)\right] (1 - e^{-\alpha \overline{H}_{Photon IMRT_{j,k}}})} \right\} \left\{ 1 - \frac{\left[\beta_j * C_{j,k} + \left(\frac{1}{\overline{H}_{Proton_{j,k}}}\right)\right]}{\beta_j * C_{j,k} + \left(\frac{1}{\overline{H}_{Photon IMRT_{j,k}}}\right)} \right\}$		
$\sigma_{C_{j,k}}$	0		
$\left(\frac{\partial RRR_{Lin Plat_{j,k}}}{\partial \overline{H}_{Proton_{j,k}}}\right)$	$\frac{e^{-\alpha \overline{H}_{Proton_{j,k}}} \left[(\alpha * \beta_j * C_{j,k}) + \left(\frac{1 + \alpha \overline{H}_{Proton_{j,k}}}{\overline{H}_{Proton_{j,k}}^2} \right) \right] - \frac{1}{\overline{H}_{Proton_{j,k}}^2}}{(1 - e^{-\alpha \overline{H}_{Photon IMRT_{j,k}}}) \left[\beta_j * C_{j,k} + \left(\frac{1}{\overline{H}_{Photon IMRT_{j,k}}} \right) \right]}$		
$\sigma_{\overline{H}_{Proton_{j,k}}}$	5% of $\overline{H}_{Proton_{j,k}}$		
$\left(\frac{\partial RRR_{Lin Plat_{j,k}}}{\partial \overline{H}_{Photon IMRT_{j,k}}}\right)$	$-\frac{\left\{ \left[\beta_j * C_{j,k} + \left(\frac{1}{\overline{H}_{Proton_{j,k}}} \right) \right] (1 - e^{-\alpha \overline{H}_{Proton_{j,k}}}) \right\} \left\{ \frac{1}{\overline{H}_{Photon IMRT_{j,k}}^2} [e^{-\alpha \overline{H}_{Photon IMRT_{j,k}}} (\alpha * \beta_j * C_{j,k} + (1 - \alpha \overline{H}_{Photon IMRT_{j,k}})) - 1] \right\}}{\left\{ (1 - e^{-\alpha \overline{H}_{Photon IMRT_{j,k}}}) \left[\beta_j * C_{j,k} + \left(\frac{1}{\overline{H}_{Photon IMRT_{j,k}}} \right) \right] \right\}^2}$		
$\sigma_{\overline{H}_{Photon IMRT_{j,k}}}$	3% of $\overline{H}_{Photon IMRT_{j,k}}$		
$\left(\frac{\partial RRR_{Lin Plat_{j,k}}}{\partial \overline{H}_{\alpha}}\right)$	$\left\{ \frac{1}{\left[\beta_j * C_{j,k} + \left(\frac{1}{\overline{H}_{Photon IMRT_{j,k}}} \right) \right] (1 - e^{-\alpha \overline{H}_{Photon IMRT_{j,k}}})} \right\} \left\{ e^{-\alpha \overline{H}_{Proton_{j,k}}} [(\beta_j * C_{j,k} * \overline{H}_{Proton_{j,k}}) + 1] \right\}$ $-\frac{\left\{ \beta_j * C_{j,k} (1 - e^{-\alpha \overline{H}_{Proton_{j,k}}}) + \left[\left(\frac{1}{\overline{H}_{Proton_{j,k}}} \right) (1 - e^{-\alpha \overline{H}_{Proton_{j,k}}}) \right] \right\} \left\{ e^{-\alpha \overline{H}_{Photon IMRT_{j,k}}} [(\beta_j * C_{j,k} * \overline{H}_{Photon IMRT_{j,k}}) + 1] \right\}}{\left\{ \left[\beta_j * C_{j,k} + \left(\frac{1}{\overline{H}_{Photon IMRT_{j,k}}} \right) \right] (1 - e^{-\alpha \overline{H}_{Photon IMRT_{j,k}}}) \right\}}$		
σ_{α}	0		

For the Linear Exponential uncertainty, we used Eq. 3.4.

$$\begin{aligned} \sigma_{\overline{RRR}_{Lin Exp_{j,k}}}^2 &= \left(\frac{\partial \overline{RRR}_{Lin Exp_{j,k}}}{\partial \beta_j} \right)^2 \sigma_{\beta_j}^2 + \left(\frac{\partial \overline{RRR}_{Lin Exp_{j,k}}}{\partial C_{j,k}} \right)^2 \sigma_{C_{j,k}}^2 + \left(\frac{\partial \overline{RRR}_{Lin Exp_{j,k}}}{\partial \overline{H}_{Proton_{j,k}}} \right)^2 \sigma_{\overline{H}_{Proton_{j,k}}}^2 + \\ &\left(\frac{\partial \overline{RRR}_{Lin Exp_{j,k}}}{\partial \overline{H}_{Photon IMRT_{j,k}}} \right)^2 \sigma_{\overline{H}_{Photon IMRT_{j,k}}}^2 + \left(\frac{\partial \overline{RRR}_{Lin Exp_{j,k}}}{\partial \alpha} \right)^2 \sigma_{\alpha}^2 \end{aligned} \quad (\text{Eq. 3.4})$$

Where $\overline{H}_{Proton_{j,k}}$, $\overline{H}_{Photon IMRT_{j,k}}$, β_j , $C_{j,k}$ are the same quantities defined in Eq. 2.22, $\overline{RRR}_{Lin Exp_{j,k}}$ is the mean RRR using the Linear Exponential dose response model, $\sigma_{\overline{RRR}_{Lin Exp_{j,k}}}$ is the uncertainty in $\overline{RRR}_{Lin Exp_{j,k}}$, α is the tissue specific parameter that accounts for cell response saturation or cell sterilization (Fontenot et al., 2009, Rechner et al., 2012a), σ_{β_j} is the known uncertainty in β_j , $\sigma_{C_{j,k}}$ is the known uncertainty in $C_{j,k}$, $\sigma_{\overline{H}_{Proton_{j,k}}}$ is the known uncertainty in $\overline{H}_{Proton_{j,k}}$, $\sigma_{\overline{H}_{Photon IMRT_{j,k}}}$ is the known uncertainty in $\overline{H}_{Photon IMRT_{j,k}}$, and σ_{α} is the known uncertainty in α .

Table 3-2 – Linear Exponential uncertainty terms and stated uncertainty for assigned variables

Quantities	Uncertainty Terms/Stated Uncertainty		
$\left(\frac{\partial RRR_{Ltn Exp_{j,k}}}{\partial \beta_j}\right)$	$\left(\frac{C_{j,k} e^{-\alpha \overline{H_{Proton_{j,k}}}}}{e^{-\alpha \overline{H_{Photon IMRT_{j,k}}} * (\beta_j * C_{j,k} * \overline{H_{Photon IMRT_{j,k}}} + 1)}}\right) \left(\overline{H_{Proton_{j,k}}} - \frac{\overline{H_{Photon IMRT_{j,k}}} (\beta_j * C_{j,k} * \overline{H_{Proton_{j,k}}} + 1)}{\beta_j * C_{j,k} * \overline{H_{Photon IMRT_{j,k}}} + 1}\right)$		
σ_{β_j}	Breast – 0.14 ERR/Sv	Lung – 0.29 ERR/Sv	Thyroid – 0.91 ERR/Sv
$\left(\frac{\partial RRR_{Ltn Exp_{j,k}}}{\partial C_{j,k}}\right)$	$\left(\frac{\beta_j e^{-\alpha \overline{H_{Proton_{j,k}}}}}{e^{-\alpha \overline{H_{Photon IMRT_{j,k}}} * (\beta_j * C_{j,k} * \overline{H_{Photon IMRT_{j,k}}} + 1)}}\right) \left(\overline{H_{Proton_{j,k}}} - \frac{\overline{H_{Photon IMRT_{j,k}}} (\beta_j * C_{j,k} * \overline{H_{Proton_{j,k}}} + 1)}{\beta_j * C_{j,k} * \overline{H_{Photon IMRT_{j,k}}} + 1}\right)$		
$\sigma_{C_{j,k}}$	0		
$\left(\frac{\partial RRR_{Ltn Exp_{j,k}}}{\partial \overline{H_{Proton_{j,k}}}}\right)$	$\frac{e^{-\alpha \overline{H_{Proton_{j,k}}}} [\beta_j * C_{j,k} (1 - \alpha \overline{H_{Proton_{j,k}}}) - \alpha]}{e^{-\alpha \overline{H_{Photon IMRT_{j,k}}} * (\beta_j * C_{j,k} * \overline{H_{Photon IMRT_{j,k}}} + 1)}}$		
$\sigma_{\overline{H_{Proton_{j,k}}}}$	5% of $\overline{H_{Proton_{j,k}}}$		
$\left(\frac{\partial RRR_{Ltn Exp_{j,k}}}{\partial \overline{H_{Photon IMRT_{j,k}}}}\right)$	$\frac{e^{-\alpha \overline{H_{Proton_{j,k}}}} (\beta_j * C_{j,k} * \overline{H_{Proton_{j,k}}} + 1) [\beta_j * C_{j,k} (1 - \alpha \overline{H_{Photon IMRT_{j,k}}}) - \alpha]}{e^{-\alpha \overline{H_{Photon IMRT_{j,k}}} * (\beta_j * C_{j,k} * \overline{H_{Photon IMRT_{j,k}}} + 1)}^2}$		
$\sigma_{\overline{H_{Photon IMRT_{j,k}}}}$	3% of $\overline{H_{Photon IMRT_{j,k}}}$		
$\left(\frac{\partial RRR_{Ltn Exp_{j,k}}}{\partial \overline{H_{\alpha}}}\right)$	$\frac{e^{-\alpha \overline{H_{Proton_{j,k}}}} (\beta_j * C_{j,k} * \overline{H_{Proton_{j,k}}} + 1)}{e^{-\alpha \overline{H_{Photon IMRT_{j,k}}} * (\beta_j * C_{j,k} * \overline{H_{Photon IMRT_{j,k}}} + 1)}} * (\overline{H_{Photon IMRT_{j,k}}} - \overline{H_{Proton_{j,k}}})$		
σ_{α}	0		

For both of these alternative dose response models, the uncertainties (σ) were the same as for the LNT model. There was no uncertainty for the additional uncertainty term, α , since this term was selected rather than measured.

3.2.6. – Sensitivity Analysis

The 8 different parameters described in 3.2.1 were varied for the sensitivity analysis to provide a comprehensive view of the possible mean RRR variations for our HL population, 19 figures which highlight different aspects of the sensitivity analysis were used to show the results. Due to this large number of permutations, Table 3.3 lists the differences between the various figures in this section in an effort to reduce confusion for the reader. Each figure is broken down into its various groupings (i.e mean equivalent dose, mean RRR, etc.) and each of the 8 parameters are listed in a separate column. Parameter values which varied were listed for each figure.

Table 3-3 – Breakdown of figures and tables described in section 3.2.6

Grouping	Figure	Patient #	Treatment Techniques Involved/Compared	OAR	Exposed Age (e)	Attained Age (a)	Mean RBE of Neutrons for Carcinogenesis (w_r)	Dose Response Model	Dose Response Inflection Point (α)	Mean RRR Value Examined	Sensitivity Parameters and Their Possible Values
Sensitivity Test for Mean Neutron Dose	Table 3.5	1-9	-	1. Total Breast 2. Total Lung 3. Thyroid	-	-	5 20 35	-	-	-	1. Patient # - 1-9 2. Treatment Plan - Photon IMRT, Proton PSPT, Proton IMPT 3. OAR - Total Breast, Total Lung, Thyroid, All OARs Average Together 4. Exposed Age [e] = 10, 26, 42 5. Attained Age [a] = 30, 60; 46, 76; 62, 92 6. Mean RBE of Neutrons for Carcinogenesis [w_r] - 5, 20, 35 7. Dose Response Model - LNT, Lin Plat, Lin Exp 8. Dose Response Inflection Point [α] - 0.025, 0.090
	Figure 3.2	1-9	-	Total Breast	-	-	5 20 35	-	-	-	
	Figure 3.3	1-9	-	Total Lung	-	-	5 20 35	-	-	-	
	Figure 3.4	1-9	-	Thyroid	-	-	5 20 35	-	-	-	
Sensitivity Test for Total Mean Equivalent Dose	Figure 3.5	1-9	1. Photon IMRT 2. Proton PSPT 3. Proton IMPT	1. Total Breast 2. Total Lung 3. Thyroid	-	-	5 20 35	-	-	-	
Sensitivity Test for Mean Relative Risk (RR)	Figure 3.6	1-9	1. Photon IMRT 2. Proton PSPT 3. Proton IMPT	1. Total Breast 2. Total Lung 3. Thyroid	26	46	5 20 35	1. LNT 2. Lin Plat 3. Lin Exp	0.025	-	
	Figure 3.7	1-9	1. Photon IMRT 2. Proton PSPT 3. Proton IMPT	1. Total Breast 2. Total Lung 3. Thyroid	26	46	5 20 35	1. LNT 2. Lin Plat 3. Lin Exp	0.090	-	
	Figure 3.8	1-9	1. Photon IMRT 2. Proton PSPT 3. Proton IMPT	1. Total Breast 2. Total Lung 3. Thyroid	26	46	5 20 35	1. LNT 2. Lin Plat 3. Lin Exp	0.025 0.090	-	
Sensitivity Test for the Propagation of Uncertainties	Table 3.6	-	-	1. Total Breast 2. Total Lung 3. Thyroid	-	-	-	1. LNT 2. Lin Plat 3. Lin Exp	-	-	
Sensitivity Test for Mean Ratio of Relative Risk (RRR)	Figures 3.9 and 3.10	1-9	1. Photon IMRT 2. Proton PSPT	1. Total Breast 2. Total Lung 3. Thyroid	26	46	20	1. LNT 2. Lin Plat 3. Lin Exp	0.025	$\overline{RRR}_{j,k}$	
	Figure 3.11	1-9	1. Photon IMRT 2. Proton PSPT 3. Proton IMPT	Total Breast	26	46	20	1. LNT 2. Lin Plat 3. Lin Exp	0.025 0.090	$\overline{RRR}_{j,k}$	
	Figure 3.12	1-9	1. Photon IMRT 2. Proton PSPT 3. Proton IMPT	Total Lung	26	46	20	1. LNT 2. Lin Plat 3. Lin Exp	0.025 0.090	$\overline{RRR}_{j,k}$	
	Figure 3.15	1-9	1. Photon IMRT 2. Proton PSPT 3. Proton IMPT	Thyroid	26	46	20	1. LNT 2. Lin Plat 3. Lin Exp	0.025 0.090	$\overline{RRR}_{j,k}$	
	Figure 3.16	-	1. Photon IMRT 2. Proton PSPT 3. Proton IMPT	1. Total Breast 2. Total Lung 3. Thyroid	26	46	20	1. LNT 2. Lin Plat 3. Lin Exp	0.025 0.090	\overline{RRR}_j	
	Figure 3.16	-	1. Photon IMRT 2. Proton PSPT	1. Total Breast 2. Total Lung 3. Thyroid	26	46	5 20 35	1. LNT 2. Lin Plat 3. Lin Exp	0.025	\overline{RRR}_j	
Statistical Tests	Figure 3.14	1-9	1. Photon IMRT 2. Proton PSPT 3. Proton IMPT	1. Total Breast 2. Total Lung 3. Thyroid 4. All OARs Averaged Together	26	46	20	1. LNT 2. Lin Plat 3. Lin Exp	0.025 0.090	$\overline{RRR}_{j,k}$	
	Table 3.7	1-9	1. Photon IMRT 2. Proton PSPT 3. Proton IMPT	1. Total Breast 2. Total Lung 3. Thyroid 4. All OARs Averaged Together	26	46	20	1. LNT 2. Lin Plat 3. Lin Exp	0.025 0.090	$\overline{RRR}_{j,k}$	

3.2.7. – Mean RRR Extrema Comparisons

From the many possible configurations, the mean RRR was found for the iterations that delivered the minimum and maximum mean RRR values for our patient set. This is not to say this occurred for every permutation. Minor differences can be seen on a case by case basis, but in general, the criteria selected for the extrema highlight the extrema of our mean RRR calculations and should provide a mechanism to view the possible range we would expect to see for our cohort.

Rather than show each $\overline{RRR}_{j,k}$, the \overline{RRR}_j (mean RRR for each OAR for all patients) was selected to eliminate excessive amounts of data. Also of note, the mean RBE of neutrons for carcinogenesis radiation weighting factor (neutron \overline{w}_R) chosen was again 20. A neutron \overline{w}_R of 35 would have of course increased the value of the mean RRR, since that contribution is added only to the proton plans, but since the variation of the mean RRR with respect to neutron \overline{w}_R was examined earlier, and to maintain consistency with patient parameters examined in Aim 1, neutron $\overline{w}_R = 20$ was selected. To further the comparison, the patient parameters examined in Aim1 were also included in the extrema comparison. While not technically the mean, those values were assumed to be a close approximation to the average mean RRR for all of the possible combinations of the parameters.

The combinations of the eight parameters described in 3.2.1 for the minimum extrema, maximum extrema, and the Aim 1 parameters are detailed in Table 3.4.

Table 3-4 – Mean RRR extrema values for sensitivity parameters

Mean RRR Test	Patient #	Treatment Techniques Involved/Compared	OAR	Exposed Age (e)	Attained Age (a)	Mean RBE of Neutrons for Carcinogenesis (w_r)	Dose Response Model	Dose Response Inflection Point (α)	Mean RRR Value Examined
Mean RRR Minimum Extrema	1-9	1. Photon IMRT	1. Total Breast	10	30	20	1. LNT	0.900	$\overline{RRR}_{j,k}$
		2. Proton PSPT	2. Total Lung						\overline{RRR}_k
		3. Proton IMPT	3. Thyroid						\overline{RRR}_k
Mean RRR Maximum Extrema	1-9	1. Photon IMRT	1. Total Breast	42	92	20	1. LNT	0.025	$\overline{RRR}_{j,k}$
		2. Proton PSPT	2. Total Lung						\overline{RRR}_k
		3. Proton IMPT	3. Thyroid						\overline{RRR}_k
Mean RRR - Aim 1 Configuration	1-9	1. Photon IMRT	1. Total Breast	26	46	20	1. LNT	0.025	$\overline{RRR}_{j,k}$
		2. Proton PSPT	2. Total Lung						\overline{RRR}_k
		3. Proton IMPT	3. Thyroid						\overline{RRR}_k

3.2. Results

3.3.1. – Sensitivity Test for Mean Neutron Dose

The mean neutron dose for each OAR was found. The mean RBE of neutrons for carcinogenesis radiation weighting factor (neutron \overline{w}_R) was varied discretely to the values of 5, 20, and 35. The mean neutron dose contribution averaged over all patients in cSv/Prescribed Gy is listed in Table 3.5, and the breakdown per patient for the various neutron \overline{w}_R is shown per OAR in Figure 3.2-3.4.

Table 3-5 – Mean neutron dose contributions averaged over all patients (cSv/Prescribed Gy) - Mean neutron equivalent dose per prescribed Gy with varying neutron \bar{w}_R for all OARs averaged over all patients. We see the expected increase in equivalent dose contribution as neutron \bar{w}_R increases. These numbers correspond well with published data for similar treatment configurations.

OAR	Wr = 5			Wr = 20			Wr = 35		
	External Neutron	Internal Neutron	Total Neutron	External Neutron	Internal Neutron	Total Neutron	External Neutron	Internal Neutron	Total Neutron
Total Breast	0.35	0.34	0.69	1.39	1.37	2.76	2.43	2.40	4.83
Total Lung	0.34	0.44	0.78	1.36	1.77	3.14	2.39	3.10	5.49
Thyroid	0.33	0.42	0.75	1.30	1.70	3.00	2.28	2.97	5.25

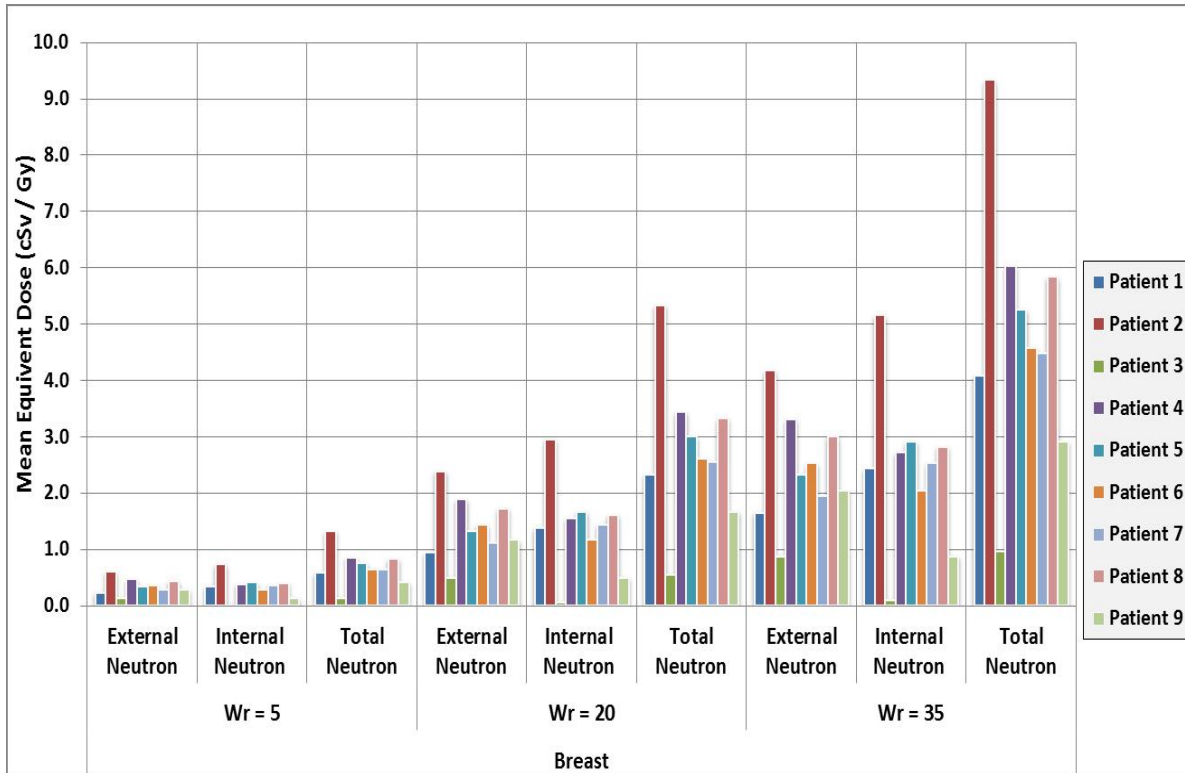


Figure 3-2 – Mean equivalent neutron dose per prescribed Gy by varying neutron \bar{w}_R – breast (cSv/Gy) - Mean neutron equivalent dose with varying \bar{w}_R for the Total Breast. We see the expected increase in equivalent dose contribution as \bar{w}_R increases. Patient 2 shows a substantial increase relative to the other patients. This could be attributed to several factors including increased nozzle entrance proton energy, width of the SOBP and water equivalent thickness relative to other patients. In addition, Patient 2 had over 3 times the amount of breast tissue in the open field relative to the average patient in the cohort.

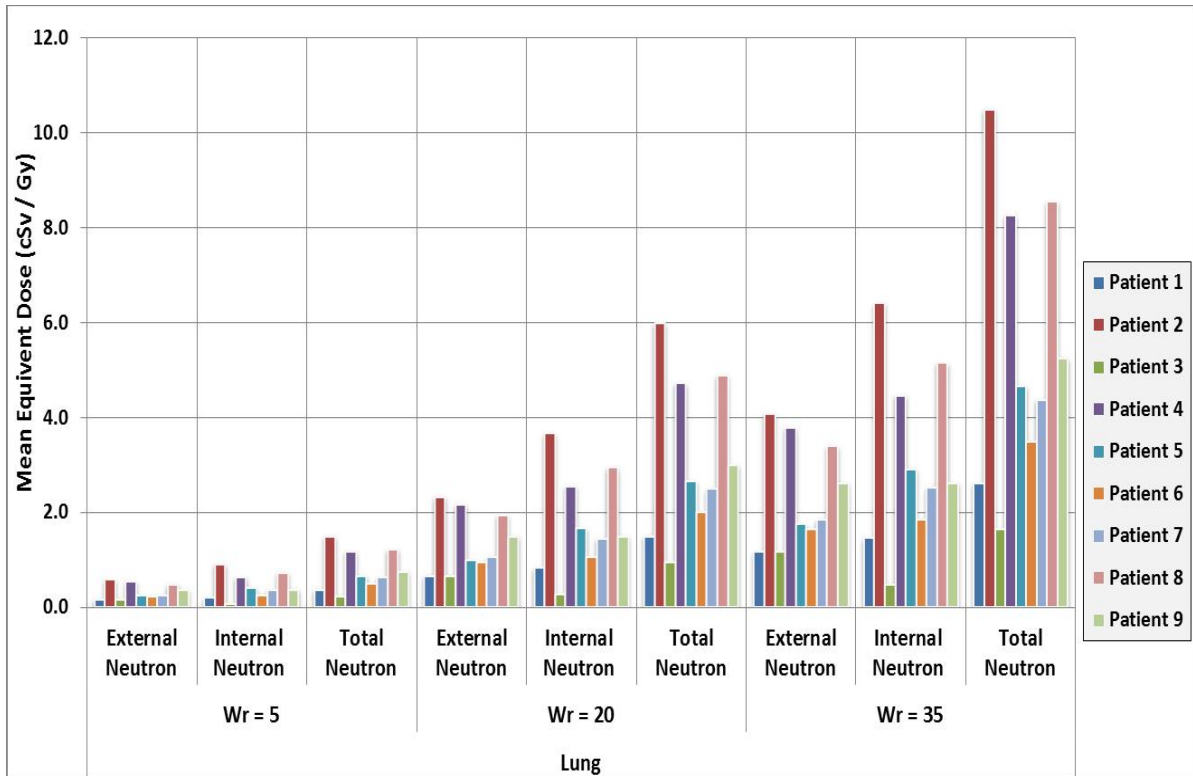


Figure 3-3 – Mean equivalent neutron dose per prescribed Gy by varying neutron \bar{w}_R – lung (cSv/Gy) - Mean neutron equivalent dose with varying \bar{w}_R for the Total Lung. We see the expected increase in equivalent dose contribution as \bar{w}_R increases. Patient 2, 4, and 8 show an increase in equivalent dose relative to the other patients. Patients 2 and 4 again had a higher than average portion of lung tissue within the field and nozzle entrance proton energy. Patient 8 did not, but was also a much smaller patient (she was the youngest in the cohort at 10 years old) and therefore had more lung tissue closer to the CTV, which increased exposure to neutron doses.

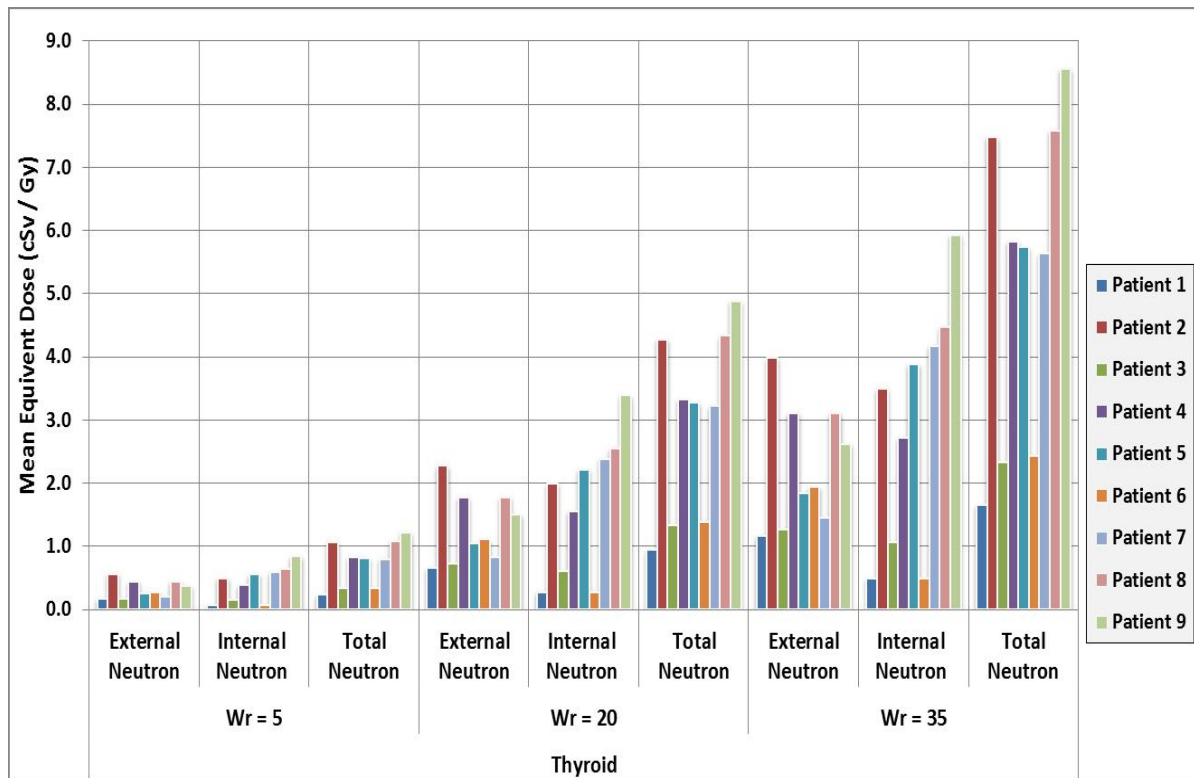


Figure 3-4 – Mean equivalent neutron dose per prescribed Gy by varying neutron \bar{w}_R – thyroid (cSv/Gy)
 - Mean neutron equivalent dose with varying \bar{w}_R for the Thyroid. We see the expected increase in equivalent dose contribution as \bar{w}_R increases. Patient 2, 8 again show increased equivalent dose relative to other patients. Those increases could be attributed to points discussed previously. Patient 9 shows a substantial increase relative to her lung and breast, however. Unlike those two OARs, which she had below the average percentage of OAR tissue in the field, nearly 70% of her thyroid was in this field (over 3 times as high as the average). This substantial increase due to the proximity to the CTV can be seen in the much higher percentage of internal neutron contribution (which is produced mainly in field) compared to the external neutrons.

3.3.2. – Sensitivity Test for Total Mean Equivalent Dose

The mean equivalent dose is shown in Figure 3.5. It delineates the dose by patient, treatment plan, OAR, and neutron \bar{w}_R .

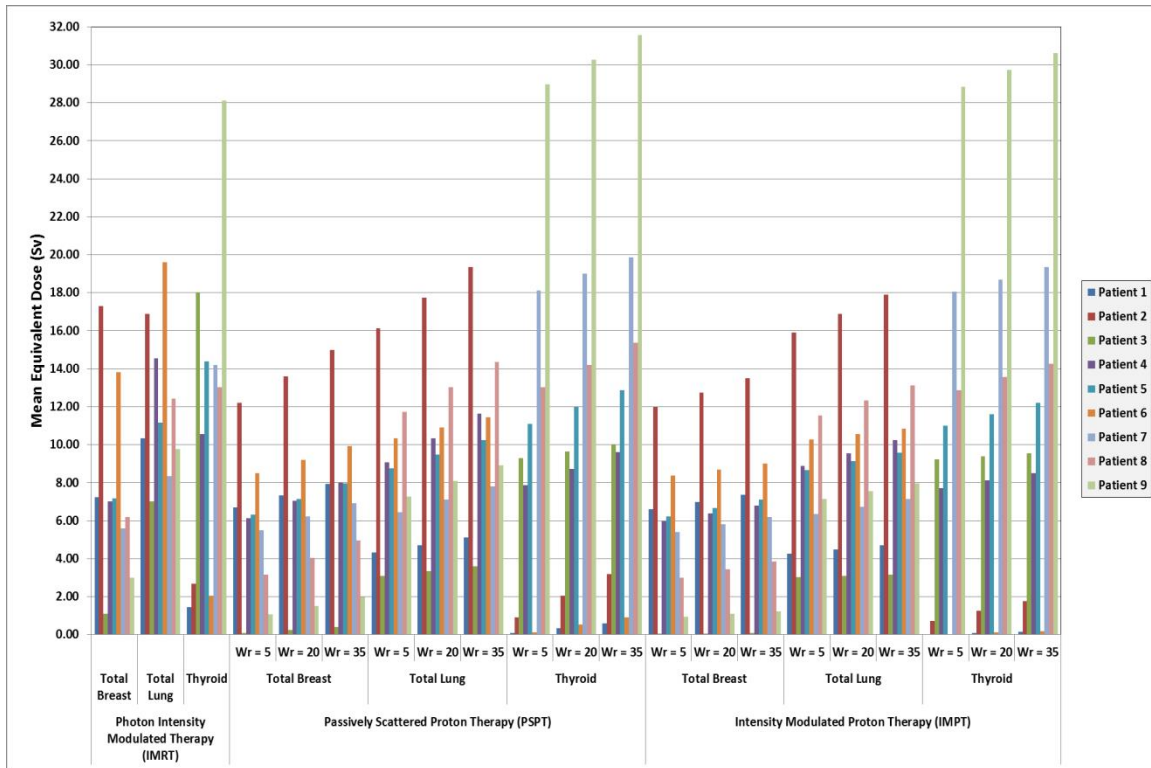


Figure 3-5 – Mean total equivalent dose to OAR by varying neutron \bar{w}_R value (Sv) - Mean total equivalent dose with varying treatment plans and \bar{w}_R for each OAR. We again see the expected increase in equivalent dose contribution as \bar{w}_R increases. Patient 2 and 9 emphasize the clustering of dose in the vicinity of the tumor volume (CTV). We see an increase in dose to the Total Breast and Lung and minimal dose to the Thyroid for Patient 2 while the opposite is true for Patient 9. Patient 2’s tumor location is located squarely in the mediastinum while Patient 9’s is located in the upper supraclavicular region.

3.3.3. – Sensitivity Test for Mean Relative Risk (RR)

Figures 3.6 and 3.7 delineate the mean RR values for each patient, treatment plan, OAR, neutron \bar{w}_R and dose response inflection point (α). Age at exposure (e) and attained age (a) were kept constant. Due to the large amounts of data displayed, Figure 3.6 showed only the $\alpha = 0.025$ calculations while Figure 3.7 showed the $\alpha = 0.090$ set. Recall, that the α value does not affect the LNT risk calculations since it is not used in the LNT equations.

Figure 3.7 in general showed a reduction in the RR relative to the corresponding data point in Figure 3.6 for the linear plateau and linear exponential risk models. This is expected since the $\alpha = 0.090$ corresponds to a much earlier inflection point at 10 Sv (i.e. the RR starts to decrease) compared to the $\alpha = 0.025$ which decrease at 40 Sv.

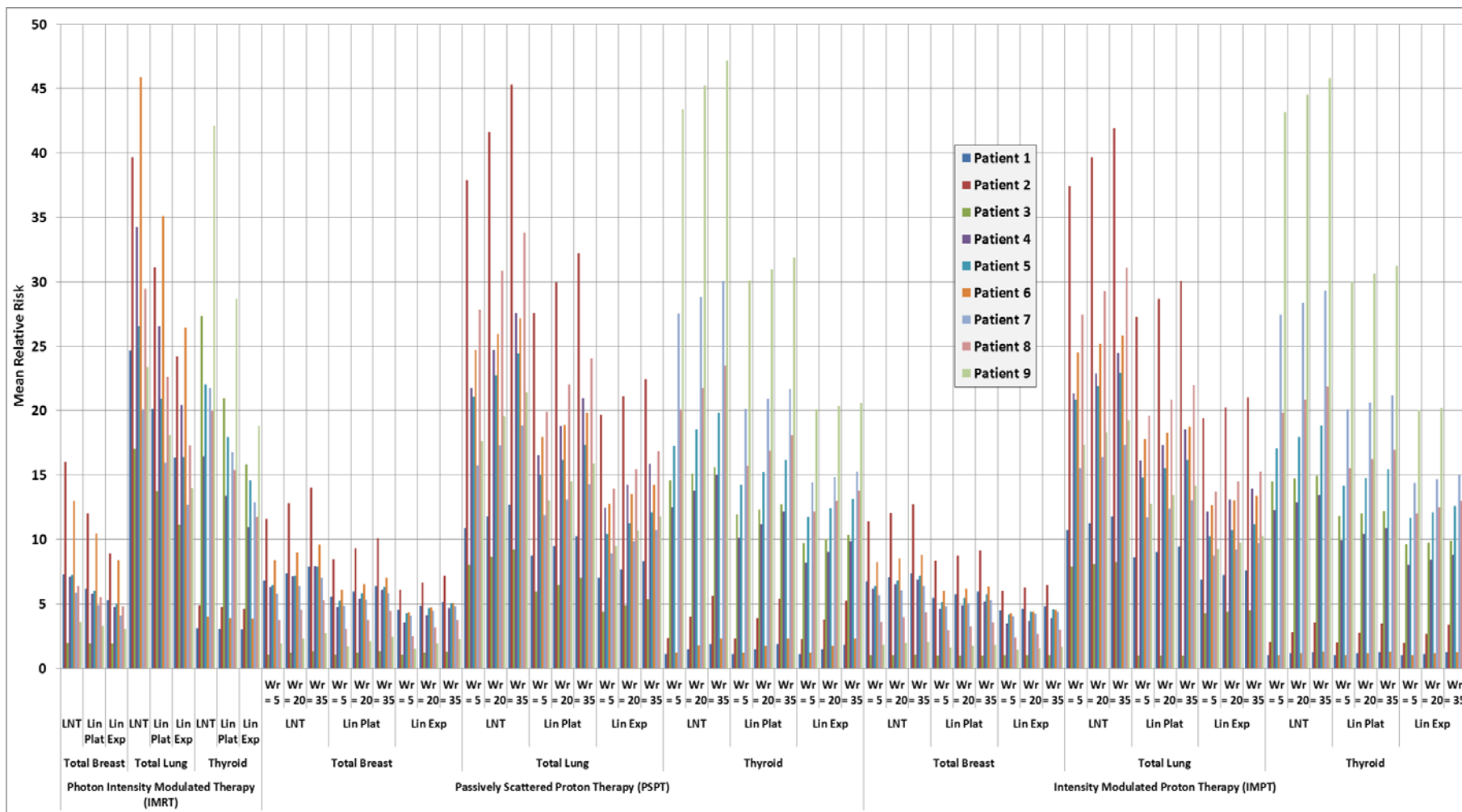


Figure 3-6 – Mean relative risk to OAR For each dose response model and neutron \bar{w}_R value - exposed age 26, attained age = 46, response inflection point (α) = 0.025 - As in Aim 1, the lung relative risk is substantial higher than the other OARs for similar mean doses to the organ. As expected, the mean RR for LNT > Linear Plateau > Linear Exponential.

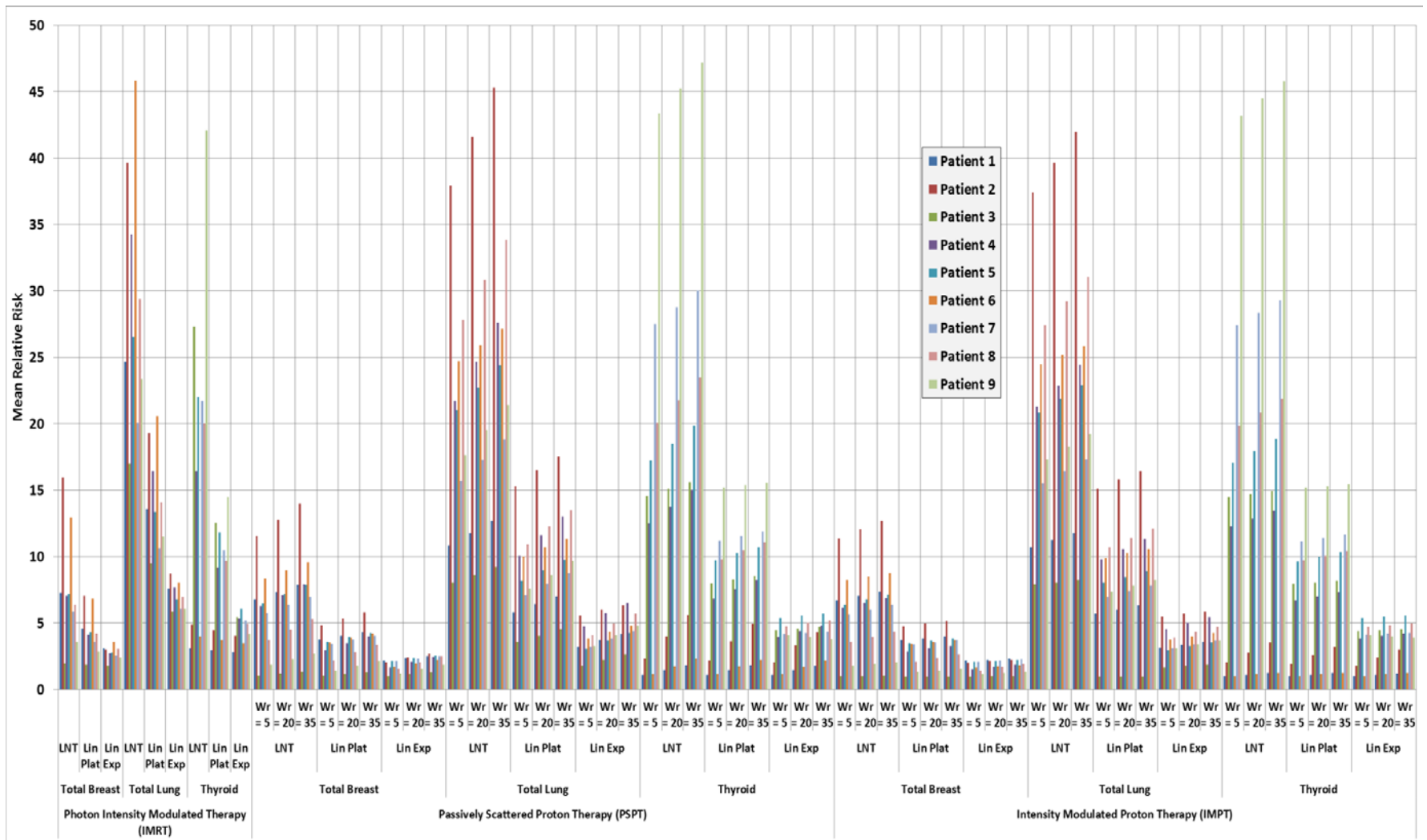


Figure 3-7 – Mean relative risk to OAR For each dose response model and neutron \overline{w}_R value - exposed age 26, attained age = 46, response inflection point (α) = 0.090 - The mean RR again was LNT > Linear Plateau > Linear Exponential, but, relative to $\alpha = 0.025$, the decrease in the mean RR values for the non-linear models was larger.

Figure 3.8 further explores the difference between the LNT and other dose response models. The ratio of the mean RR averaged over all of the patients between the LNT and the Linear Plateau and Linear Exponential models was taken and displayed for each examined parameter in Figure 3.8.

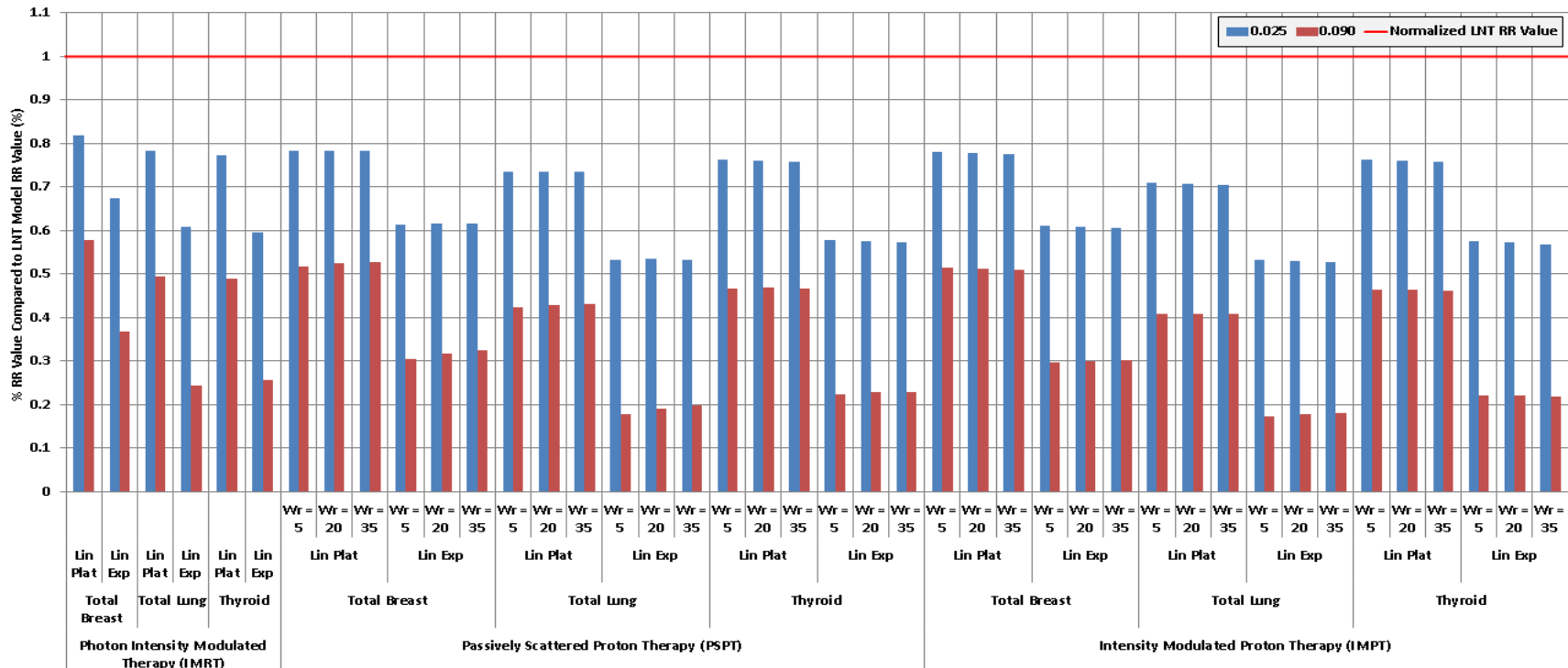


Figure 3-8 – % decrease in RR compared to LNT model RR – all patients averaged together - The % decrease in the Mean RR average over all patients of the non-linear dose response models vs the LNT model. The models which used $\alpha = 0.025$ are in blue and $\alpha = 0.090$ are in red. Again, the increased reduction was seen for the $\alpha = 0.090$ model compared to the $\alpha = 0.025$ model due to the earlier dose inflection point. There was a fairly constant decrease between the LNT and the Lin Plat and Lin Exp across all treatments plans, OARs, and neutron $\overline{w_R}$ values, with the proton plans seeing a slightly higher drop relative to the LNT compared to the photon IMRT plan. The lung, however, seems to decrease more than the other OARs. This would imply a larger percentage of voxels which had a higher equivalent dose value. Higher doses would benefit more from a decrease in the risk associated with the non-linear models.

3.3.4. – Sensitivity Test for the Propagation of Uncertainties

Similar to Aim 1, the percent contribution of each component of the propagation of uncertainty equations was shown, but this time for all 3 dose response models. Similar trends were seen for the non-linear models as with the LNT. The proton dose again was the majority of the component contribution to the uncertainty.

Table 3-6 – % contribution breakdown of propagation of uncertainty error for dose response models - The mean % contribution of to the propagation of uncertainty average over all patients for each component used to calculate the value. Values that specific a percentage of 0% (i.e. Total lung/LNT for the β contribute an amount, but that value rounded to 0. Similarities between the three dose response models were seen with the proton dose dominating the source of error.

Dose Response Model	$\left(\frac{\partial RRR_{Response Model_j}}{\partial \beta_j}\right)^2 \sigma_{\beta_j}^2$			$\left(\frac{\partial RRR_{Response Model_j}}{\partial C_j}\right)^2 \sigma_{C_j}^2$			$\left(\frac{\partial RRR_{Response Model_j}}{\partial H_{Proton_j}}\right)^2 \sigma_{H_{Proton_j}}^2$			$\left(\frac{\partial RRR_{Response Model_j}}{\partial H_{Photon IMRT_j}}\right)^2 \sigma_{H_{Photon IMRT_j}}^2$			$\left(\frac{\partial RRR_{Response Model_j}}{\partial H_a}\right)^2 \sigma_a^2$		
	Total Breast	Total Lung	Thyroid	Total Breast	Total Lung	Thyroid	Total Breast	Total Lung	Thyroid	Total Breast	Total Lung	Thyroid	Total Breast	Total Lung	Thyroid
LNT	4%	0%	10%	-	-	-	93%	83%	89%	3%	17%	1%	-	-	-
Lin Plat	5%	0%	9%	-	-	-	85%	100%	91%	10%	0%	0%	-	-	-
Lin Exp	5%	1%	9%	-	-	-	73%	78%	80%	22%	21%	11%	-	-	-

3.3.5. – Sensitivity Test for Mean RRR

The endpoint metric tested in this work, the mean RRR, is shown in the following figures. Figure 3.9 and Figure 3.10 show the same data in two different ways and is intended to more simply focus on looking at differences between dose response models for each patient (Figure 3.9) and then differences between patients for each dose response model (Figure 3.10) while displaying the data for each OAR on each graph as well.

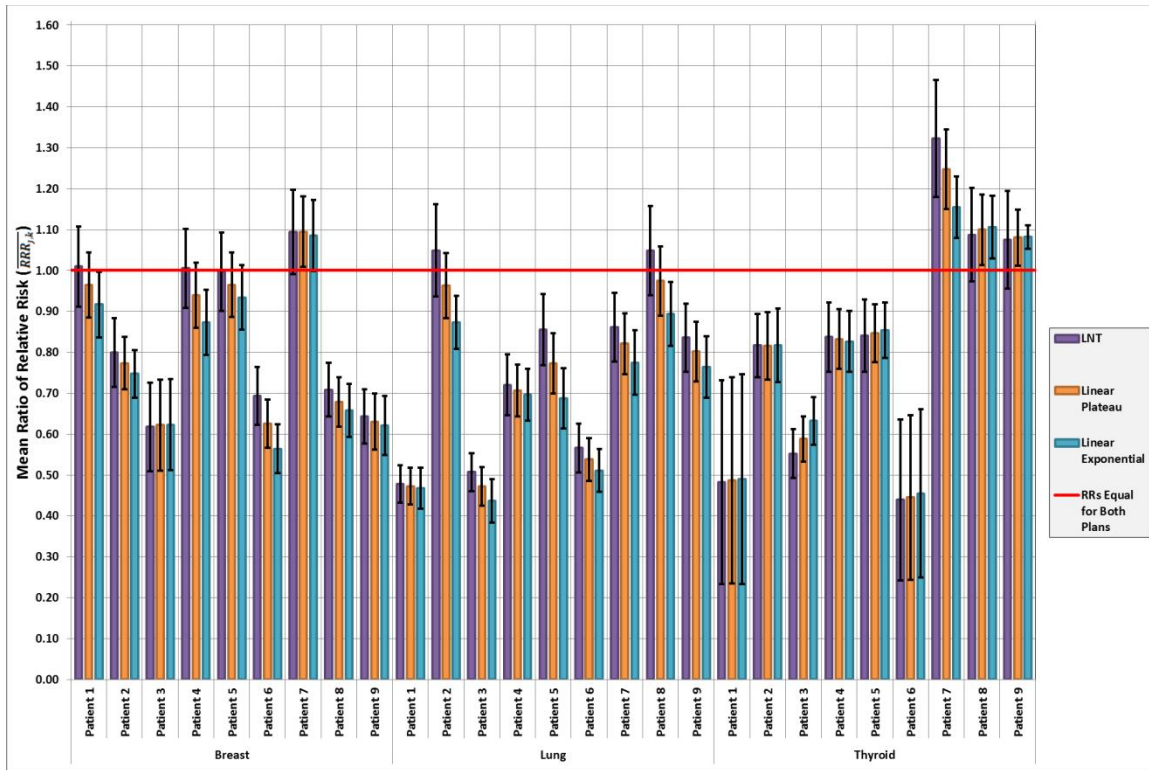


Figure 3-9 – $\overline{RRR}_{J,k}$ for all patients and OARs, PSPT vs IMRT, exposed age = 26, attained age (a) = 46, neutron $\overline{w}_R = 20$, response inflection pt (α) = 0.025 – dose response model comparison - For the majority of cases, the mean RRR for the LNT > Lin Plat > Lin Exp. There are some isolated instances where this is not the case (i.e. patient #1Thyroid). Recall that the mean RRR is a measurement of the RR ratio between the proton and photon IMRT plans. Higher doses will yield lower RR values with the non-linear response models relative to LNT, which could benefit higher dose yielding plans. For all patients, none of the different dose response models fell outside of any of the other’s range of uncertainty. 28% of comparisons showed a mean RRR value over 1.

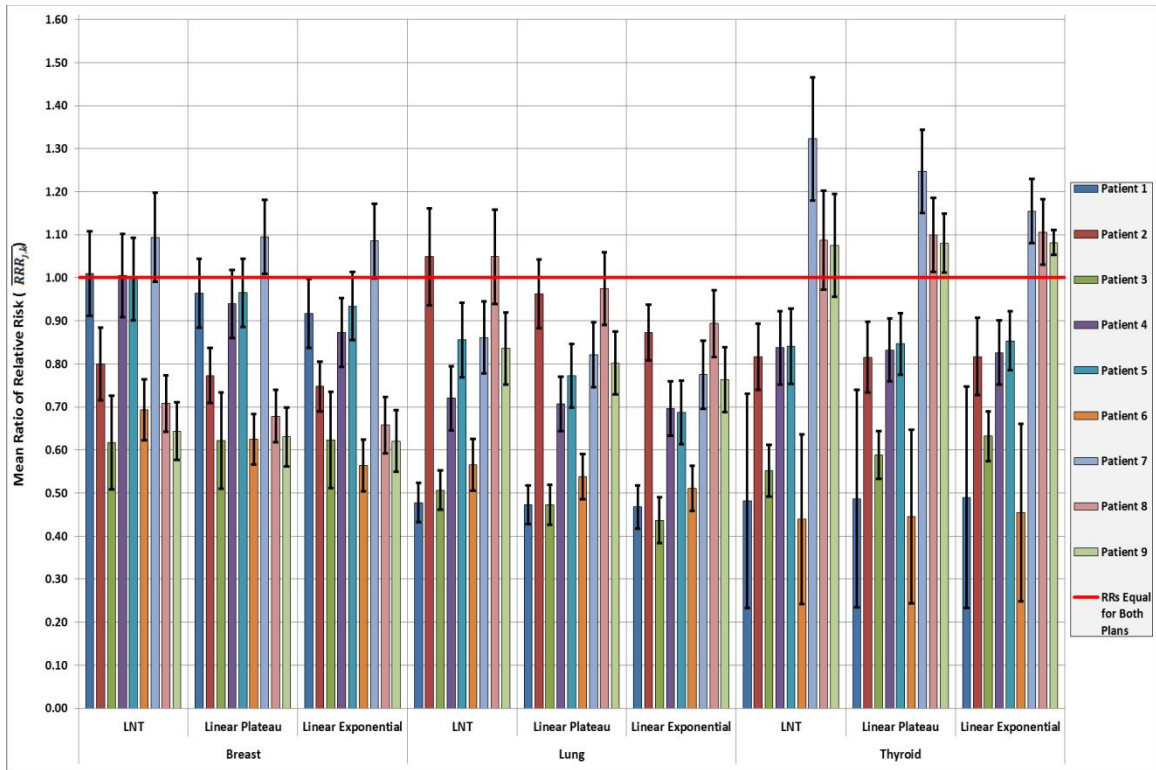


Figure 3-10 – $\overline{RRR}_{j,k}$ for all patients and OARs, PSPT vs IMRT, exposed age = 26, attained age (a) = 46, neutron $\overline{w}_R = 20$, response inflection pt (α) = 0.025 – patient comparison - Emphasis is placed on how individual patients compared relative to each other. Patients #7-9 show statistically significant increases in the thyroid relative to all other patients. It is worth noting that these three patients were the youngest in the cohort (two 15 year olds (#7 and 9) and a 10 year old (#8)). The smaller body and geographical location likely contributed to increased scatter dose to these patients relative to the older members of the cohort.

Figures 3.9 and 3.10 focused on examining the differences between patients, OARs, and dose response models while keeping the treatment plan, neutron \overline{w}_R , and dose response model parameters fixed. Figures 3.11-3.13 focuses on only one OAR apiece while showing the differences in the mean RRR when the treatment plan and dose response model parameters vary. General trends for the three graphs showed the majority of mean RRR values below 1.0, including the statistical uncertainty, indicating improved risk control for the various proton plans compared to the photon IMRT plan.

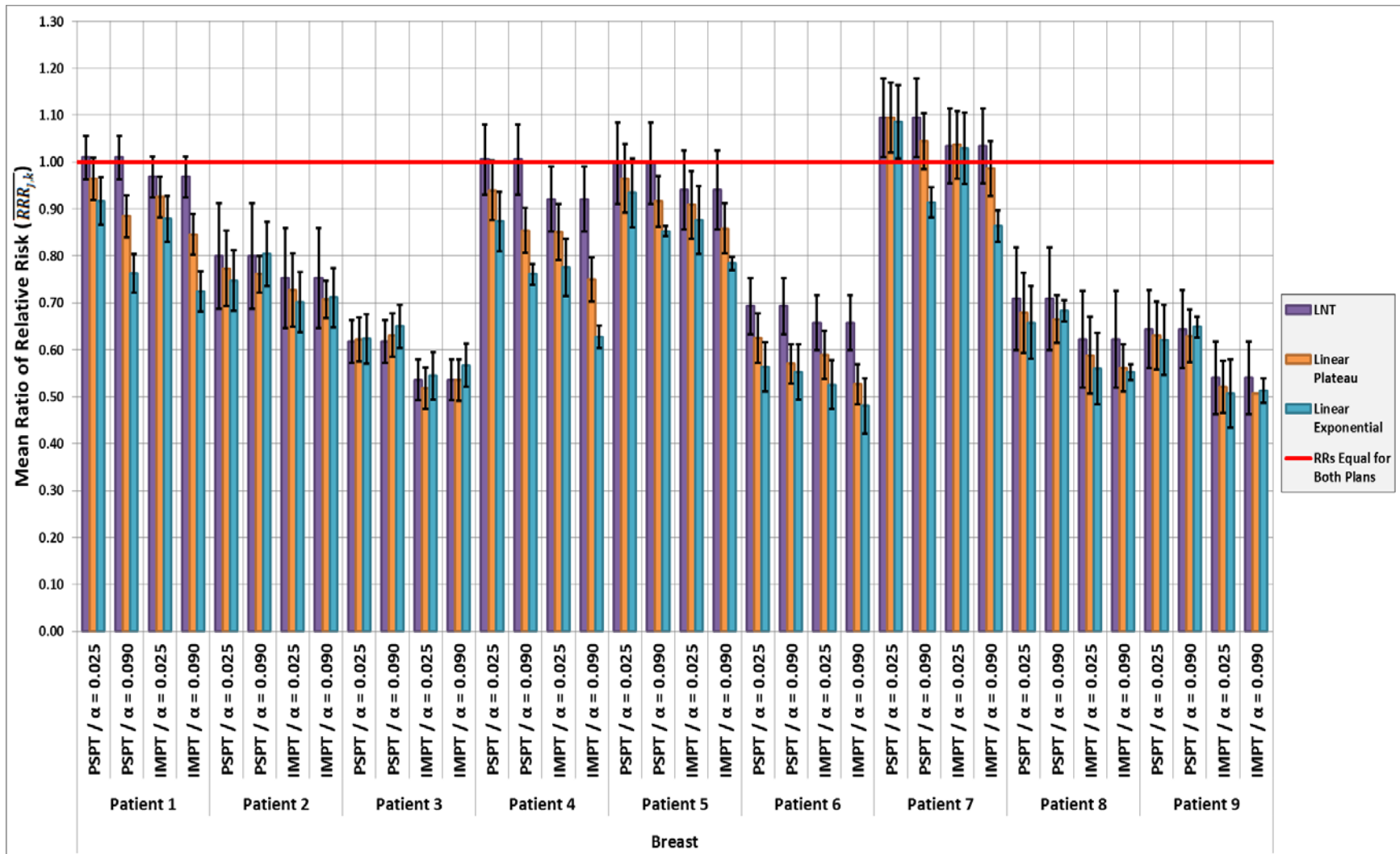


Figure 3-11 – $\overline{RRR}_{j,k}$ – BREAST ONLY – proton plans vs IMRT, exposed age (e) = 26, attained age (a) = 46, neutron $\overline{w}_R = 20$, All α - Since the LNT values are the same for each individual patient per treatment plan, in the graph there are 90 individual $\overline{RRR}_{j,k}$ values with their corresponding error bars. Of the 90, 15 (16.7%) showed a $\overline{RRR}_{j,k} > 1$. Of these 22, 11 were seen from the PSPT plan comparisons.

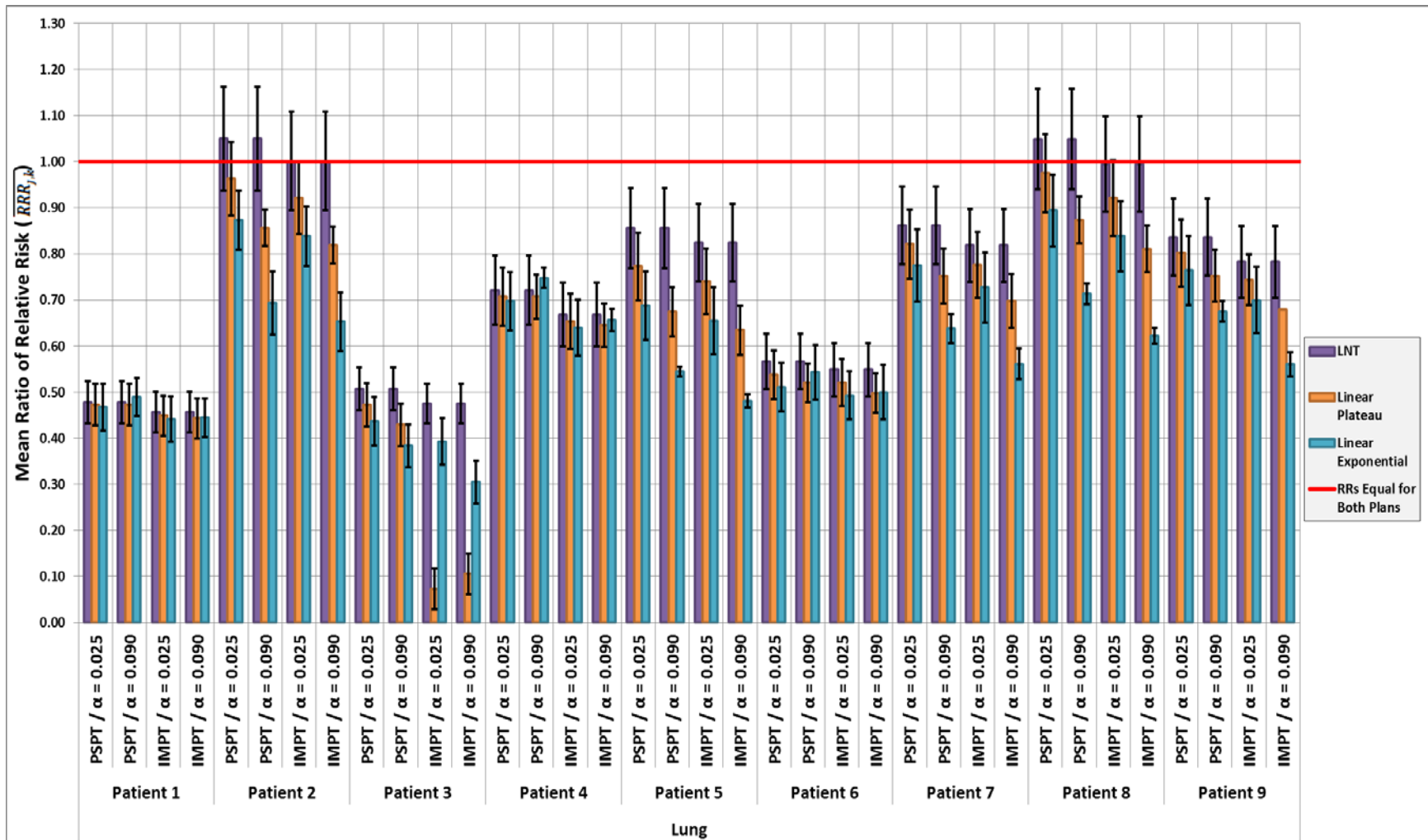


Figure 3-12 – $\overline{RRR}_{j,k}$ – LUNG ONLY – proton plans vs IMRT, exposed age (e) = 26, attained age (a) = 46, neutron $\overline{w}_R = 20$, All α - Since the LNT values are the same for each individual patient per treatment plan, in the graph there are 90 individual $\overline{RRR}_{j,k}$ values with their corresponding error bars. Of the 90, 7 (7.8%) showed a $\overline{RRR}_{j,k} > 1$. The total lung gave the strongest indication for the use of a proton plan compared to the photon IMRT plan of the three OARs examined with respect to the reduction of RSCs.

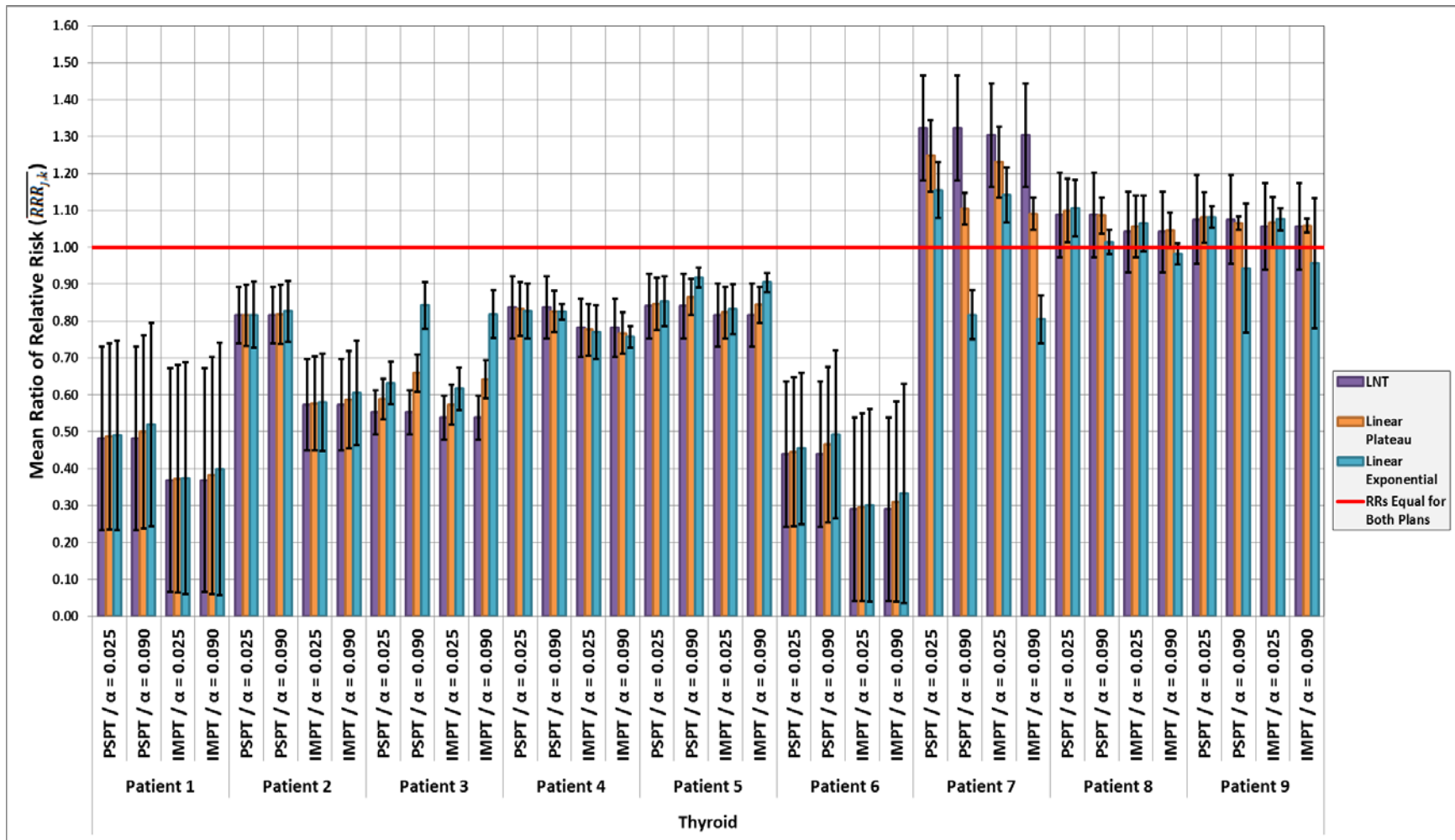


Figure 3-13 – $\overline{RRR}_{j,k}$ – THYROID ONLY – proton plans vs IMRT, exposed age (e) = 26, attained age (a) = 46, neutron $\overline{w}_r = 20$, All α - Since the LNT values are the same for each individual patient per treatment plan, in the graph there are 90 individual $\overline{RRR}_{j,k}$ values with their corresponding error bars. Of the 90, 28 (31.1%) showed a $\overline{RRR}_{j,k} > 1$. Of these 28, 14 were seen from the PSPT plan comparisons. The thyroid, gave the strongest indication for the use of a photon plan compared to the proton plans of the three OARs examined with respect to the reduction of RSCs. All $\overline{RRR}_{j,k}$ with a value over 1 were again seen in the last 3 patients, which were the youngest in the cohort.

The sign (Figure 3.14) and Student's t-test (Table 3.7) were done for the data shown in Figures 3.11-13. The majority of the data points indicate a mean RRR < 1 although they thyroid showed a higher percentage of parameter configurations that showed no significance for either plan examined. No configuration indicated significance for photon plans.

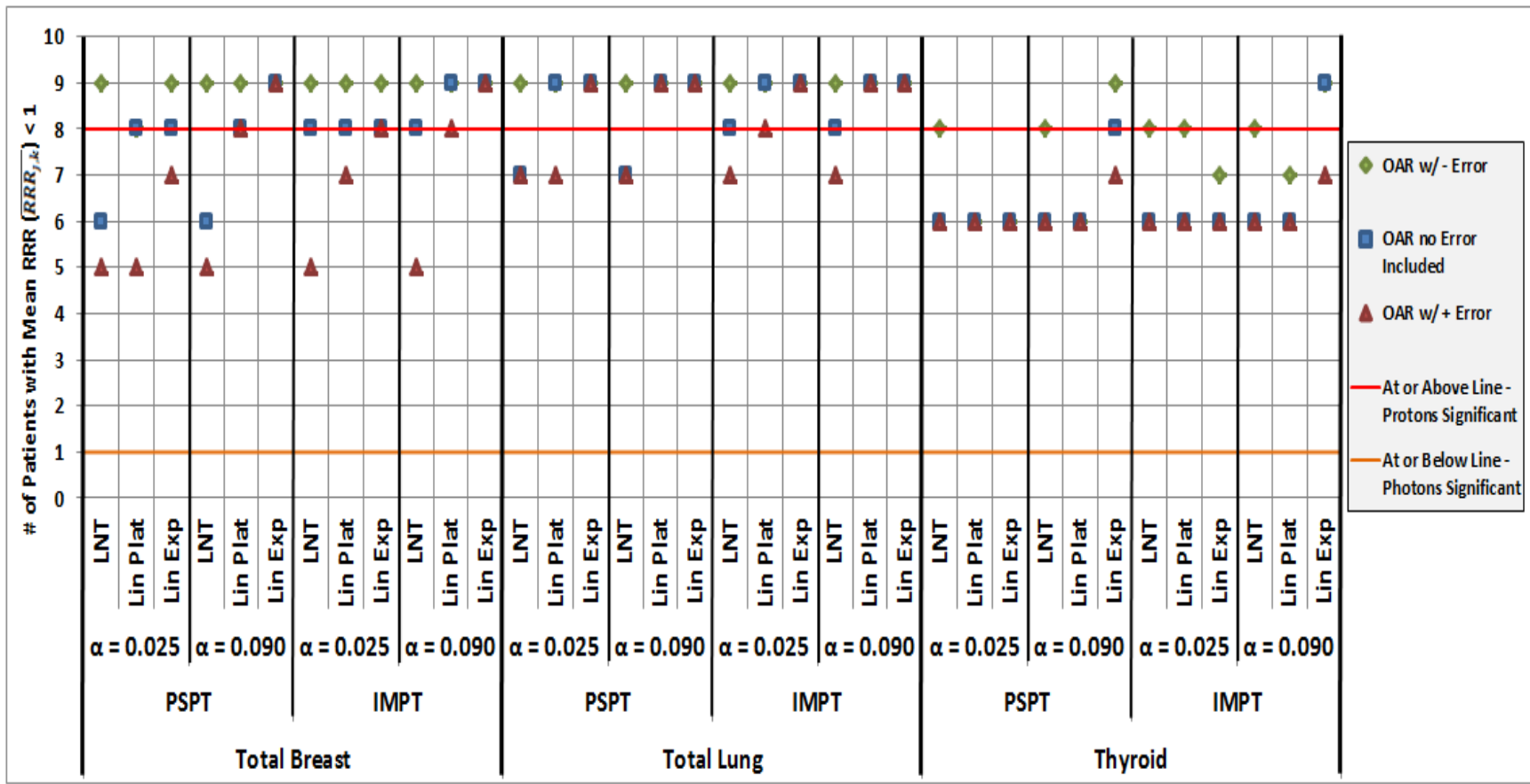


Figure 3-14 – Sign test of $\overline{RRR}_{j,k}$ for proton treatments vs IMRT, exposed age (e) = 26, attained age (a) = 46, neutron $\overline{w}_R = 20$, all dose response models, all α - Sign Test for $\overline{RRR}_{j,k}$ for both proton plans vs the corresponding photon IMRT plan. The blue square indicates the nominal $\overline{RRR}_{j,k}$ values. The red triangles designate the nominal $\overline{RRR}_{j,k}$ plus its corresponding error, and the green diamonds are the nominal $\overline{RRR}_{j,k}$ minus the corresponding error. All points at or below the Orange Line indicates the $\overline{RRR}_{j,k}$ is significantly > 1. All points at or above the Red Line indicates the $\overline{RRR}_{j,k}$ is significantly < 1. All points between the Red and Orange line indicate the $\overline{RRR}_{j,k}$ is not significantly different than 1. Since the LNT values are identical values for each individual patient per unique treatment plan, there were 90 unique $\overline{RRR}_{j,k}$ values in the figure. Of the 90, 60 (66.7%), indicated the $\overline{RRR}_{j,k}$ was significantly < 1, 30 (33.3%) showed no significance, and 0 (0%) indicated the $\overline{RRR}_{j,k}$ was significantly > 1.

Table 3-7 – Student’s t-test of $\overline{RRR}_{j,k}$ for proton treatments vs IMRT, exposed age (e) = 26, attained age (a) = 46, neutron $\overline{w}_R = 20$, all dose response models, all α - Values show any potential statistical significance for a given treatment plan if the uncertainty is subtracted from the nominal $\overline{RRR}_{j,k}$ (- Error), the uncertainty is added to the nominal $\overline{RRR}_{j,k}$ value (+ Error), and with just the nominal $\overline{RRR}_{j,k}$ value (OAR name only). Since the LNT values are identical values for each individual patient per unique treatment plan, there were 90 unique $\overline{RRR}_{j,k}$ values in the figure. Of the 90, 71 (78.9%), indicated the $\overline{RRR}_{j,k}$ was significantly < 1, 19 (21.1%) showed no significance, and 0 (0%) indicated the $\overline{RRR}_{j,k}$ was significantly > 1.

Treatment Type Compared to IMRT	α Value	Dose Response Model	Treatment Significance								
			Breast w/ - Error	Breast	Breast w/ + Error	Lung w/ - Error	Lung	Lung w/ + Error	Thyroid w/ - Error	Thyroid	Thyroid w/ + Error
PSPT	0.025	LNT	Protons	Protons	None	Protons	Protons	None	Protons	None	None
		Lin Plat	Protons	Protons	None	Protons	Protons	Protons	Protons	None	None
		Lin Exp	Protons	Protons	Protons	Protons	Protons	Protons	Protons	None	None
	0.09	LNT	Protons	Protons	None	Protons	Protons	None	Protons	None	None
		Lin Plat	Protons	Protons	Protons	Protons	Protons	Protons	Protons	None	None
		Lin Exp	Protons	Protons	Protons	Protons	Protons	Protons	Protons	Protons	None
IMPT	0.025	LNT	Protons	Protons	None	Protons	Protons	Protons	Protons	None	None
		Lin Plat	Protons	Protons	Protons	Protons	Protons	Protons	Protons	None	None
		Lin Exp	Protons	Protons	Protons	Protons	Protons	Protons	Protons	Protons	None
	0.09	LNT	Protons	Protons	None	Protons	Protons	Protons	Protons	None	None
		Lin Plat	Protons	Protons	Protons	Protons	Protons	Protons	Protons	Protons	None
		Lin Exp	Protons	Protons	Protons	Protons	Protons	Protons	Protons	Protons	Protons

The \overline{RRR}_j for the same parameter configuration as Figures 3.11-3.13 were examined in Figure 3.15. Results were decidedly in favor of the two proton treatments relative to the photon IMRT plan. All reported values showed a $\overline{RRR}_j < 1$ for all OARs varied over both proton plans for all dose response models and inflection points. As has been the case throughout the results in this chapter thus far, the Age of Exposure (e) = 26, the Attained Age (a) = 46, and the neutron $\overline{w}_R = 20$.

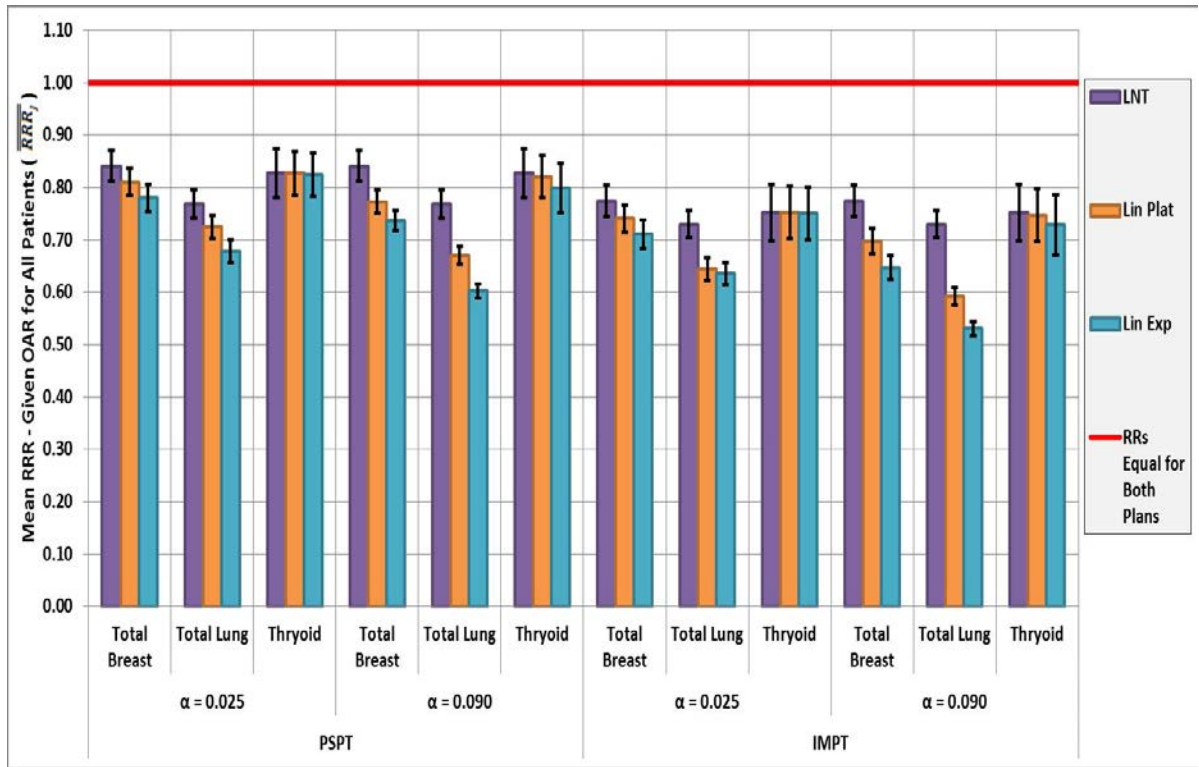


Figure 3-15 – \overline{RRR}_j for a given OAR for all patients, proton plans vs IMRT, exposed age (e) = 26, attained age (a) = 46, neutron $\overline{w}_R = 20$, all dose response models, all α - All iterations showed a \overline{RRR}_j value of below 1, including error bars. As has been seen throughout, generally, the LNT values show the highest \overline{RRR}_j values, $\alpha = 0.090$ has a lower mean \overline{RRR}_j , and the total lung has the lowest \overline{RRR}_j of the OARs.

Figure 3.16 depart from the data shown up to this point by focusing on the \overline{RRR}_j when the neutron \overline{w}_R value is varied. Recall that all data up to this point kept the neutron \overline{w}_R constant at 20. For this graph, both proton plans were compared to the photon IMRT plan. The age of exposure (e) is still 26, the attained age (a) is still 46, and $\alpha = 0.025$.

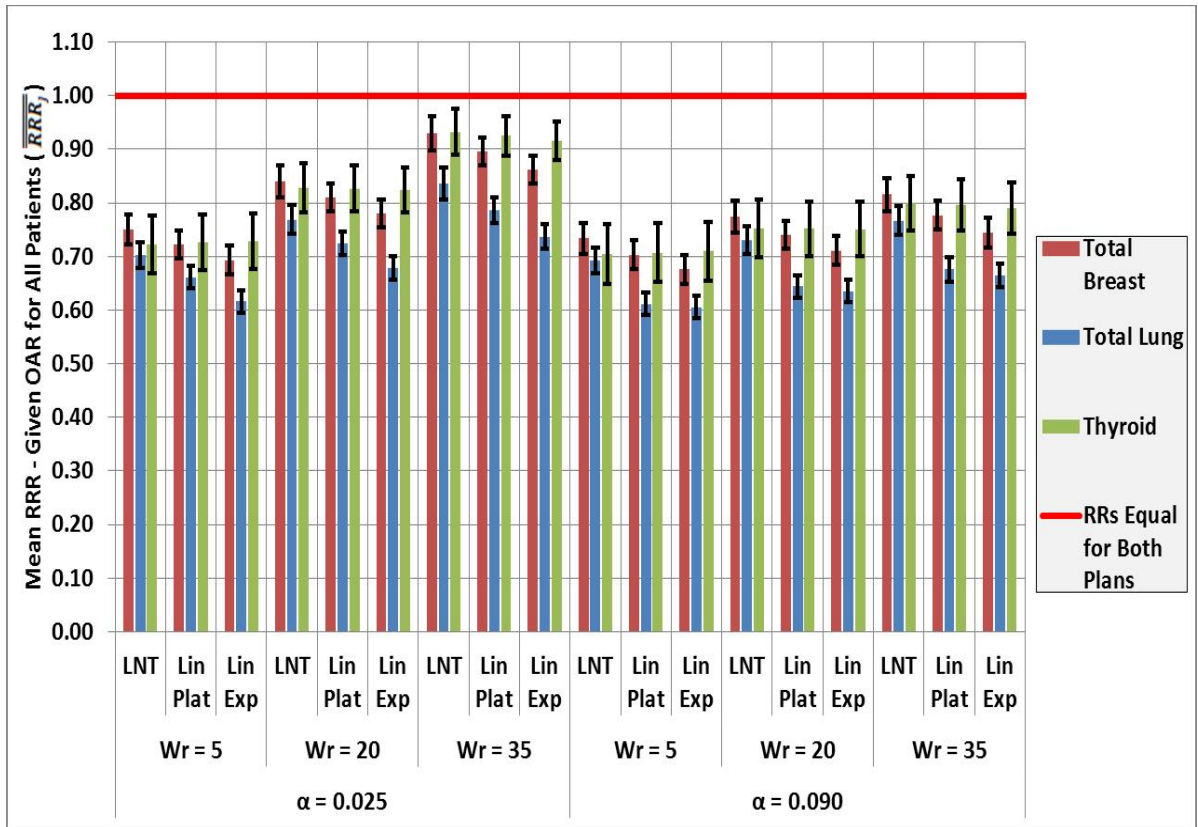


Figure 3-16 – \overline{RRR}_j for a given OAR for all patients, PSPT vs IMRT, exposed age (e) = 26, attained age (a) = 46, neutron \overline{w}_R , all α - Mean RRR (\overline{RRR}_j) for all patients and both proton plans as the neutron \overline{w}_R is varied. Including the error bars, none of the \overline{RRR}_j values in the figure were > 1. While the LNT values will stay the same when $\alpha = 0.090$, the \overline{RRR}_j values decrease on average for the non-linear dose response models.

3.3.6. – Mean RRR Extrema Comparisons

\overline{RRR}_j was examined in the case of its extrema for the Proton PSPT plan vs the Photon IMRT plan in Figure 3.17. Each OAR was tested over each dose response model. The oldest age of exposure (e) and attained age (a) combined with the dose response inflection point (α) = 0.025 gave the largest mean RRR values. The youngest (e) and (a) values in concert with $\alpha = 0.090$ gave the smallest \overline{RRR}_j . To compare, the average patient tested in Aim 1 (e = 26, a = 46, $\alpha = 0.025$) is displayed as well.

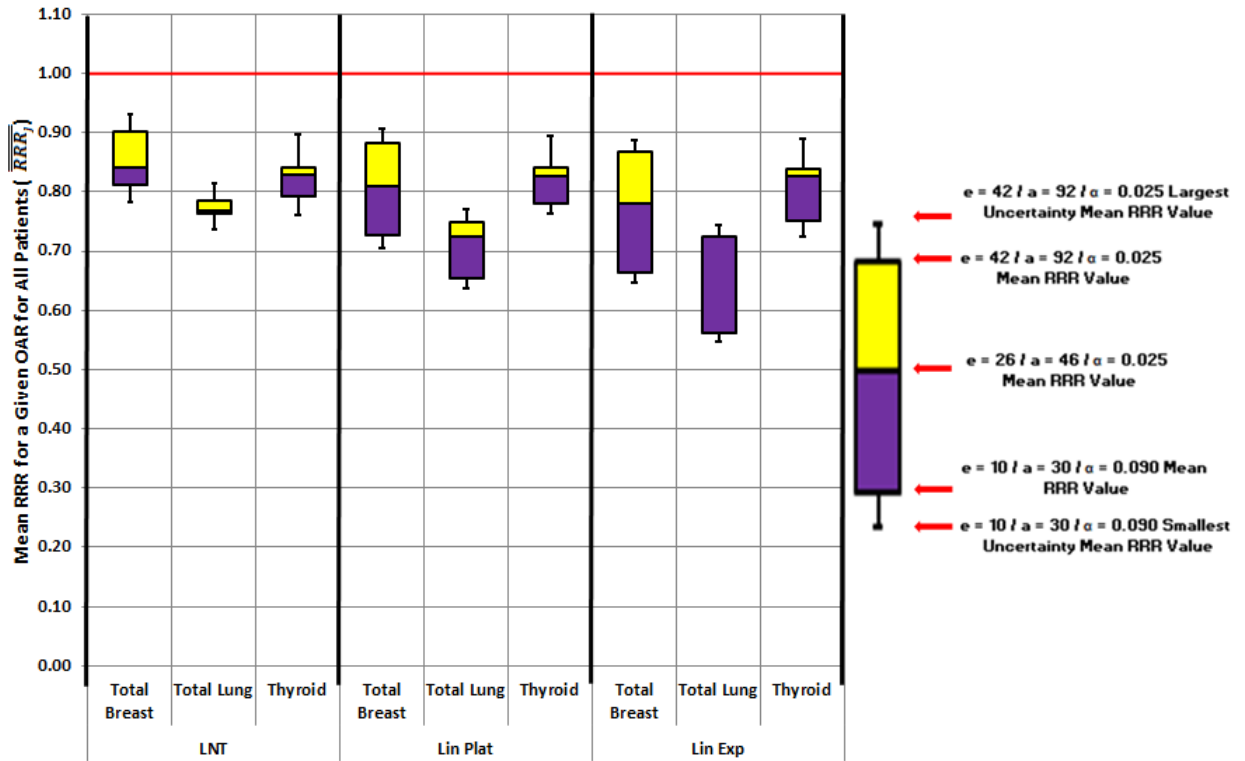


Figure 3-17 – Extrema \overline{RRR}_j for PSPT vs IMRT, exposed age (e), attained age (a), α , and neutron $\overline{w}_R = 20$ - Of note, the display is not a standard box and whisker graph, but rather a way of displaying the extrema in one image concisely. See legend to the right of the figure. Including the error bars, none of the \overline{RRR}_j values in the figure had a mean RRR value > 1 . The average patient tested in Aim 1 ($e = 26, a = 46, \alpha = 0.025$) is the interface between the yellow and purple portions of the graph. Including error bars, the range of outcomes for this figure show a \overline{RRR}_j value between 0.55 and 0.94.

The sign (Figure 3.17) and Student's t-test (Table 3.8) were applied to the data shown in Figures 3.17. Outcomes were similar to those figures with the majority of the data points indicating a mean $RRR < 1$. Again, the thyroid showed a higher percentage of parameter configurations that showed no significance. No configuration indicated significance for photon plans.

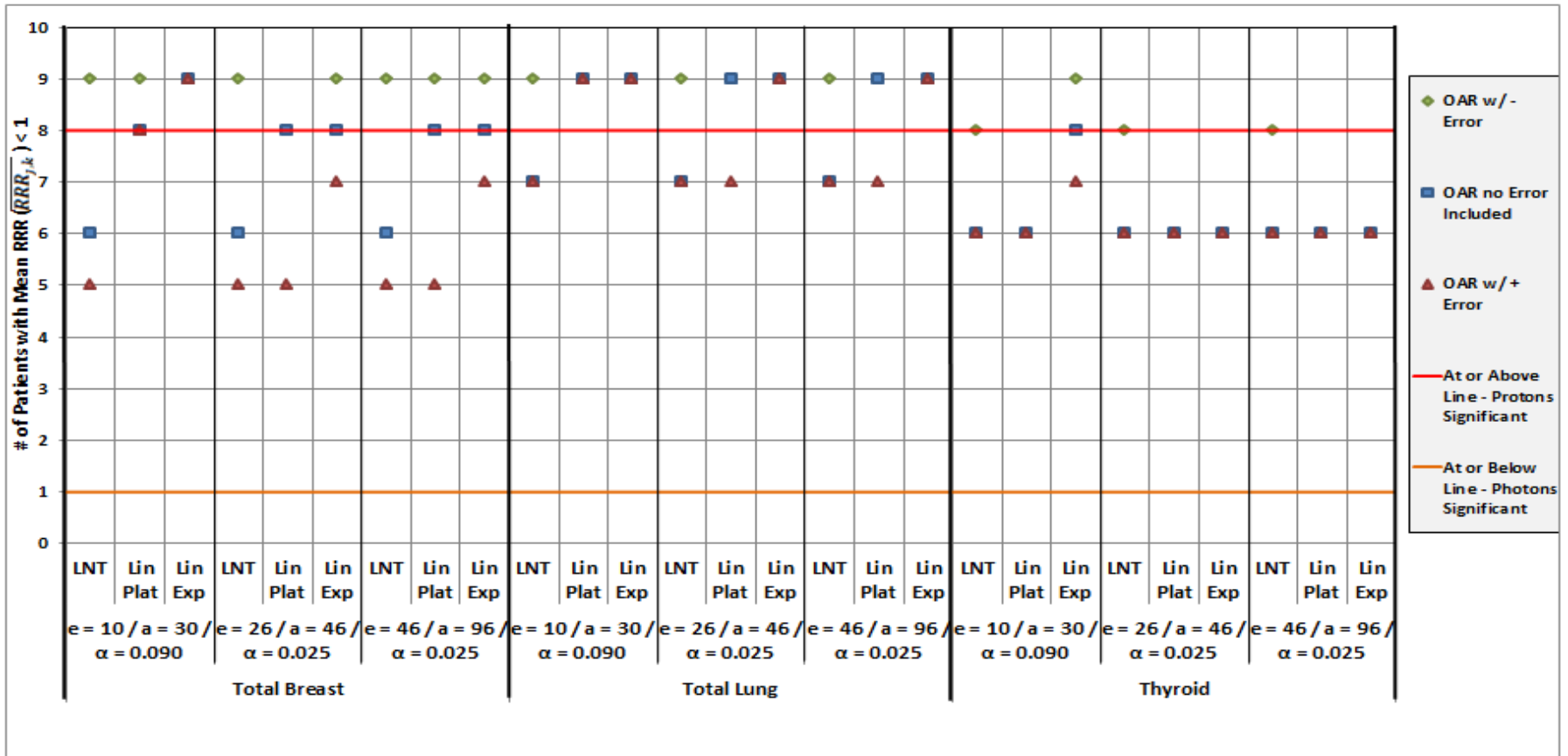


Figure 3-18 – Sign test of $\overline{RRR}_{j,k}$ extrema for PSPT vs IMRT, exposed age (e), attained age (a), neutron $\overline{w}_R = 20$, all dose response models, and α - The blue square indicates the nominal $\overline{RRR}_{j,k}$ values. The red triangles designate the nominal $\overline{RRR}_{j,k}$ plus its corresponding error, and the green diamonds are the nominal $\overline{RRR}_{j,k}$ minus the corresponding error. All points at or below the Orange Line indicates the $\overline{RRR}_{j,k}$ is significantly > 1. All points at or above the Red Line indicates the $\overline{RRR}_{j,k}$ is significantly < 1. All points between the Red and Orange line indicate the $\overline{RRR}_{j,k}$ is not significantly different than 1. There are 81 unique $\overline{RRR}_{j,k}$ values in the figure. Of the 81, 40 (49.4%), indicated the $\overline{RRR}_{j,k}$ was not significantly different than 1. 22 of the 40 points that indicated no significance were for the thyroid.

Table 3-8 – Student’s t-test of $\overline{RRR}_{j,k}$ extrema for PSPT vs IMRT, exposed age (e), attained age (a), neutron $\overline{w}_R = 20$, all dose response models, and α -
 Values show any potential statistical significance for a given treatment plan if the uncertainty is subtracted from the nominal $\overline{RRR}_{j,k}$ (- Error), the uncertainty is added to the nominal $\overline{RRR}_{j,k}$ value (+ Error), and with just the nominal $\overline{RRR}_{j,k}$ value (OAR name only). Of the 81, 25 (30.9%), indicated the $\overline{RRR}_{j,k}$ was not significantly different than 1. 16 of the 25 points that indicated no significance were for the thyroid.

PSPT Treatment Parameters for Comparisons to IMRT	Dose Response Model	Treatment Significance								
		Breast w/ - Error	Breast	Breast w/ + Error	Lung w/ - Error	Lung	Lung w/ + Error	Thyroid w/ - Error	Thyroid	Thyroid w/ + Error
e = 10 / a = 30 / $\alpha = 0.090$	LNT	Protons	Protons	None	Protons	Protons	None	Protons	None	None
	Lin Plat	Protons	Protons	Protons	Protons	Protons	Protons	Protons	None	None
	Lin Exp	Protons	Protons	Protons	Protons	Protons	Protons	Protons	Protons	Protons
e = 26 / a = 46 / $\alpha = 0.025$	LNT	Protons	Protons	None	Protons	Protons	None	Protons	None	None
	Lin Plat	Protons	Protons	None	Protons	Protons	Protons	Protons	None	None
	Lin Exp	Protons	Protons	Protons	Protons	Protons	Protons	Protons	None	None
e = 46 / a = 96 / $\alpha = 0.025$	LNT	Protons	Protons	None	Protons	Protons	None	Protons	None	None
	Lin Plat	Protons	Protons	None	Protons	Protons	Protons	Protons	None	None
	Lin Exp	Protons	Protons	None	Protons	Protons	Protons	Protons	None	None

As in Aim 1, tables summarizing the finding of Aim 2 are now listed. Due to the amount of data they have been broken into three separate tables. Table 3.9 compares the differences between the dose response models to the Aim 1 data. Table 3.10 shows the variation in the results as the neutron \bar{w}_R varies, and Table 3.11 displays the extrema comparisons.

Table 3-9 – Summary of all major finding from Aim 2 - comparisons to Aim 1 – Breaks down the results by PSPT and IMPT tests compared to IMRT. Note that the column labeled “Mean for All 9 Patients” averages all 9 of the respective $\overline{RRR}_{j,k}$ values together. These values correspond to \overline{RRR}_j . A mark like this (*) indicates that the given proton plan significantly ($p \leq 0.05$) reduced the risk of RSC compared to IMRT.

Patient Parameters	Metric Examined	Corresponding Figure	Mean for All 9 Patients	Sign Test	Student's T-Test	Comment	
e = 26, a = 46, Lin Plat, neutron $\overline{w}_R = 20, \alpha = 0.025$	PSPT vs IMRT						
		$\overline{RRR}_{j,k}$				Non-linear dose response models increased the significance of PSPT plan relative to LNT. Thyroid still showed no significant difference between the two modalities	
	Breast	Figure 3.11	0.81 ± .03	P = 0.046*	P = 0.014*		
	Lung	Figure 3.12	0.72 ± .02	P = 0.008*	P = 0.003*		
	Thyroid	Figure 3.13	0.83 ± .04	P = 0.503	P = 0.102		
		IMPT vs IMRT					
		$\overline{RRR}_{j,k}$				IMPT again improves upon the PSPT result. There is roughly a 10% decrease in risk compared to the PSPT plan but the qualitative findings remain the same	
	Breast	Figure 3.11	0.74 ± .03	P = 0.046*	P = 0.004*		
	Lung	Figure 3.12	0.64 ± .02	P = 0.046*	P = 0.004*		
	Thyroid	Figure 3.13	0.75 ± .05	P = 0.503	P = 0.051		
	e = 26, a = 46, Lin Exp, neutron $\overline{w}_R = 20, \alpha = 0.025$	PSPT vs IMRT					
			$\overline{RRR}_{j,k}$				The Lin Exp model reduces mean RRR values below the Lin Plat model. In general with respect to mean RRR Lin Exp < Lin Plat < LNT
Breast		Figure 3.11	0.78 ± .03	P = 0.046*	P = 0.006*		
Lung		Figure 3.12	0.68 ± .02	P = 0.008*	P = 0.000*		
Thyroid		Figure 3.13	0.82 ± .04	P = 0.503	P = 0.077		
		IMPT vs IMRT					
		$\overline{RRR}_{j,k}$				This is the only configuration that shows a significant reduction in mean RRR for a proton plan compared to IMRT for the thyroid.	
Breast		Figure 3.11	0.71 ± .03	P = 0.046*	P = 0.002*		
Lung		Figure 3.12	0.64 ± .02	P = 0.008*	P = 0.000*		
Thyroid		Figure 3.13	0.75 ± .05	P = 0.503	P = 0.041*		

Table 3-10 – Summary of all major finding from Aim 2 - neutron $\overline{w_R}$ variation – Breaks down the results by PSPT and IMPT tests compared to IMRT. Note that the column labeled “Mean for All 9 Patients” averages all 9 of the respective $\overline{RRR}_{j,k}$ values together. These values correspond to \overline{RRR}_j . A mark like this (*) indicates that the given proton plan significantly ($p \leq 0.05$) reduced the risk of RSC compared to IMRT.

Patient Parameters	Metric Examined	Corresponding Figure	Mean for All 9 Patients	Sign Test	Student's T-Test	Comment	
e = 26, a = 46, LNT, neutron $\overline{w_R} = 5, \alpha = 0.025$	PSPT vs IMRT						
	$\overline{RRR}_{j,k}$	Figure 3.16					
	Breast		0.75 ± .03	P = 0.008*	P = 0.003*	The reduction in neutron dose compared to Aim 1 results shows increased significance for all three individual OARs including the thyroid	
	Lung		0.70 ± .02	P = 0.008*	P = 0.002*		
	Thyroid		0.72 ± .05	P = 0.503	P = 0.037*		
	IMPT vs IMRT						
$\overline{RRR}_{j,k}$	Figure 3.16						
Breast			0.73 ± .03	P = 0.008*	P = 0.002*	Again we see an increase in significance for the IMPT compared to the PSPT. It did not change the qualitative findings, however	
Lung			0.69 ± .02	P = 0.008*	P = 0.001*		
Thyroid			0.70 ± .06	P = 0.184	P = 0.033*		
e = 26, a = 46, Lin Exp, neutron $\overline{w_R} = 5, \alpha = 0.025$	PSPT vs IMRT						
	$\overline{RRR}_{j,k}$	Figure 3.16					
	Breast			0.69 ± .03	P = 0.008*	P = 0.001*	The Lin Exp dose response model increased significance compared to the LNT model
	Lung			0.62 ± .02	P = 0.008*	P = 0.000*	
	Thyroid			0.73 ± .05	P = 0.503	P = 0.028*	
	IMPT vs IMRT						
$\overline{RRR}_{j,k}$	Figure 3.16						
Breast			0.68 ± .03	P = 0.008*	P = 0.001*	This is the only time we see an decrease in significance using a non-linear dose response model compared to LNT. Higher doses for the photon IMRT plan led to an increased reduction in RSC risk compared to the lower dose IMPT plan	
Lung			0.61 ± .02	P = 0.008*	P = 0.000*		
Thyroid			0.71 ± .05	P = 0.503	P = 0.026*		
e = 26, a = 46, LNT, neutron $\overline{w_R} = 35, \alpha = 0.025$	PSPT vs IMRT						
	$\overline{RRR}_{j,k}$	Figure 3.16					
	Breast			0.93 ± .03	P = 1.000	P = 0.313	This represents the worst outcome for proton plans compared to IMRT. No significant difference is seen between the two plans, however the majority of patients still show a mean RRR < 1
	Lung			0.84 ± .03	P = 0.184	P = 0.076	
	Thyroid			0.93 ± .04	P = 1.000	P = 0.516	
	IMPT vs IMRT						
$\overline{RRR}_{j,k}$	Figure 3.16						
Breast			0.82 ± .03	P = 0.184	P = 0.028*	IMPT still maintains significance for some OARs compared to the neutron $\overline{w_R} = 5$ but thyroid again shows no significant difference between the plan comparisons	
Lung			0.77 ± .03	P = 0.184	P = 0.014*		
Thyroid			0.80 ± .05	P = 0.503	P = 0.115		
e = 26, a = 46, Lin Exp, neutron $\overline{w_R} = 35, \alpha = 0.025$	PSPT vs IMRT						
	$\overline{RRR}_{j,k}$	Figure 3.16					
	Breast			0.86 ± .03	P = 0.184	P = 0.054	The Lin Exp dose response model again decreases the mean RRR values, even to the point of showing PSPT to be significantly better than IMRT for some OARs
	Lung			0.74 ± .02	P = 0.008*	P = 0.003*	
	Thyroid			0.92 ± .04	P = 0.503	P = 0.330	
	IMPT vs IMRT						
$\overline{RRR}_{j,k}$	Figure 3.16						
Breast			0.74 ± .03	P = 0.046*	P = 0.005*	Breast now sees significant improvement in RSC risk for IMPT compared to IMRT	
Lung			0.66 ± .03	P = 0.008*	P = 0.000*		
Thyroid			0.79 ± .05	P = 0.503	P = 0.069		

Table 3-11 – Summary of all major finding from Aim 2 - extrema comparison – Breaks down the results for PSPT compared to IMRT only. Note that the column labeled “Mean for All 9 Patients” averages all 9 of the respective $\overline{RRR}_{j,k}$ values together. These values correspond to \overline{RRR}_j . A mark like this (*) indicates that the given proton plan significantly ($p \leq 0.05$) reduced the risk of RSC compared to IMRT.

Patient Parameters	Metric Examined	Corresponding Figure	Mean for All 9 Patients	Sign Test	Student's T-Test	Comment			
e = 10, a = 30, LNT, neutron $\overline{w}_R = 20$, $\alpha = 0.090$	PSPT vs IMRT	Figure 3.17				This is the best case scenario for LNT when the neutron $\overline{w}_R = 20$ for the PSPT plan compared to the IMRT plan. While significance is improved relative to Aim 1 results for PSPT, there is no change in the qualitative findings			
	$\overline{RRR}_{j,k}$								
	Breast						0.81 ± .03	P = 0.503	P = 0.037*
	Lung						0.76 ± .02	P = 0.184	P = 0.013*
	Thyroid	0.79 ± .03	P = 0.503	P = 0.112					
e = 10, a = 30, Lin Exp, neutron $\overline{w}_R = 20$, $\alpha = 0.090$	PSPT vs IMRT	Figure 3.17				As seen throughout, non-linear dose response models further reduces the risk of RSC for PSPT compared to IMRT in most instances. These are the absolute lowest mean RRR value			
	$\overline{RRR}_{j,k}$								
	Breast						0.66 ± .02	P = 0.008*	P = 0.000*
	Lung						0.56 ± .01	P = 0.008*	P = 0.000*
	Thyroid	0.75 ± .03	P = 0.046*	P = 0.014*					
e = 42, a = 92, LNT, neutron $\overline{w}_R = 20$, $\alpha = 0.025$	PSPT vs IMRT	Figure 3.17				This is the worst case scenario for LNT when the neutron $\overline{w}_R = 20$ for the PSPT plan compared to the IMRT plan. Compared to the best case immediately above, we see no change in the qualitative findings			
	$\overline{RRR}_{j,k}$								
	Breast						0.90 ± .03	P = 0.503	P = 0.033*
	Lung						0.79 ± .03	P = 0.184	P = 0.013*
	Thyroid	0.84 ± .06	P = 0.503	P = 0.131					
e = 42, a = 92, Lin Exp, neutron $\overline{w}_R = 20$, $\alpha = 0.025$	PSPT vs IMRT	Figure 3.17				Compared to the Lin Exp for e = 10, a = 30, we see the same qualitative findings with the exception of thyroid which showed no significance			
	$\overline{RRR}_{j,k}$								
	Breast						0.87 ± .02	P = 0.046*	P = 0.007*
	Lung						0.71 ± .02	P = 0.008*	P = 0.000*
	Thyroid	0.84 ± .05	P = 0.503	P = 0.079					

4. Discussion

4.1. Outcome of Specific Aim 1

The goal of Specific Aim 1 was to determine baseline \overline{RRR} values calculated between proton PSPT and IMPT treatment plans vs the corresponding photon IMRT plan for the total breast, total lung, and thyroid of 9 patients using a representative patient exposed at the age of 26 years and attaining the age of 46 years. The neutron \bar{w}_R value equaled 20 and the LNT dose response model was used to calculate the \overline{RRR} .

Several \overline{RRR} endpoints were used (See Table 2.3). With respect to significant difference, each gave variable answers. While the majority of parameter permutations for each patient indicated a mean RRR value < 1 , a statistically significant difference from a value of 1 was not always found. Two statistical tests were used, the sign test and the Student's t-test. Analysis was conducted for both the PSPT/IMRT and IMPT/IMRT comparison.

The sign test for PSPT/IMRT comparison showed no significant difference from a value of 1 ($p \leq 0.05$) for $\overline{RRR}_{j,k}$ for any of the OARs considered. The IMPT plan increased the differences compared to the IMRT plan by demonstrating a mean RRR < 1 for the total breast and total lung.

Student's t-test (which takes the magnitude of the mean RRR value into account) gave the same qualitative results as the sign test for the IMPT/IMRT comparison. The PSPT/IMRT comparison again showed a statistically significant reduction relative to the IMRT plan when all 3 OARs were averaged together, but also showed a statistically significant reduction for the total breast and total lung as well. Thyroid showed no difference for either comparison again.

Note that these results are for the nominal mean RRR values. If the error bars were taken into account, the answers either gave a more favorable view of the photon IMRT plan (by adding the error to the nominal mean RRR) or to the proton plans (by subtracting the error). Regardless of the permutation, though, statistically significant reduction in the \overline{RRR} 's, if any, only favored the proton plans.

Additionally, the other mean RRR endpoint examined ($\overline{\overline{RRR}}_j$) also showed a reduction (including error bars) in the RSC risk relative to the IMRT plan for all endpoints. For the PSPT/IMRT comparison, the $\overline{\overline{RRR}}_j$ for total breast was 0.84, for total lung, 0.77, and for thyroid, 0.84. For the IMPT/IMRT comparison the $\overline{\overline{RRR}}_j$ for total breast was 0.77, for total lung, 0.73, and for thyroid, 0.75.

Tests of the correlation of any host or treatment factors to mean RRR values showed minimal or negligible correlation for all OARS save the thyroid, which showed moderate correlation as a

function of the patient's exposed age (decreases as patients get older) and the mean RRR values of all OARs except thyroid (increases as the other mean RRR values of other OARs increase).

4.2. Outcome of Specific Aim 2

The goal of Specific Aim 2 was to determine the uncertainty associated with the baseline mean RRR values found in Specific Aim 1 by varying the parameters that affect the mean RR calculations used to compare the treatment plans.

When varying the dose response models for the representative patient in Aim 1 (with a fixed neutron $\overline{w_R}$ of 20), the greatest range of mean RRR for any combination of dose response model, dose response inflection point, and OAR ($\overline{RRR_j}$) was between 0.60-0.84 for PSPT/IMRT and 0.53-0.77 for IMPT/IMRT. The non-linear dose response model generally decreased the mean RRR relative to the LNT model, and the IMPT plan lowered the mean RRR value on average by an additional 12% compared to the PSPT plan.

Mean RRR values varied by a slightly larger amount as a function of neutron $\overline{w_R}$. Once again using the representative patient from Aim 1 as a baseline, the greatest range of the nominal mean RRR for any combination of dose response model, dose response inflection point, and OAR ($\overline{RRR_j}$) was between 0.51-0.93 for PSPT/IMRT and 0.49-0.82 for IMPT/IMRT.

The smaller range for the IMPT is expected due to the lack of external neutrons and therefore reduced total neutron dose added to the dose distribution relative to IMRT. While a neutron $\overline{w_R}$ of 20 is a very plausible value to use for calculations, values closer to 10 have been reported in the literature for other radiotherapy sites (Newhauser et al., 2009), so this value could be considered conservative.

Extrema variations from OAR to OAR (Figure 3.20), were much less diverse. Including dose response model variation, the $\overline{RRR_j}$ for total breast ranged from 0.64-0.93 for a variation of $\sim \pm 17\%$ from the mean, total lung ranged from 0.55-0.82 for a variation of $\sim \pm 18\%$ from the mean, and thyroid ranged from 0.72-0.90.

With respect to statistical significance for the extrema, the sign test showed no significant differences between the PSPT and IMRT treatments when the LNT model was used. Use of non-linear dose response models led to significance for some additional configurations of the total breast and total lung, but the thyroid never did.

Compared to the sign test results, the Student's t-test increased the number of PSPT configurations where PSPT significantly reduced the RSC risk *versus* IMRT. Significance was seen in the total breast, total lung, and all 3 OARs averaged together. There were no \overline{RRR} configurations

throughout this entire work that indicated the photon plan would be statistically significantly better than either proton plan at reducing RSC risk.

Evidently, the majority of patients tend to favor the proton treatments compared to the photon IMRT treatment with respect to RSC risk for the lungs and breast. The thyroid, however, showed no significant reduction in RSC risk for the proton plans, even when non-linear dose response models were used. Overall, with the exception of thyroid, our data indicated that patients exposed at younger ages saw reduced RSC risk using the proton plans compared to the photon IMRT than older patients did.

Despite the majority of patients indicating RSC risk reduction by using proton therapy, one patient, #7, almost exclusively displayed $\overline{RRR} > 1$, even showing values that exceeded the range of uncertainty of all other patients. Patient #7 showed no great deviation from the mean for most host factors, such as height, weight, etc. She was, however, one of the three youngest in the cohort (15 years at the time of exposure) which, for thyroid, indicated a small tendency to increase \overline{RRR} . She also had larger than average OAR volumes, which provided more tissue used in the calculation of OAR RSC risk to be exposed to radiation. In addition, her proton beam orientation was not an AP/PA setup as was done for the majority of the patients, but an AP/Lateral configuration.

Only one other patient (#1) had this field arrangement. Their mean RRR value was higher than the average for the total breast, which is attributed to the lateral beam traversing the left breast in order to treat the tumor volume. While these two share similarities with respect to the total breast, the mean RRR for the thyroid of Patient #7 is substantially higher than Patient #1. This is attributed to the CTV being much more superior in the patient body for #7 compared to #1. Figure 4.1 compares the photon IMRT dose distribution for two axial slices compared to the proton PSPT plan (therapeutic dose only) for Patient #7.

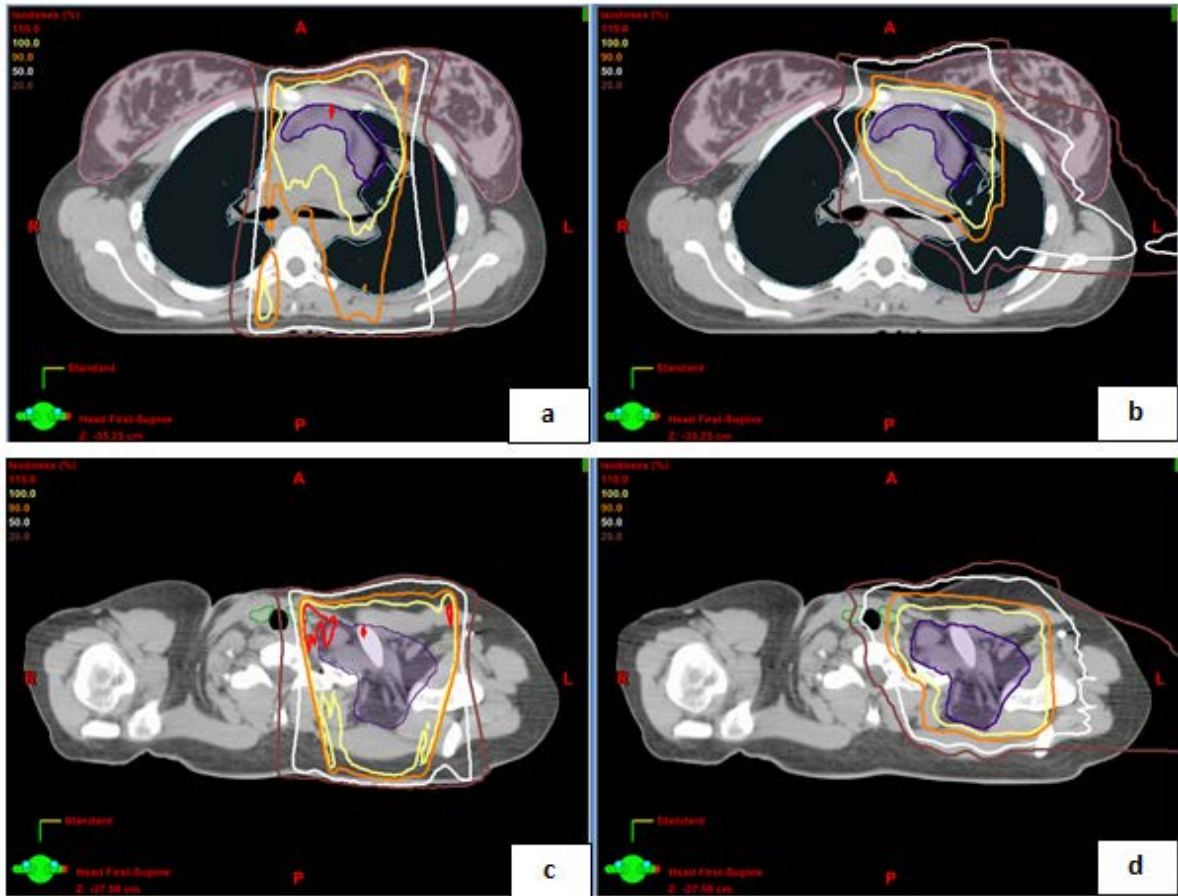


Figure 4-1 – Axial slices of Patient #7 highlighting increased dose from the IMRT plan vs the PSPT plan
 - a) IMRT plan highlighting the reduction in dose to the breast (pink) compared to the PSPT plan in b), which is the same axial slice as a). c) IMRT plan highlighting the significant reduction to the thyroid (green) compared to the PSPT plan in d), which is also the same axial slice as c). The lateral beam appears to significantly increase the dose incident of these two OARs, which have mean RRR values > 1.

In general, proton plans lowered the \overline{RRR} compared to photon IMRT for all OARs except the thyroid, for which no significant deviation from a mean RRR value of 1 was observed.

4.3. Coherence with Existing Literature

With respect to the major endpoints of the work, the mean RRR, the work which most closely resembles ours was that of Cella et al. (2013). In it, they benchmarked a similar calculation to the RRR (they called it the risk ratio) using dose volume histograms (DVH) bins rather than voxel by voxel calculations to account for dose heterogeneity. They also only calculated for an IMPT configuration, which excludes an external neutron component. Other differences included, they only used one representative patient with artificially drawn CTVs, applied a model based internal neutron component within the primary (i.e. open) field only and used a neutron $\overline{w}_R = 7$ instead of using direct

calculation in and out of field, and they included cell kill, repopulation, and fractionation variations in their risk calculations using methods from Schneider (2009).

In their work, they used three CTV/PTV volumes to compare their version of the RRR. Our patients spanned the spectrum of these volumes, and we selected patients that most closely resembled theirs. Several aspects of their representative patient differed from ours; however, a comparison of their results and ours is shown in Figure 4.2.

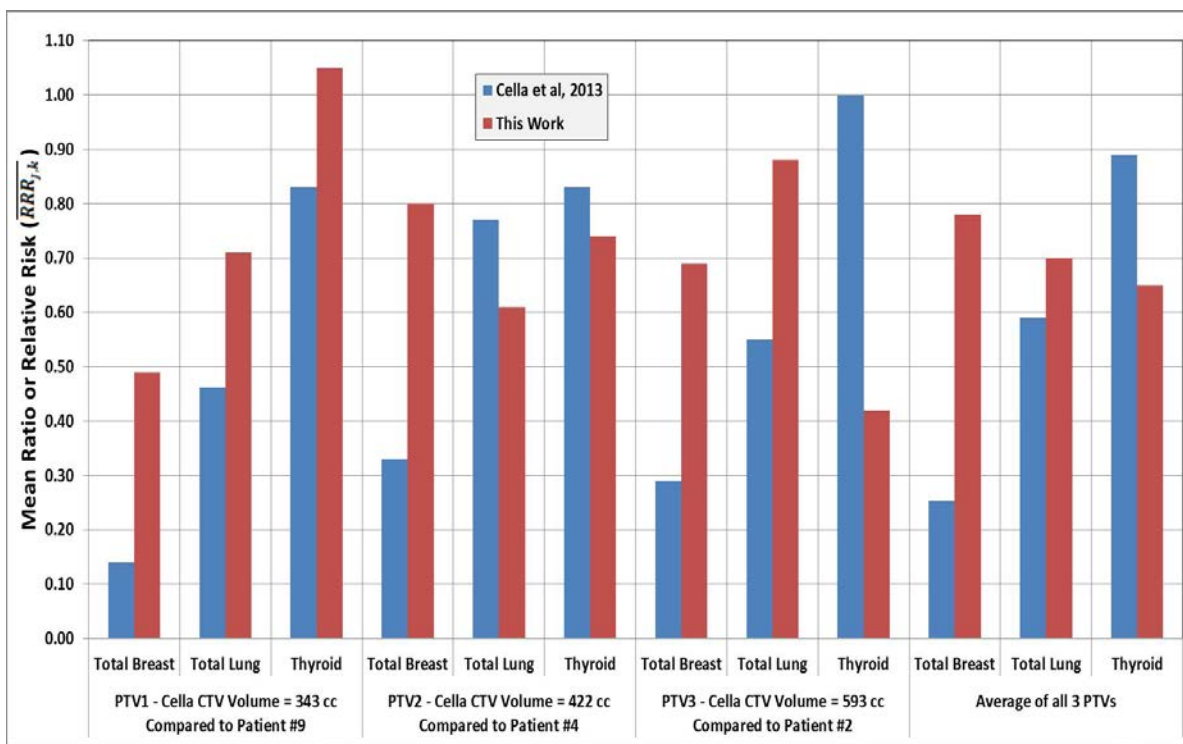


Figure 4-2 – Comparison of Cella *et al*, 2013 mean RRR values to this work – Comparison between our configuration that most closely mirrored the work by Cella *et al* (IMPT treatment, linear plateau dose response model, neutron $\overline{w_R}$). The various PTV designations (1,2,3) indicate the varying size of the contoured PTV in the Cella *et al* paper. The mean of the OARs for each of the three PTV sizes is shown in the fourth column designated as “Average of all 3 PTVs”. Their results indicate a reduction in $\overline{RRR}_{j,k}$ values relative to our study. In addition, each PTV examined shows increasing $\overline{RRR}_{j,k}$ values (from lowest to highest) to the total breast, total lung, and thyroid. This differs from our results and is likely caused by tumor location.

Their results favored the IMPT plans compared to our findings especially for the total breast. While they also found the mean RRR to be < 1 , their data indicated a more significant reduction compared to our results. There are several possible reasons for this.

1) The proton beam energies they used ranged from 62-180 MeV. Ours were much higher (often above 200 MeV and up to 250 MeV) which would have increased the neutron dose, which they only accounted for in field. Additionally, they prescribed a dose of 30 Gy instead of 36 Gy as we did,

which would reduce risk values slightly as well due to a reduction in neutron contributions. 2) The PTV was constructed to largely be symmetrical bi-laterally in the patient both laterally and in the superior/inferior direction. This is a fairly idealized setup for treatments, and was often not seen in our patients, including the patients in this comparison. Patient #4 (used to compare PTV2 above) was a close approximation to this geometry and is the closest replication to the results from Cella *et al.* 3) Their IMRT treatment used seven fields and ours were five field setups. A reduction in the number of fields and therefore, volume of healthy tissue irradiated, will lower the patient's risk of RSC using IMRT (De Bruin et al., 2009, Ng et al., 2010, Weber et al., 2011, Paganetti et al., 2012). 4) Their study only included one patient which eliminates the variations seen in patient anatomy and tumor location across a cohort.

Despite these differences, the overall results generally agree. Several other studies have also indicated a clear advantage for proton plans versus photon plans for HL, either dosimetrically (Chera et al., 2009, Andolino et al., 2011) or with risk calculations included (Schneider et al., 2000, Cella et al., 2013). Additionally, both Schneider *et al* and Cella *et al* found that there was minimal improvement in the thyroid when comparing the photon and proton therapies. This agreed with our findings, further strengthening this result.

While our overall results are generally consistent with the previous works, the advantage for the proton treatments is not as significant as their studies suggested. Possible reasons for this include: 1) Some previous studies conducted measurements on only one representative patient. 2) No previous studies included neutron exposures, either forgoing them completely or introducing static in-field neutron estimations from Schneider et al. (2002). 3) As stated previously, certain aspects of their treatment parameters for both the proton and photon fields tend to provide a best case scenario for the proton setup.

Comparisons to other published data similar to our studies also matched up fairly well. Our adjustment of the photon dose to voxels beyond the 5% isodose line led to an average increase in our OAR mean dose by 14.5% in total breast, 2.6% in total lung, 4.6% for the thyroid. Papers by Howell et al. (2010a) and Joosten et al. (2011) reported an under dosage by the commercial TPS to voxels which fell below the 5% isodose line by 40 - 60%. Since voxels with values greater than the 5% isodose line were unchanged, and the majority of OARs for the 9 patients had larger portions of their volume above the 5% isodose line, our adjustments were lower than the value reported by Howell *et al* and Joosten *et al*.

While the average increases in mean doses were the values reported above, there were a few instances where individual patients registered an increase in dose above the 60% threshold. This was attributed to the use of an IMRT fields compared to the open fields used in the previously cited

works. The many small fields used by the IMRT plan causes the peripheral dose profile to be largely comprised of scatter from the linear accelerator treatment head. Multiple studies, including Howell et al. (2006b) and Ruben et al. (2011) showed in a comparison between IMRT and three dimensional conformal therapy (3DCRT) that head scatter and leakage was significantly higher for IMRT compared to 3DCRT since it was proportional to the number of monitor units (MU) delivered.

The neutron calculations for our proton plans also match up well with previous studies. Taddei et al. (2010a) is the closest comparison to our work, most closely corresponding to Patient #2 from our work. They treated a tumor located in the liver with 2 proton fields using the same proton energies (225 and 250 MeV) and have similar spread out Bragg peak widths (SOBP).

If one adjusts Taddei's work to equate the neutron \overline{w}_R value to 20 and to deliver the same prescribed dose, the mean cSv/Gy for his work to the liver is 3.8 cSv/Gy. The mean H/D value for the total breast and total lung together (which is as close to a similar OAR location as we had) in our work was 5.7 cSv/Gy. The increased value of our calculations compared to Taddei *et al* can be partially explained by their use of an intermediate snout size (corresponding to an 18x18 cm² open field) in their work while we used a larger snout configuration (25x25 cm²). Stray neutron exposures have been shown to be sensitive to the position of the snout (Mesoloras et al., 2006, Zheng et al., 2007). In addition, Zheng et al. (2008) have shown that a change from the intermediate snout to the larger size for a 250 MeV beam can lead to an increase in neutron equivalent dose by more than 25%. Adjusting the values to account for this brings the values closely in line.

It is important to point out that Patient #2 was the patient with the maximum neutron dose contributions compared to other patients. Averaging all OARs together for all patients, the mean neutron dose was 2.97 cSv/Gy.

Our work also saw an increase in neutron dose as a function of proton beam energy, which corresponds to other works (Zheng et al., 2007, Zheng et al., 2008, Fontenot et al., 2008). With the exception of Patient #8, patients with the largest neutron dose contribution came from the plans with the highest proton beam energies. Patient #8, recall, was our youngest patient (and also one of our smaller ones as well) and had larger portions of her anatomy exposed to scatter dose.

The increase in the contribution of neutrons to the OARs followed closely with that of Newhauser et al. (2009). Their work showed that internal neutron and external neutron spectra deliver roughly the same amount of dose when accounted for. Our work showed a slight increase of internal neutron dose compared to the external neutrons. Our fields were also much larger relative to their study which would account for the increased internal neutron dose production in the patient. Of note, the total neutron contribution is no more than 20% of the total risk contribution for neutron $\overline{w}_r =$

20 for PSPT, and can be as little as 3% when the neutron $\overline{w_R} = 5$. The coherence with these previous works provides further confidence of out of field scatter dose contributions values in our study.

Our findings demonstrate an advantage for proton treatments relative to photon IMRT treatments for HL patients with respect to RSC risk, which is in qualitative agreement with previous studies. However, our studies suggest the need for taking into account neutron exposures and individualized treatment planning in performing risk assessment.

4.4. Implications and Significance of Findings

From a public health perspective, the high cure rates and long survival times after HL treatment make plausible reductions of RSC risks an important and relevant study. Since the turn of the millennium, many epidemiological and radiation exposure studies have examined this topic. Unlike other studies which have shown clear advantages of protons vs photon treatments (Schneider et al., 2000, Newhauser et al., 2009, Fontenot et al., 2009, Chera et al., 2009, Taddei et al., 2010b, Taddei et al., 2010a, Paganetti et al., 2012, Rechner et al., 2012a, Cella et al., 2013), our work has a more nuanced conclusion.

In the majority of patients considered, the proton plans offered a lower predicted mean RR to the OARs of interest. This was not the case for all patients, however, and can be attributed to several unique contributions of this work.

To the best of our knowledge, this study is the first to conduct a full neutron dose calculation for a HL proton plan. The significance of this increase in mean dose to the OAR is, of course, highly dependent on the neutron $\overline{w_R}$ value. For a neutron $\overline{w_R}$ of 5, the increase in mean dose to the OARs is around 5%. For a neutron $\overline{w_R}$ of 20, however, the OAR mean doses increased between 16-20% for PSPT plans, which for a LNT dose response would increase the risk by a corresponding percentage. This is a non-negligible amount that needs to be incorporated before making definitive statements about the RSC risk comparisons between plans.

Our plans also had one of the higher prescribed doses (36 Gy) in the spectrum for HL treatments. Many other similar works used 20-30 Gy and can even go as low as 20 Gy. Reducing the dose would lower the proton treatment's mean RRR at a faster rate than the IMRT plan because of the additional reduction of the neutron dose component.

Additionally, to the best of our knowledge, this is the first study to make corrections to the under-dosed areas calculated for the IMRT photon plan by the commercial TPS with direct field measurements made in phantom. The increase in the mean dose for organs which are far away from

the tumor, such as a superiorly placed HL tumor that largely spares the breast (which increased the mean dose by 10-15%) could also change the qualitative outcome of modality comparisons.

This is also the first study that included RSC risk sensitivity analysis for an HL cohort. Dosimetric studies have been conducted on more than one patient, but other recent risk analysis have been done on one representative patient (Cella et al., 2013). The extrema testing conducted in this work attempts to bracket the range of uncertainties associated with this patient set. While there are still questions as to the exact biological mechanisms involved in the development of RSCs, the insensitivity of the qualitative findings to the choice of risk models should greatly increase confidence in the results.

When examining proton vs photons, the majority of RSC risk studies in the literature only looked at IMPT plans (Schneider et al., 2000, Cella et al., 2013). While our studies showed that IMPT would reduce the risk compared to PSPT, on average this reduction for the LNT dose response model was 8% for total breast, 5% for total lung, and 12% for thyroid and never exceeded the error bars for PSPT. This is important for several reasons, but emphasis is focused on the fact that none of our studies take into account breathing motion, instead assuming the tumor volumes found from the CT scan represent the average CT position of the tumor and subsequent OARs.

Since supra-diaphragmatic HL tumors are located in the thorax, motion should be examined. Studies have shown that for lung tumors, assumed dose to the tumor (and lack thereof to healthy tissue) is not delivered as intended due to geographic misses of the tumor as a result of respiratory motion (Engelsman et al., 2006, Starkschall et al., 2009).

The nature of the IMPT beam delivery compared to the more stable PSPT could cause hot and cold spots due to dosimetric misses of the tumor as a result of the interplay between the organ and tumor motion and the beam (Grozinger et al., 2006, Newhauser et al., 2009). Recent studies have discussed the uses and need for 4D imaging of HL patients to better improve treatment outcomes as well (Stromberg et al., 2000, Claude et al., 2007, Specht et al., 2013, Eley et al., 2013).

Finally, the findings revealed that large inter-patient variations necessitate population based studies. Furthermore, clinical care decisions made from the sole perspective of RSC risk seem to, in general, favor the various proton plans over photon IMRT, but personalized RSC predictions are needed.

4.5. Strengths of the Study

This study was unique from several different aspects. The full dosimetric analysis due to the inclusion of the secondary dose contributions of both the proton and photon treatment plans increases the confidence of our risk analysis, which has been noted by the authors of other studies as

a shortcoming of their results (Schneider et al., 2000, Chera et al., 2009, Weber et al., 2011, Cella et al., 2013).

The sensitivity analysis of Specific Aim 2 addressed several of the most important sources of uncertainty associated with the calculation of the RSC risk. Rather than make a single assumption, a range of possibilities were calculated via brute force calculation to assist in drawing more meaningful and confident choices regarding treatment selection of HL patients with respect to RSC risk.

Another strength, as pointed out earlier, was the inclusion of multiple patients in the dosimetric analysis of this study. Incorporating multiple patients allowed us to observe and account for the variation found between each patient, both in their anatomy and in their tumor characteristics. Importantly, clinically significant differences were seen which would not have been observed had a phantom of a single representative patient been used.

One final strength was the calculation of the risk on a voxel by voxel basis. While these voxels were averaged together for each OAR and then reported as the mean RR in this work, there is potential to use the voxel based calculations to visualize the risk calculations as commercial TPSs' visualize dose as seen in Figure 4.3. Other works used similar techniques to account for the heterogeneity but used data from a DVH, which allocates the dose appropriately, but loses the spatial location of that dose in the process (Rechner et al., 2012a, Cella et al., 2013).

There are many unanswered questions in personalized RSC, such as is it appropriate to use risk models based off of mean dose to calculate on a per voxel basis (Berrington de Gonzalez et al., 2013). If these questions are answered in the future, these techniques can be used to determine where the risk is most prevalent (not a straightforward answer if the dose response is non-linear) or to optimize plans based off of risk in addition to dose.

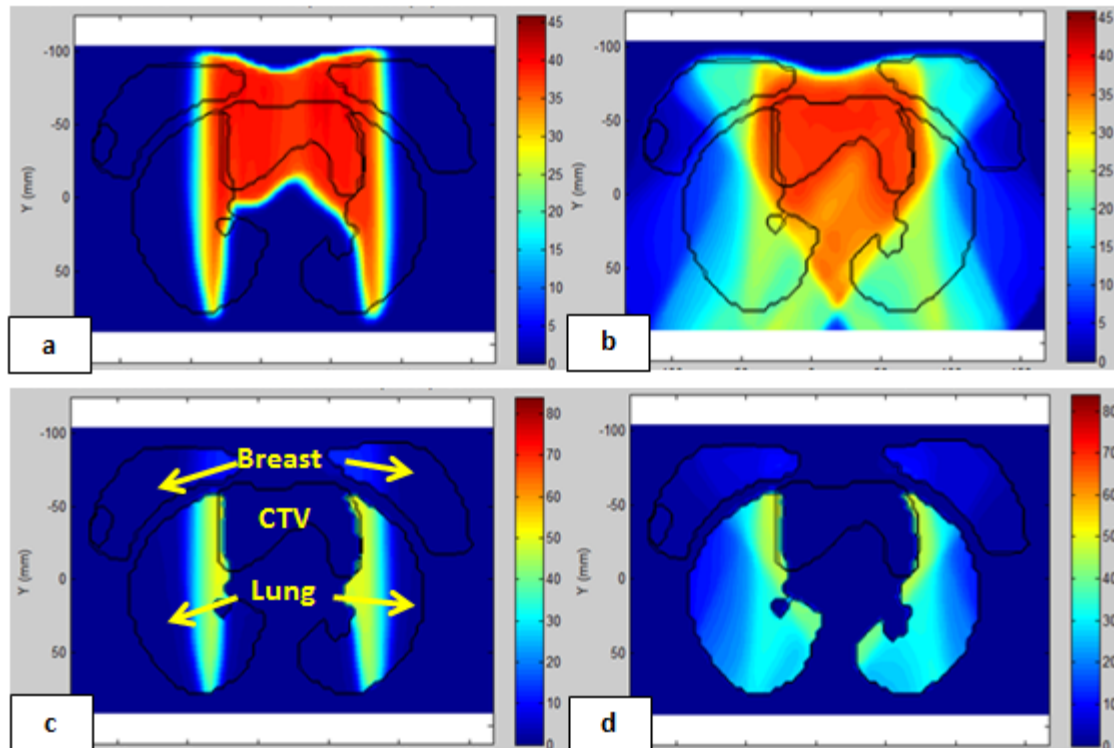


Figure 4-3 – Example of risk visualization tools – Images from Patient #2. The CTV and OARs in the image are pointed out in c). a) equivalent dose distribution from PSPT plan b) equivalent dose distribution for IMRT plan c) relative risk (RR) from same slice of PSPT plan d) RR from same slice of IMRT plan. Several questions remain regarding the appropriate value of risk on voxel by voxel basis, but calculating risk in the future can be used to visualize locations of higher or lower risk between treatment plans.

4.6. Limitations of the Study

Our study also had several limitations. As stated previously, the lack of 4D CT data sets or 4D planning when calculating dose could lead to discrepancies between the dose, and subsequently the RSC risk, calculated compared to what is actually delivered.

Another shortcoming is the lack of risk calculations for other potential OARs in the field of treatment, such as the esophagus and heart. All of the studies mentioned previously focus on the breast, lung, and thyroid, and for good reason. Breast and lung cancer are the most prevalent among young adults (Ng et al., 2010) after undergoing HL treatment, even compared to the thyroid which is up to 7 times less common as a RSC for HL patients. However, a more comprehensive review of OARs potentially affected would provide a more complete picture of possible issues when making clinical determinations.

Our study was an *in-silico* trial as opposed to an *in-vivo* trial. This is a common issue in radiation dosimetry/risk analysis and is difficult to overcome due to the amount of time required to acquire statistically meaningful results before the treatment technique is rendered technologically obsolete.

On a similar note, while the 9 patients in our study was the largest of HL risk analysis involving proton therapy to our knowledge, additional patients will be required to attain the necessary statistical power to draw definitive conclusions. In the short term, similar analysis of more patients in a similar manner will increase confidence in the result going forward.

While we feel our sensitivity tests cover a substantial amount of uncertainty associated with these risk calculations, there are still several unknowns regarding RSC outcomes for medically irradiated populations, not only compared to the LSS cohort we used from RadRAT and BEIR VII, but also from variations in techniques for medically exposed populations over the last 40 years, which were largely treated with EFRT (mantle fields).

Most institutions have moved from EFRT to IFRT over the last decade, however. These smaller field sizes which reduce the dose to healthy tissue combined with the heterogeneity of the dose distribution relative to EFRT have led many epidemiologists to caution against use of these risk models (Little, 2001, Dores et al., 2002, Suit et al., 2007, Koh et al., 2007, De Bruin et al., 2009, Ng et al., 2010, Berrington de Gonzalez et al., 2013). By taking the ratio of two plans against each other, many of these confounders have been removed, but when calculating absolute risk as opposed to relative risk as we have, care should be taken.

In the same vein, for photon treatments, 3DCRT has been compared to IMRT in other HL studies. While there are several advantages for IMRT treatments, including higher dose conformity and reduced hot spots to healthy tissue compare to 3DCRT, which may reduce acute side effects of radiation treatment, IMRT delivers low dose irradiations to larger volumes of healthy tissue. With the use of current models, this characteristic has led to lower dose or risk values for the organ at large compared for 3DCRT compared to IMRT (Chera et al., 2009, Andolino et al., 2011, Cella et al., 2013).

Additionally, both photon and proton treatments, there has been substantial interest in moving to even smaller fields than IFRT. These fields, called Involved Node Radiation Therapy (INRT) (Girinsky et al., 2006) are gaining in popularity and have been shown to irradiate less healthy tissue than IFRT (Weber et al., 2011). To further validate our results, a more comprehensive study of all available treatment techniques could be explored in the future.

Despite the above limitations, we feel our study is the most comprehensive for a HL patient cohort comparing photon treatments *vs* proton therapy to date and will only be strengthened by further studies in the future.

4.7. Future Work

Several different steps which have been highlighted in the above sections can be taken in the short term to further advance the topic of HL RSC risk. Several other treatment techniques, including the aforementioned INRT field setups in conjunction with the treatment setups from this work as well as the more recently used volumetric modulated arc therapy (VMAT) for both photon and proton modalities can be explored. VMAT risk values have been looked at in the prostate (Rechner et al., 2012a, Rechner et al., 2012b) and have shown similar results as IMRT in HL patients (Weber et al., 2011).

Extensive work has also been done on the implementation of Monte Carlo based calculations for photon IMRT treatments in our research group. Incorporating this into future studies would be the first validation of a complete photon IMRT treatment plan using deterministic methods and would provide a more comprehensive dosimetric evaluation than the analytical model employed here.

Finally, the risk visualization analysis previewed in Figure 4.3 can be further refined by streamlining the in house code written to prototype its function. More important, however, will be the validation of a model from epidemiological studies regarding the incidence of RSC for heterogeneous dose distributions in the treated HL population. With this information, the visualization becomes more than just a tool for comparisons of likely locations of dose and therefore potential risk. It can instead be used to help optimize treatment plans to not only reduce dose to healthy tissue, but risk as well.

4.8. Conclusion

Individualized PSPT and IMPT proton treatment plans which included a comprehensive dose calculation were compared for RSC risk to a corresponding photon IMRT plans for 9 patients. Evaluation of the range of possible mean RRR values with the sign test showed that while the majority of patient's individual OARs displayed decreased RSC risk for each proton plan compared to the IMRT plan, significant reductions were only seen when the average of all nine patients for each OAR ($\overline{RRR_j}$) were compared. Inclusion of out of field and secondary doses were shown to be important to accurately calculate risk as its absence for both the proton and photon plans would have resulted in a mean RRR value to incorrectly being greater than or lesser than 1. Due to the high variability of each patient with respect to patient anatomy and tumor location, individualized analysis is paramount to ensuring the best possible prediction of RSCs.

References

- AGOSTEO, S., BIRATTARI, C., CARAVAGGIO, M., SILARI, M. & TOSI, G. 1998. Secondary neutron and photon dose in proton therapy. *Radiother Oncol*, 48, 293-305.
- AGOSTEO, S., ROLLET, S., SILARI, M. & THEIS, C. 2008. Dosimetry in radiation fields around high-energy proton accelerators. *Radiat Meas*, 43, 1024-1032.
- ALEMAN, B. M., VAN DEN BELT-DUSEBOUT, A. W., KLOKMAN, W. J., VAN'T VEER, M. B., BARTELINK, H. & VAN LEEUWEN, F. E. 2003. Long-term cause-specific mortality of patients treated for Hodgkin's disease. *J Clin Oncol*, 21, 3431-9.
- ALMOND, P. R., BIGGS, P. J., COURSEY, B. M., HANSON, W. F., HUQ, M. S., NATH, R. & ROGERS, D. W. O. 1999. AAPM's TG-51 protocol for clinical reference dosimetry of high-energy photon and electron beams. *Med Phys*, 26, 1847-1870.
- ANDOLINO, D. L., HOENE, T., XIAO, L., BUCHSBAUM, J. & CHANG, A. L. 2011. Dosimetric comparison of involved-field three-dimensional conformal photon radiotherapy and breast-sparing proton therapy for the treatment of Hodgkin's lymphoma in female pediatric patients. *Int J Radiat Oncol Biol Phys*, 81, e667-71.
- ARCHAMBEAU, J. O., BENNETT, G. W., LEVINE, G. S., COWEN, R. & AKANUMA, A. 1974. Proton radiation therapy. *Radiology*, 110, 445-57.
- ARMITAGE, J. O. 2010. Early-stage Hodgkin's lymphoma. *N Engl J Med*, 363, 653-62.
- BEEBE, G. W., ISHIDA, M. & JABLON, S. 1962. Studies of the mortality of A-bomb survivors. I. Plan of study and mortality in the medical subsample (selection 1), 1950-1958. *Radiat Res*, 16, 253-80.
- BERRINGTON DE GONZALEZ, A., GILBERT, E., CURTIS, R., INSKIP, P., KLEINERMAN, R., MORTON, L., RAJARAMAN, P. & LITTLE, M. P. 2013. Second solid cancers after radiation therapy: a systematic review of the epidemiologic studies of the radiation dose-response relationship. *Int J Radiat Oncol Biol Phys*, 86, 224-33.

- BERRINGTON DE GONZALEZ, A., IULIAN APOSTOAEI, A., VEIGA, L. H., RAJARAMAN, P., THOMAS, B. A., OWEN HOFFMAN, F., GILBERT, E. & LAND, C. 2012. RadRAT: a radiation risk assessment tool for lifetime cancer risk projection. *J Radiol Prot*, 32, 205-22.
- BHATIA, S., YASUI, Y., ROBISON, L. L., BIRCH, J. M., BOGUE, M. K., DILLER, L., DELAAT, C., FOSSATI-BELLANI, F., MORGAN, E., OBERLIN, O., REAMAN, G., RUYMANN, F. B., TERSAK, J. & MEADOWS, A. T. 2003. High risk of subsequent neoplasms continues with extended follow-up of childhood Hodgkin's disease: report from the Late Effects Study Group. *J Clin Oncol*, 21, 4386-94.
- BHATTI, P., VEIGA, L. H., RONCKERS, C. M., SIGURDSON, A. J., STOVALL, M., SMITH, S. A., WEATHERS, R., LEISENRING, W., MERTENS, A. C., HAMMOND, S., FRIEDMAN, D. L., NEGLIA, J. P., MEADOWS, A. T., DONALDSON, S. S., SKLAR, C. A., ROBISON, L. L. & INSKIP, P. D. 2010. Risk of second primary thyroid cancer after radiotherapy for a childhood cancer in a large cohort study: an update from the childhood cancer survivor study. *Radiat Res*, 174, 741-52.
- BLEYER, A., VINY, A. & BARR, R. 2006. Cancer in 15- to 29-year-olds by primary site. *Oncologist*, 11, 590-601.
- BONADONNA, G., ZUCALI, R., MONFARDINI, S., DE LENA, M. & USLENGHI, C. 1975. Combination chemotherapy of Hodgkin's disease with adriamycin, bleomycin, vinblastine, and imidazole carboxamide versus MOPP. *Cancer*, 36, 252-9.
- BORTFELD, T. 2006. IMRT: a review and preview. *Phys Med Biol*, 51, R363-79.
- BORTFELD, T. R., KAHLER, D. L., WALDRON, T. J. & BOYER, A. L. 1994. X-ray field compensation with multileaf collimators. *Int J Radiat Oncol Biol Phys*, 28, 723-30.
- BRAHME, A. 1988. Optimal setting of multileaf collimators in stationary beam radiation therapy. *Strahlentherapie Und Onkologie*, 164, 343-50.
- BRENNER, D. J. & HALL, E. J. 2008. Secondary neutrons in clinical proton radiotherapy: a charged issue. *Radiother Oncol*, 86, 165-70.

- CASTELLINO, S. M., GEIGER, A. M., MERTENS, A. C., LEISENRING, W. M., TOOZE, J. A., GOODMAN, P., STOVALL, M., ROBISON, L. L. & HUDSON, M. M. 2011. Morbidity and mortality in long-term survivors of Hodgkin lymphoma: a report from the Childhood Cancer Survivor Study. *Blood*, 117, 1806-16.
- CELLA, L., CONSON, M., PRESSELLO, M. C., MOLINELLI, S., SCHNEIDER, U., DONATO, V., ORECCHIA, R., SALVATORE, M. & PACELLI, R. 2013. Hodgkin's lymphoma emerging radiation treatment techniques: trade-offs between late radio-induced toxicities and secondary malignant neoplasms. *Radiat Oncol*, 8, 22.
- CHAM, W. C., TAN, C. T., MARTINEZ, A., EXELBY, P. R., TEFFT, M., MIDDLEMAN, P. & D'ANGIO, G. J. 1976. Involved field radiation therapy for early stage Hodgkin's disease in children: preliminary results. *Cancer*, 37, 1625-32.
- CHERA, B. S., RODRIGUEZ, C., MORRIS, C. G., LOUIS, D., YEUNG, D., LI, Z. & MENDENHALL, N. P. 2009. Dosimetric comparison of three different involved nodal irradiation techniques for stage II Hodgkin's lymphoma patients: conventional radiotherapy, intensity-modulated radiotherapy, and three-dimensional proton radiotherapy. *Int J Radiat Oncol Biol Phys*, 75, 1173-80.
- CHUNG, C. S., KEATING, N., YOCK, T. & TARBELL, N. 2008. Comparative analysis of second malignancy risk in patients treated with proton therapy versus conventional photon therapy. *International Journal of Radiation Oncology Biology Physics*, 72, S8-S8.
- CLAUDE, L., MALET, C., POMMIER, P., THIESSE, P., CHABAUD, S. & CARRIE, C. 2007. Active breathing control for Hodgkin's disease in childhood and adolescence: feasibility, advantages, and limits. *Int J Radiat Oncol Biol Phys*, 67, 1470-5.
- CONNORS, J. M., KLIMO, P., FAIREY, R. N. & VOSS, N. 1987. Brief chemotherapy and involved field radiation therapy for limited-stage, histologically aggressive lymphoma. *Ann Intern Med*, 107, 25-30.

- CONSTINE, L. S., TARBELL, N., HUDSON, M. M., SCHWARTZ, C., FISHER, S. G., MUHS, A. G., BASU, S. K., KUN, L. E., NG, A., MAUCH, P., SANDHU, A., CULAKOVA, E., LYMAN, G. & MENDENHALL, N. 2008. Subsequent malignancies in children treated for Hodgkin's disease: associations with gender and radiation dose. *Int J Radiat Oncol Biol Phys*, 72, 24-33.
- COX, J. D. & HA, C. S. 1999. Prevention of diagnostic and treatment-related sequelae in stage I and II Hodgkin's disease. *Radiation Injury*, 32, 85-97.
- DASU, A. & TOMA-DASU, I. 2005. Dose-effect models for risk-relationship to cell survival parameters. *Acta Oncol*, 44, 829-35.
- DE BRUIN, M. L., SPARIDANS, J., VAN'T VEER, M. B., NOORDIJK, E. M., LOUWMAN, M. W., ZIJLSTRA, J. M., VAN DEN BERG, H., RUSSELL, N. S., BROEKS, A., BAAIJENS, M. H., ALEMAN, B. M. & VAN LEEUWEN, F. E. 2009. Breast cancer risk in female survivors of Hodgkin's lymphoma: lower risk after smaller radiation volumes. *J Clin Oncol*, 27, 4239-46.
- DE LANEY, T. F. & KOOY, H. M. 2008. *Proton and charged particle radiotherapy*, Philadelphia, Wolters Kluwer Health/Lippincott Williams & Wilkins.
- DE VATHAIRE, F., HARDIMAN, C., SHAMSALDIN, A., CAMPBELL, S., GRIMAUD, E., HAWKINS, M., RAQUIN, M., OBERLIN, O., DIALLO, I., ZUCKER, J. M., PANIS, X., LAGRANGE, J. L., DALY-SCHVEITZER, N., LEMERLE, J., CHAUAUDRA, J., SCHLUMBERGER, M. & BONAITI, C. 1999. Thyroid carcinomas after irradiation for a first cancer during childhood. *Arch Intern Med*, 159, 2713-9.
- DEVESA, S. S., SILVERMAN, D. T., YOUNG, J. L., JR., POLLACK, E. S., BROWN, C. C., HORM, J. W., PERCY, C. L., MYERS, M. H., MCKAY, F. W. & FRAUMENI, J. F., JR. 1987. Cancer incidence and mortality trends among whites in the United States, 1947-84. *J Natl Cancer Inst*, 79, 701-70.

- DIEZ, P., HOSKIN, P. J. & AIRD, E. G. 2007. Treatment planning and delivery of involved field radiotherapy in advanced Hodgkin's disease: results from a questionnaire-based audit for the UK Stanford V regimen vs ABVD clinical trial quality assurance programme (ISRCTN 64141244). *Br J Radiol*, 80, 816-21.
- DORES, G. M., METAYER, C., CURTIS, R. E., LYNCH, C. F., CLARKE, E. A., GLIMELIUS, B., STORM, H., PUKKALA, E., VAN LEEUWEN, F. E., HOLOWATY, E. J., ANDERSSON, M., WIKLUND, T., JOENSUU, T., VAN'T VEER, M. B., STOVALL, M., GOSPODAROWICZ, M. & TRAVIS, L. B. 2002. Second malignant neoplasms among long-term survivors of Hodgkin's disease: a population-based evaluation over 25 years. *J Clin Oncol*, 20, 3484-94.
- EASSON, E. & RUSSELL, M. H. 1963. Cure of Hodgkins Disease. *British Medical Journal*, 682-&.
- ELEY, J., NEWHAUSER, W., BERT, C., HOWELL, R. M., MAHAJAN, A., ETZEL, C. & STARKSCHALL, G. 2013. *Scanned Ion Beam Therapy for Thoracic Tumors*. Ph.D., The University of Texas at Houston.
- ENGELSMAN, M., RIETZEL, E. & KOOY, H. M. 2006. Four-dimensional proton treatment planning for lung tumors. *Int J Radiat Oncol Biol Phys*, 64, 1589-95.
- ENGERT, A., FRANKLIN, J., EICH, H. T., BRILLANT, C., SEHLEN, S., CARTONI, C., HERRMANN, R., PFREUNDSCHUH, M., SIEBER, M., TESCH, H., FRANKE, A., KOCH, P., DE WIT, M., PAULUS, U., HASENCLEVER, D., LOEFFLER, M., MULLER, R. P., MULLER-HERMELINK, H. K., DUHMKE, E. & DIEHL, V. 2007. Two cycles of doxorubicin, bleomycin, vinblastine, and dacarbazine plus extended-field radiotherapy is superior to radiotherapy alone in early favorable Hodgkin's lymphoma: final results of the GHSG HD7 trial. *J Clin Oncol*, 25, 3495-502.
- ENGERT, A., SCHILLER, P., JOSTING, A., HERRMANN, R., KOCH, P., SIEBER, M., BOISSEVAIN, F., DE WIT, M., MEZGER, J., DUHMKE, E., WILLICH, N., MULLER, R. P., SCHMIDT, B. F., RENNER, H., MULLER-HERMELINK, H. K., PFISTNER, B.,

- WOLF, J., HASENCLEVER, D., LOFFLER, M. & DIEHL, V. 2003. Involved-field radiotherapy is equally effective and less toxic compared with extended-field radiotherapy after four cycles of chemotherapy in patients with early-stage unfavorable Hodgkin's lymphoma: results of the HD8 trial of the German Hodgkin's Lymphoma Study Group. *J Clin Oncol*, 21, 3601-8.
- FERME, C., EGHBALI, H., MEERWALDT, J. H., RIEUX, C., BOSQ, J., BERGER, F., GIRINSKY, T., BRICE, P., VAN'T VEER, M. B., WALEWSKI, J. A., LEDERLIN, P., TIRELLI, U., CARDE, P., VAN DEN NESTE, E., GYAN, E., MONCONDUIT, M., DIVINE, M., RAEMAEKERS, J. M., SALLES, G., NOORDIJK, E. M., CREEMERS, G. J., GABARRE, J., HAGENBEEK, A., REMAN, O., BLANC, M., THOMAS, J., VIE, B., KLUIN-NELEMANS, J. C., VISEU, F., BAARS, J. W., POORTMANS, P., LUGTENBURG, P. J., CARRIE, C., JAUBERT, J. & HENRY-AMAR, M. 2007. Chemotherapy plus involved-field radiation in early-stage Hodgkin's disease. *N Engl J Med*, 357, 1916-27.
- FOLLOWILL, D., GEIS, P. & BOYER, A. 1997. Estimates of whole-body dose equivalent produced by beam intensity modulated conformal therapy. *International Journal of Radiation Oncology Biology Physics*, 38, 667-672.
- FONTENOT, J., TADDEI, P., ZHENG, Y., MIRKOVIC, D., JORDAN, T. & NEWHAUSER, W. 2008. Equivalent dose and effective dose from stray radiation during passively scattered proton radiotherapy for prostate cancer. *Phys Med Biol*, 53, 1677-88.
- FONTENOT, J. D., BLOCH, C., FOLLOWILL, D., TITT, U. & NEWHAUSER, W. D. 2010. Estimate of the uncertainties in the relative risk of secondary malignant neoplasms following proton therapy and intensity-modulated photon therapy. *Phys Med Biol*, 55, 6987-98.
- FONTENOT, J. D., LEE, A. K. & NEWHAUSER, W. D. 2009. Risk of secondary malignant neoplasms from proton therapy and intensity-modulated x-ray therapy for early-stage prostate cancer. *Int J Radiat Oncol Biol Phys*, 74, 616-22.

- FONTENOT, J. D., NEWHAUSER, W. D. & TITT, U. 2005. Design tools for proton therapy nozzles based on the double-scattering foil technique. *Radiat Prot Dosimetry*, 116, 211-5.
- FRIEDMAN, D. L., WHITTON, J., LEISENRING, W., MERTENS, A. C., HAMMOND, S., STOVALL, M., DONALDSON, S. S., MEADOWS, A. T., ROBISON, L. L. & NEGLIA, J. P. 2010. Subsequent neoplasms in 5-year survivors of childhood cancer: the Childhood Cancer Survivor Study. *J Natl Cancer Inst*, 102, 1083-95.
- GIEBELER, A., NEWHAUSER, W., ETZEL, C., HOWELL, R. M., MIRKOVIC, D. & COUTRAKON, G. 2011. *The Role of Cell Sterilization in Population Based Studies of Radiogenic Second Cancers Following Radiation Therapy*. Ph.D., The University of Texas at Houston.
- GILBERT, E. S., STOVALL, M., GOSPODAROWICZ, M., VAN LEEUWEN, F. E., ANDERSSON, M., GLIMELIUS, B., JOENSUU, T., LYNCH, C. F., CURTIS, R. E., HOLOWATY, E., STORM, H., PUKKALA, E., VAN'T VEER, M. B., FRAUMENI, J. F., BOICE, J. D., JR., CLARKE, E. A. & TRAVIS, L. B. 2003. Lung cancer after treatment for Hodgkin's disease: focus on radiation effects. *Radiat Res*, 159, 161-73.
- GILBERT, R. 1939. Radiotherapy in Hodgkin's disease (malignant granulomatosis) anatomic and clinical foundations governing principles, results. *American Journal of Roentgenology and Radium Therapy*, 41, 198-241.
- GIRINSKY, T., VAN DER MAAZEN, R., SPECHT, L., ALEMAN, B., POORTMANS, P., LIEVENS, Y., MEIJNDERS, P., GHALIBAFIAN, M., MEERWALDT, J. & NOORDIJK, E. 2006. Involved-node radiotherapy (INRT) in patients with early Hodgkin lymphoma: concepts and guidelines. *Radiother Oncol*, 79, 270-7.
- GRAGOUDAS, E. S. 1986. Proton-Beam Therapy of Uveal Melanomas. *Archives of Ophthalmology*, 104, 349-351.

- GROZINGER, S. O., RIETZEL, E., LI, Q., BERT, C., HABERER, T. & KRAFT, G. 2006. Simulations to design an online motion compensation system for scanned particle beams. *Phys Med Biol*, 51, 3517-31.
- GUIBOUT, C., ADJADJ, E., RUBINO, C., SHAMSALDIN, A., GRIMAUD, E., HAWKINS, M., MATHIEU, M. C., OBERLIN, O., ZUCKER, J. M., PANIS, X., LAGRANGE, J. L., DALY-SCHVEITZER, N., CHAVAUDRA, J. & DE VATHAIRE, F. 2005. Malignant breast tumors after radiotherapy for a first cancer during childhood. *J Clin Oncol*, 23, 197-204.
- HALL, E. J. 2004. Henry S. Kaplan Distinguished Scientist Award 2003. The crooked shall be made straight; dose-response relationships for carcinogenesis. *Int J Radiat Biol*, 80, 327-37.
- HALL, E. J. 2006. Intensity-modulated radiation therapy, protons, and the risk of second cancers. *Int J Radiat Oncol Biol Phys*, 65, 1-7.
- HALL, E. J. & WUU, C. S. 2003. Radiation-induced second cancers: the impact of 3D-CRT and IMRT. *Int J Radiat Oncol Biol Phys*, 56, 83-8.
- HANSEN, E. K. & ROACH, M. 2010. *Handbook of evidence-based radiation oncology*, New York, Springer.
- HODGKIN, T. 1832. On some Morbid Appearances of the Absorbent Glands and Spleen. *Med Chir Trans*, 17, 68-114.
- HODGSON, D. C., GILBERT, E. S., DORES, G. M., SCHONFELD, S. J., LYNCH, C. F., STORM, H., HALL, P., LANGMARK, F., PUKKALA, E., ANDERSSON, M., KAIJSER, M., JOENSUU, H., FOSSA, S. D. & TRAVIS, L. B. 2007a. Long-term solid cancer risk among 5-year survivors of Hodgkin's lymphoma. *J Clin Oncol*, 25, 1489-97.
- HODGSON, D. C., KOH, E. S., TRAN, T. H., HEYDARIAN, M., TSANG, R., PINTILIE, M., XU, T., HUANG, L., SACHS, R. K. & BRENNER, D. J. 2007b. Individualized estimates of second cancer risks after contemporary radiation therapy for Hodgkin lymphoma. *Cancer*, 110, 2576-86.

- HOPPE, B. S., FLAMPOURI, S., SU, Z., MORRIS, C. G., LATIF, N., DANG, N. H., LYNCH, J., LI, Z. & MENDENHALL, N. P. 2012. Consolidative involved-node proton therapy for Stage IA-IIIB mediastinal Hodgkin lymphoma: preliminary dosimetric outcomes from a Phase II study. *Int J Radiat Oncol Biol Phys*, 83, 260-7.
- HOWELL, R. M., HERTEL, N. E., WANG, Z. L., HUTCHINSON, J. & FULLERTON, G. D. 2006a. Calculation of effective dose from measurements of secondary neutron spectra and scattered photon dose from dynamic MLC IMRT for 6 MV, 15 MV, and 18 MV beam energies. *Med Phys*, 33, 360-368.
- HOWELL, R. M., KOONTZ-RAISIG, W. & JOHNSTONE, P. A. S. 2006b. The trade-off between neutron dose and skin dose for 6MV versus 18MV for prostate IMRT: Does the 20cm rule still apply? *International Journal of Radiation Oncology Biology Physics*, 66, S678-S678.
- HOWELL, R. M., SCARBORO, S. B., KRY, S. F. & YALDO, D. Z. 2010a. Accuracy of out-of-field dose calculations by a commercial treatment planning system. *Phys Med Biol*, 55, 6999-7008.
- HOWELL, R. M., SCARBORO, S. B., TADDEI, P. J., KRISHNAN, S., KRY, S. F. & NEWHAUSER, W. D. 2010b. Methodology for determining doses to in-field, out-of-field and partially in-field organs for late effects studies in photon radiotherapy. *Phys Med Biol*, 55, 7009-23.
- HOWLADER, N., NOONE, A. M., KRAPCHO, M., GARSHELL, J., NEYMAN, N., ALTERKRUSE, S. F., KOSARY, C. L., YU, M., RUHL, J., TATALOVICH, Z., CHO, H., MARIOTTO, A., LEWIS, D. R., CHEN, H. S., FEUER, E. J. & CRONIN, K. A. 2013. SEER Cancer Statistics Review, 1975-2010. based on November 2012 SEER data submission, posted to the SEER web site, April 2013 ed. Bethesda, MD: U.S. Department of Health and Human Services, National Institutes of Health, National Cancer Institute.
- INSKIP, P. D., ROBISON, L. L., STOVALL, M., SMITH, S. A., HAMMOND, S., MERTENS, A. C., WHITTON, J. A., DILLER, L., KENNEY, L., DONALDSON, S. S., MEADOWS, A. T.

- & NEGLIA, J. P. 2009. Radiation dose and breast cancer risk in the childhood cancer survivor study. *J Clin Oncol*, 27, 3901-7.
- JIANG, H., WANG, B., XU, X. G., SUIT, H. D. & PAGANETTI, H. 2005. Simulation of organ-specific patient effective dose due to secondary neutrons in proton radiation treatment. *Phys Med Biol*, 50, 4337-53.
- JOOSTEN, A., BOCHUD, F., BAECHLER, S., LEVI, F., MIRIMANOFF, R. O. & MOECKLI, R. 2011. Variability of a peripheral dose among various linac geometries for second cancer risk assessment. *Phys Med Biol*, 56, 5131-51.
- KALLMAN, P., LIND, B., EKLOF, A. & BRAHME, A. 1988. Shaping of Arbitrary Dose Distributions by Dynamic Multileaf Collimation. *Phys Med Biol*, 33, 1291-1300.
- KAPLAN, H. S. 1962. The radical radiotherapy of regionally localized Hodgkin's disease. *Radiology*, 78, 553-61.
- KAPLAN, S. & GARRICK, B. J. 1981. On The Quantitative Definition of Risk. *Risk Anal*, 1, 11-27.
- KASE, K. R., SVENSSON, G. K., WOLBARST, A. B. & MARKS, M. A. 1983. Measurements of Dose from Secondary Radiation Outside a Treatment Field. *International Journal of Radiation Oncology Biology Physics*, 9, 1177-1183.
- KELLERER, A. M., RUHM, W. & WALSH, L. 2006. Indications of the neutron effect contribution in the solid cancer data of the A-bomb survivors. *Health Phys*, 90, 554-64.
- KIRBY, T. H., HANSON, W. F., GASTORF, R. J., CHU, C. H. & SHALEK, R. J. 1986. Mailable TLD system for photon and electron therapy beams. *Int J Radiat Oncol Biol Phys*, 12, 261-5.
- KIRBY, T. H., HANSON, W. F. & JOHNSTON, D. A. 1992. Uncertainty analysis of absorbed dose calculations from thermoluminescence dosimeters. *Med Phys*, 19, 1427-33.
- KJELLBERG, R. N., HANAMURA, T., DAVIS, K. R., LYONS, S. L. & ADAMS, R. D. 1983. Bragg-peak proton-beam therapy for arteriovenous malformations of the brain. *N Engl J Med*, 309, 269-74.

- KJELLBERG, R. N., SWEET, W. H., PRESTON, W. M. & KOEHLER, A. M. 1962. The Bragg peak of a proton beam in intracranial therapy of tumors. *Trans Am Neurol Assoc*, 87, 216-8.
- KOECK, J., ABO-MADYAN, Y., LOHR, F., STIELER, F., KRIZ, J., MUELLER, R. P., WENZ, F. & EICH, H. T. 2012. Radiotherapy for early mediastinal Hodgkin lymphoma according to the German Hodgkin Study Group (GHSG): the roles of intensity-modulated radiotherapy and involved-node radiotherapy. *Int J Radiat Oncol Biol Phys*, 83, 268-76.
- KOEHLER, A. M., SCHNEIDER, R. J. & SISTERTON, J. M. 1977. Flattening of proton dose distributions for large-field radiotherapy. *Med Phys*, 4, 297-301.
- KOH, E. S., TRAN, T. H., HEYDARIAN, M., SACHS, R. K., TSANG, R. W., BRENNER, D. J., PINTILIE, M., XU, T., CHUNG, J., PAUL, N. & HODGSON, D. C. 2007. A comparison of mantle versus involved-field radiotherapy for Hodgkin's lymphoma: reduction in normal tissue dose and second cancer risk. *Radiat Oncol*, 2, 13.
- KRIKORIAN, J. G., PORTLOCK, C. S. & MAUCH, P. M. 1986. Hodgkin's disease presenting below the diaphragm: a review. *J Clin Oncol*, 4, 1551-62.
- KRY, S. F., SALEHPOUR, M., FOLLOWILL, D. S., STOVALL, M., KUBAN, D. A., WHITE, R. A. & ROSEN, I. I. 2005. Out-of-field photon and neutron dose equivalents from step-and-shoot intensity-modulated radiation therapy. *International Journal of Radiation Oncology Biology Physics*, 62, 1204-1216.
- LEVIN, W. P., KOOY, H., LOEFFLER, J. S. & DELANEY, T. F. 2005. Proton beam therapy. *British Journal of Cancer*, 93, 849-854.
- LINDSAY, K. A., WHELDON, E. G., DEEHAN, C. & WHELDON, T. E. 2001. Radiation carcinogenesis modelling for risk of treatment-related second tumours following radiotherapy. *Br J Radiol*, 74, 529-36.
- LITTLE, M. P. 2001. Comparison of the risks of cancer incidence and mortality following radiation therapy for benign and malignant disease with the cancer risks observed in the Japanese A-bomb survivors. *Int J Radiat Biol*, 77, 431-64.

- MACDONALD, D. A., DING, K., GOSPODAROWICZ, M. K., WELLS, W. A., PEARCEY, R. G., CONNORS, J. M., WINTER, J. N., HORNING, S. J., DJURFELDT, M. S., SHEPHERD, L. E. & MEYER, R. M. 2007. Patterns of disease progression and outcomes in a randomized trial testing ABVD alone for patients with limited-stage Hodgkin lymphoma. *Annals of Oncology*, 18, 1680-4.
- MACMAHON, B. 1957. Epidemiological evidence of the nature of Hodgkin's disease. *Cancer*, 10, 1045-54.
- MEADOWS, A. T., FRIEDMAN, D. L., NEGLIA, J. P., MERTENS, A. C., DONALDSON, S. S., STOVALL, M., HAMMOND, S., YASUI, Y. & INSKIP, P. D. 2009. Second Neoplasms in Survivors of Childhood Cancer: Findings From the Childhood Cancer Survivor Study Cohort. *Journal of Clinical Oncology*, 27, 2356-2362.
- MESOLORAS, G., SANDISON, G. A., STEWART, R. D., FARR, J. B. & HSI, W. C. 2006. Neutron scattered dose equivalent to a fetus from proton radiotherapy of the mother. *Med Phys*, 33, 2479-90.
- MEYER, R. M., GOSPODAROWICZ, M. K., CONNORS, J. M., PEARCEY, R. G., WELLS, W. A., WINTER, J. N., HORNING, S. J., DAR, A. R., SHUSTIK, C., STEWART, D. A., CRUMP, M., DJURFELDT, M. S., CHEN, B. E. & SHEPHERD, L. E. 2012. ABVD alone versus radiation-based therapy in limited-stage Hodgkin's lymphoma. *N Engl J Med*, 366, 399-408.
- MOYERS, M. F., BENTON, E. R., GHEBREMEDHIN, A. & COUTRAKON, G. 2008. Leakage and scatter radiation from a double scattering based proton beamline. *Med Phys*, 35, 128-44.
- MUNZENRIDER, J. E. 1999. Proton therapy for uveal melanomas and other eye lesions. *Strahlentherapie Und Onkologie*, 175, 68-73.
- MUNZENRIDER, J. E., GRAGOUDAS, E., VERHEY, L., GOITEIN, M., KOEHLER, A. & SUIT, H. D. 1980. Radiotherapy of Ocular Melanomas - Precision High-Dose External Beam

- Proton Therapy. *International Journal of Radiation Oncology Biology Physics*, 6, 1410-1411.
- NATH, R., BIGGS, P. J., BOVA, F. J., LING, C. C., PURDY, J. A., VAN DE GEIJN, J. & WEINHOUS, M. S. 1994. AAPM code of practice for radiotherapy accelerators: report of AAPM Radiation Therapy Task Group No. 45. *Med Phys*, 21, 1093-121.
- NATIONAL RESEARCH COUNCIL (U.S.). COMMITTEE TO ASSESS HEALTH RISKS FROM EXPOSURE TO LOW LEVEL OF IONIZING RADIATION. 2006. *Health risks from exposure to low levels of ionizing radiation : BEIR VII Phase 2*, Washington, D.C., National Academies Press.
- NCRP 2011. Report No. 170 - Second Primary Cancers and Cardiovascular Disease After Radiation Therapy (2011). NCRP Publications.
- NEUHAUSER, W., FONTENOT, J., ZHENG, Y., POLF, J., TITT, U., KOCH, N., ZHANG, X. & MOHAN, R. 2007a. Monte Carlo simulations for configuring and testing an analytical proton dose-calculation algorithm. *Phys Med Biol*, 52, 4569-84.
- NEUHAUSER, W., FONTENOT, J., ZHENG, Y., TADDEI, P., MIRKOVIC, D., TITT, U., ZHU, X., SAHOO, N., SCHAFFNER, B., LANGENEGGER, A., KOCH, N., ZHANG, X. & MOHAN, R. 2007b. A Monte-Carlo based dose engine for proton radiotherapy treatment planning. *Med Phys*, 34, 2406-2406.
- NEUHAUSER, W., KOCH, N., HUMMEL, S., ZIEGLER, M. & TITT, U. 2005. Monte Carlo simulations of a nozzle for the treatment of ocular tumours with high-energy proton beams. *Phys Med Biol*, 50, 5229-49.
- NEUHAUSER, W. D. & DURANTE, M. 2011. Assessing the risk of second malignancies after modern radiotherapy. *Nat Rev Cancer*, 11, 438-48.
- NEUHAUSER, W. D., FONTENOT, J. D., MAHAJAN, A., KORNGUTH, D., STOVALL, M., ZHENG, Y., TADDEI, P. J., MIRKOVIC, D., MOHAN, R., COX, J. D. & WOO, S. 2009.

- The risk of developing a second cancer after receiving craniospinal proton irradiation. *Phys Med Biol*, 54, 2277-91.
- NG, A. K., BERNARDO, M. P., WELLER, E., BACKSTRAND, K. H., SILVER, B., MARCUS, K. C., TARBELL, N. J., FRIEDBERG, J., CANELLOS, G. P. & MAUCH, P. M. 2002. Long-term survival and competing causes of death in patients with early-stage Hodgkin's disease treated at age 50 or younger. *J Clin Oncol*, 20, 2101-8.
- NG, A. K., KENNEY, L. B., GILBERT, E. S. & TRAVIS, L. B. 2010. Secondary malignancies across the age spectrum. *Semin Radiat Oncol*, 20, 67-78.
- OZASA, K., SHIMIZU, Y., SUYAMA, A., KASAGI, F., SODA, M., GRANT, E. J., SAKATA, R., SUGIYAMA, H. & KODAMA, K. 2012. Studies of the mortality of atomic bomb survivors, Report 14, 1950-2003: an overview of cancer and noncancer diseases. *Radiat Res*, 177, 229-43.
- PAGANETTI, H., ATHAR, B. S., MOTEABBED, M., J, A. A., SCHNEIDER, U. & YOCK, T. I. 2012. Assessment of radiation-induced second cancer risks in proton therapy and IMRT for organs inside the primary radiation field. *Phys Med Biol*, 57, 6047-61.
- PAUMIER, A., GHALIBAFIAN, M., BEAUDRE, A., FERREIRA, I., PICHENOT, C., MESSAI, T., LESSARD, N. A., LEFKOPOULOS, D. & GIRINSKY, T. 2011. Involved-node radiotherapy and modern radiation treatment techniques in patients with Hodgkin lymphoma. *Int J Radiat Oncol Biol Phys*, 80, 199-205.
- PEREZ-ANDUJAR, A., NEWHAUSER, W. D. & DELUCA, P. M. 2009. Neutron production from beam-modifying devices in a modern double scattering proton therapy beam delivery system. *Phys Med Biol*, 54, 993-1008.
- PETERS, M. V. 1950. A Study of Survivals in Hodgkins Disease Treated Radiologically. *American Journal of Roentgenology*, 63, 299-311.
- POLF, J. C. & NEWHAUSER, W. D. 2005. Calculations of neutron dose equivalent exposures from range-modulated proton therapy beams. *Phys Med Biol*, 50, 3859-73.

- POWERS, W. E., KINZIE, J. J., DEMIDECKI, A. J., BRADFIELD, J. S. & FELDMAN, A. 1973. A new system of field shaping for external-beam radiation therapy. *Radiology*, 108, 407-11.
- PRESTON, D. L., MATTSSON, A., HOLMBERG, E., SHORE, R., HILDRETH, N. G. & BOICE, J. D., JR. 2002. Radiation effects on breast cancer risk: a pooled analysis of eight cohorts. *Radiat Res*, 158, 220-35.
- PRESTON, D. L., RON, E., TOKUOKA, S., FUNAMOTO, S., NISHI, N., SODA, M., MABUCHI, K. & KODAMA, K. 2007. Solid cancer incidence in atomic bomb survivors: 1958-1998. *Radiat Res*, 168, 1-64.
- RAMSEY, C. R., CORDREY, I. L., SPENCER, K. M. & OLIVER, A. L. 1999. Dosimetric verification of two commercially available three-dimensional treatment planning systems using the TG 23 test package. *Med Phys*, 26, 1188-95.
- RECHNER, L. A., HOWELL, R. M., ZHANG, R., ETZEL, C., LEE, A. K. & NEWHAUSER, W. D. 2012a. Risk of radiogenic second cancers following volumetric modulated arc therapy and proton arc therapy for prostate cancer. *Phys Med Biol*, 57, 7117-32.
- RECHNER, L. A., HOWELL, R. M., ZHANG, R. & NEWHAUSER, W. D. 2012b. Impact of margin size on the predicted risk of radiogenic second cancers following proton arc therapy and volumetric modulated arc therapy for prostate cancer. *Phys Med Biol*, 57, N469-79.
- RIES, L. A. G. & SEER PROGRAM (NATIONAL CANCER INSTITUTE (U.S.)) 2007. Cancer survival among adults U.S. SEER program, 1988-2001 : patient and tumor characteristics. *SEER survival monograph*. Bethesda, MD: U.S. Dept. of Health and Human Services, National Institutes of Health, National Cancer Institute ,.
- RON, E., LUBIN, J. H., SHORE, R. E., MABUCHI, K., MODAN, B., POTTERN, L. M., SCHNEIDER, A. B., TUCKER, M. A. & BOICE, J. D., JR. 1995. Thyroid cancer after exposure to external radiation: a pooled analysis of seven studies. *Radiat Res*, 141, 259-77.
- RONCKERS, C. M., SIGURDSON, A. J., STOVALL, M., SMITH, S. A., MERTENS, A. C., LIU, Y., HAMMOND, S., LAND, C. E., NEGLIA, J. P., DONALDSON, S. S., MEADOWS, A.

- T., SKLAR, C. A., ROBISON, L. L. & INSKIP, P. D. 2006. Thyroid cancer in childhood cancer survivors: a detailed evaluation of radiation dose response and its modifiers. *Radiat Res*, 166, 618-28.
- ROSENBERG, S. A. & KAPLAN, H. S. 1982. *Malignant lymphomas : etiology, immunology, pathology, treatment*, New York, Academic Press.
- ROSNER, B. 2011. *Fundamentals of biostatistics*, Boston, Brooks/Cole, Cengage Learning.
- RUBEN, J. D., LANCASTER, C. M., JONES, P. & SMITH, R. L. 2011. A comparison of out-of-field dose and its constituent components for intensity-modulated radiation therapy versus conformal radiation therapy: implications for carcinogenesis. *Int J Radiat Oncol Biol Phys*, 81, 1458-64.
- SCHAFFNER, B. 2008. Proton dose calculation based on in-air fluence measurements. *Phys Med Biol*, 53, 1545-62.
- SCHNEIDER, U. 2009. Mechanistic model of radiation-induced cancer after fractionated radiotherapy using the linear-quadratic formula. *Med Phys*, 36, 1138-43.
- SCHNEIDER, U., AGOSTEO, S., PEDRONI, E. & BESSERER, J. 2002. Secondary neutron dose during proton therapy using spot scanning. *Int J Radiat Oncol Biol Phys*, 53, 244-51.
- SCHNEIDER, U. & KASER-HOTZ, B. 2005. Radiation risk estimates after radiotherapy: application of the organ equivalent dose concept to plateau dose-response relationships. *Radiat Environ Biophys*, 44, 235-9.
- SCHNEIDER, U., LOMAX, A. & LOMBRISER, N. 2000. Comparative risk assessment of secondary cancer incidence after treatment of Hodgkin's disease with photon and proton radiation. *Radiat Res*, 154, 382-8.
- SCHNEIDER, U., SUMILA, M. & ROBOTKA, J. 2011. Site-specific dose-response relationships for cancer induction from the combined Japanese A-bomb and Hodgkin cohorts for doses relevant to radiotherapy. *Theor Biol Med Model*, 8, 27.

- SCHNEIDER, U., ZWAHLEN, D., ROSS, D. & KASER-HOTZ, B. 2005. Estimation of radiation-induced cancer from three-dimensional dose distributions: Concept of organ equivalent dose. *Int J Radiat Oncol Biol Phys*, 61, 1510-5.
- SIGURDSON, A. J., RONCKERS, C. M., MERTENS, A. C., STOVALL, M., SMITH, S. A., LIU, Y., BERKOW, R. L., HAMMOND, S., NEGLIA, J. P., MEADOWS, A. T., SKLAR, C. A., ROBISON, L. L. & INSKIP, P. D. 2005. Primary thyroid cancer after a first tumour in childhood (the Childhood Cancer Survivor Study): a nested case-control study. *Lancet*, 365, 2014-23.
- SPECHT, L., YAHALOM, J., ILLIDGE, T., BERTHELSEN, A. K., CONSTINE, L. S., EICH, H. T., GIRINSKY, T., HOPPE, R. T., MAUCH, P., MIKHAEEL, N. G. & NG, A. 2013. Modern Radiation Therapy for Hodgkin Lymphoma: Field and Dose Guidelines From the International Lymphoma Radiation Oncology Group (ILROG). *Int J Radiat Oncol Biol Phys*.
- STARCKSCHALL, G., BRITTON, K., MCALEER, M. F., JETER, M. D., KAUS, M. R., BZDUSEK, K., MOHAN, R. & COX, J. D. 2009. Potential dosimetric benefits of four-dimensional radiation treatment planning. *Int J Radiat Oncol Biol Phys*, 73, 1560-5.
- STROMBERG, J. S., SHARPE, M. B., KIM, L. H., KINI, V. R., JAFFRAY, D. A., MARTINEZ, A. A. & WONG, J. W. 2000. Active breathing control (ABC) for Hodgkin's disease: reduction in normal tissue irradiation with deep inspiration and implications for treatment. *Int J Radiat Oncol Biol Phys*, 48, 797-806.
- SUIT, H., GOLDBERG, S., NIEMIERKO, A., ANCUKIEWICZ, M., HALL, E., GOITEIN, M., WONG, W. & PAGANETTI, H. 2007. Secondary carcinogenesis in patients treated with radiation: a review of data on radiation-induced cancers in human, non-human primate, canine and rodent subjects. *Radiat Res*, 167, 12-42.

- TADDEI, P. J., FONTENOT, J. D., ZHENG, Y., MIRKOVIC, D., LEE, A. K., TITT, U. & NEWHAUSER, W. D. 2008. Reducing stray radiation dose to patients receiving passively scattered proton radiotherapy for prostate cancer. *Phys Med Biol*, 53, 2131-47.
- TADDEI, P. J., HOWELL, R. M., KRISHNAN, S., SCARBORO, S. B., MIRKOVIC, D. & NEWHAUSER, W. D. 2010a. Risk of second malignant neoplasm following proton versus intensity-modulated photon radiotherapies for hepatocellular carcinoma. *Phys Med Biol*, 55, 7055-65.
- TADDEI, P. J., MAHAJAN, A., MIRKOVIC, D., ZHANG, R., GIEBELER, A., KORNGUTH, D., HARVEY, M., WOO, S. & NEWHAUSER, W. D. 2010b. Predicted risks of second malignant neoplasm incidence and mortality due to secondary neutrons in a girl and boy receiving proton craniospinal irradiation. *Phys Med Biol*, 55, 7067-80.
- TADDEI, P. J., MIRKOVIC, D., FONTENOT, J. D., GIEBELER, A., ZHENG, Y., KORNGUTH, D., MOHAN, R. & NEWHAUSER, W. D. 2009. Stray radiation dose and second cancer risk for a pediatric patient receiving craniospinal irradiation with proton beams. *Phys Med Biol*, 54, 2259-75.
- TAYAMA, R., FUJITA, Y., TADOKORO, M., FUJIMAKI, H., SAKAE, T. & TERUNUMA, T. 2006. Measurement of neutron dose distribution for a passive scattering nozzle at the Proton Medical Research Center (PMRC). *Nuclear Instruments & Methods in Physics Research Section a-Accelerators Spectrometers Detectors and Associated Equipment*, 564, 532-536.
- TITT, U., ZHENG, Y., ZHU, X., MOHAN, R. & NEWHAUSER, W. 2006. Verification of a proton treatment-planning pencil-beam dose algorithm with Monte Carlo. *Med Phys*, 33, 2149-2149.
- TRAVIS, L. B. 2006. The epidemiology of second primary cancers. *Cancer Epidemiology Biomarkers & Prevention*, 15, 2020-2026.
- TRAVIS, L. B., GOSPODAROWICZ, M., CURTIS, R. E., CLARKE, E. A., ANDERSSON, M., GLIMELIUS, B., JOENSUU, T., LYNCH, C. F., VAN LEEUWEN, F. E., HOLOWATY,

- E., STORM, H., GLIMELIUS, I., PUKKALA, E., STOVALL, M., FRAUMENI, J. F., JR., BOICE, J. D., JR. & GILBERT, E. 2002. Lung cancer following chemotherapy and radiotherapy for Hodgkin's disease. *J Natl Cancer Inst*, 94, 182-92.
- TRAVIS, L. B., HILL, D. A., DORES, G. M., GOSPODAROWICZ, M., VAN LEEUWEN, F. E., HOLOWATY, E., GLIMELIUS, B., ANDERSSON, M., WIKLUND, T., LYNCH, C. F., VANT VEER, M. B., GLIMELIUS, I., STORM, H., PUKKALA, E., STOVALL, M., CURTIS, R., BOICE, J. D., JR. & GILBERT, E. 2003. Breast cancer following radiotherapy and chemotherapy among young women with Hodgkin disease. *JAMA*, 290, 465-75.
- TRAVIS, L. B., NG, A. K., ALLAN, J. M., PUI, C. H., KENNEDY, A. R., XU, X. G., PURDY, J. A., APPLGATE, K., YAHALOM, J., CONSTINE, L. S., GILBERT, E. S. & BOICE, J. D., JR. 2012. Second malignant neoplasms and cardiovascular disease following radiotherapy. *J Natl Cancer Inst*, 104, 357-70.
- VAN ESCH, A., TILLIKAINEN, L., PYYKKONEN, J., TENHUNEN, M., HELMINEN, H., SILJAMAKI, S., ALAKUIJALA, J., PAIUSCO, M., LORI, M. & HUYSKENS, D. P. 2006. Testing of the analytical anisotropic algorithm for photon dose calculation. *Med Phys*, 33, 4130-48.
- WAMBERSIE, A., JONES, D. T. L. & SUIT, H. D. 2007. Presentation of the ICRU-IAEA joint report "Prescribing, Recording, and Reporting Proton-beam Therapy". *Strahlentherapie Und Onkologie*, 183, 87-89.
- WAMBERSIE, A., LANDBERG, T. & GAHBAUER, R. 1999. Prescribing, recording and reporting photon beam therapy: the problem of margins (the recent ICRU recommendations, Report #62, 1999). *Patras Medical Physics* 99, 25-31.
- WEBB, S. 1992. Optimization by Simulated Annealing of 3-Dimensional, Conformal Treatment Planning for Radiation-Fields Defined by a Multileaf Collimator .2. Inclusion of 2-Dimensional Modulation of the X-Ray-Intensity. *Phys Med Biol*, 37, 1689-1704.

- WEBER, D. C., JOHANSON, S., PEGURET, N., COZZI, L. & OLSEN, D. R. 2011. Predicted risk of radiation-induced cancers after involved field and involved node radiotherapy with or without intensity modulation for early-stage hodgkin lymphoma in female patients. *Int J Radiat Oncol Biol Phys*, 81, 490-7.
- WOOD, M. E., VOGEL, V., NG, A., FOXHALL, L., GOODWIN, P. & TRAVIS, L. B. 2012. Second malignant neoplasms: assessment and strategies for risk reduction. *J Clin Oncol*, 30, 3734-45.
- YAN, X., TITT, U., KOEHLER, A. M. & NEWHAUSER, W. D. 2002. Measurement of neutron dose equivalent to proton therapy patients outside of the proton radiation field. *Nuclear Instruments & Methods in Physics Research Section a-Accelerators Spectrometers Detectors and Associated Equipment*, 476, 429-434.
- ZHANG, R., PEREZ-ANDUJAR, A., FONTENOT, J. D., TADDEI, P. J. & NEWHAUSER, W. D. 2010. An analytic model of neutron ambient dose equivalent and equivalent dose for proton radiotherapy. *Phys Med Biol*, 55, 6975-6985.
- ZHENG, Y., FONTENOT, J., TADDEI, P., MIRKOVIC, D. & NEWHAUSER, W. 2008. Monte Carlo simulations of neutron spectral fluence, radiation weighting factor and ambient dose equivalent for a passively scattered proton therapy unit. *Phys Med Biol*, 53, 187-201.
- ZHENG, Y., NEWHAUSER, W., FONTENOT, J. & KOCH, N. 2006. Automation of Monte Carlo simulations for a proton therapy system. *Med Phys*, 33, 2073-2074.
- ZHENG, Y., NEWHAUSER, W., FONTENOT, J., TADDEI, P. & MOHAN, R. 2007. Monte Carlo study of neutron dose equivalent during passive scattering proton therapy. *Phys Med Biol*, 52, 4481-96.

Vita

Kenneth Lois Homann was born in Aransas Pass, Texas, in 1979. He was raised by his parents, Ronnie and Debbie Homann, and grew up with his younger brother, Scott Homann, in several small towns in Texas including Hallettsville, Cushing, and Nacogdoches, where he graduated from high school in 1997. In the fall of 1997 he began his undergraduate studies at Northwestern State University in Natchitoches, Louisiana, graduating with a bachelor of science in physics in the spring of 2001. Kenneth then attended the University of Texas Health Science Center-Houston and received his Specialized Masters of Science in medical physics in 2005. From 2005 to 2009, he worked as a clinical medical physics at Baylor College of Medicine in Houston, Texas before returning to the Health Science Center to pursue his Ph.D. in medical physics. Kenny married the former Sarah Bourgeois in September of 2012, and upon completion of his degree requirements, he will join the medical physics group at Houston Methodist Hospital's where he will serve as a clinical physicist and the director of the Houston Methodist medical physics residency program.